COVER PAGE

Federal award number: **2020-R2-CX-0050**

Project Title: **Experimental and numerical investigations for the prediction of depth of calcination of gypsum plasterboards under fire exposure**

PD/PI Name, Title and Contact Information (e-mail address and phone number):

Shijin P. Kozhumal, Ph.D.

Assistant Professor

Fire Protection & Safety Engineering Technology Program

College of Justice, Safety & Military Science

Eastern Kentucky University

128 Ashland Fire and Safety Lab.

521 Lancaster Ave, Richmond, KY, 40475

Phone: 859-622-7136

e-mail: shijin.kozhumal@eku.edu

Recipient Organization (Name and Address):

Eastern Kentucky University

521 Lancaster Avenue

Richmond, KY 40475-3102

Project/Grant Period: **01/01/2021 to 12/31/2022**

Award amount: **$ 241,30**

TABLE OF CONTENTS

NOMENCLATURE

$\emptyset$	Porosity
${\rho_g}^k$	Mass concentration of the kth gas phase component (kg/m^3)
t	Time (s)
D_{eff}	Effective diffusion coefficient (m^2/s)
${U_g}^D$	Darcy velocity vector (m/s)
${\dot{Q}_m}^{'''k}$	Mass production/consumption rate of the kth gas phase per unit volume (kg/m^3 s)
K	Permeability tensor (m^2)
μ_g	Dynamic viscosity of the gas mixture (Pa s)
P_g	Total pressure of the gas mixture (Pa)
ρ_s	Density of the solid (kg/m^3)
c_s	Specific heat of the solid component (J/ kg K)
N^g	Number of gas phase components
${c_{p,g}}^k$	Constant pressure specific heat of the kth gas phase component (J/ kg K)
T	Temperature (K)
K_{eff}	Effective thermal conductivity (W/m K)
${j_{diff}}^k$	Mass flux vector per unit area of the kth gas phase component due to concentration gradients (kg/s m^2)

$j_{pres}{}^{k}$	Mass flux vector per unit area of the kth gas phase component due to pressure gradients (kg/s m^2)
$\dot{Q}_T{}'''$	Energy production/consumption rate per unit volume (W/m^3)
D_{AB}	Binary diffusion coefficient of water vapor in the air (m^2/s)
τ	Tortuosity factor
∂	Partial derivative operator
∇	Gradient operator
$\vec{X}$	Vector of sensitivity inputs
Y	Generalized model output
var	variance operator
$E(Y\|X_i)$	expected value of model output given some constrained value X_i
S_i^G	Global sensitivity of parameter X_i (first order Sobol index)
S_k^L	Local sensitivity of parameter k

LIST OF FIGURES

1. SUMMARY OF THE PROJECT

1.1: Major goals and objectives

Scientific studies with in-depth analysis of the physical and chemical process of gypsum calcination are very limited despite the wide use of gypsum plasterboards and its significance in forensic fire investigations. Based on our preliminary numerical studies and literature review we identified the areas where significant improvements are required to develop a reliable predictive tool for the analysis of gypsum calcination and the prediction of depth of calcination. The objectives of the proposed project, include:

1. Chemistry model that considers the multi-stage endothermic dehydration of the gypsum and decomposition of calcium carbonate.
2. Characterization of different gypsum boards available in the market from different manufacturers.
3. Validation of the numerical model and characterization of the sensitivity of each modeling parameter in the entire practical range
4. A computational model that considers the endothermic dehydration of chemically bound water in calcium sulfate dihydrate, variable thermo-physical properties, variable porosity, and heat and mass transfer through the porous material
5. Development of a three-dimensional computational model that can predict the depth of calcination based on the measured or simulated heat fluxes or temperature of fire.
6. Validation of the numerical model based on experiments where heat flux, spatial gradients in heat flux, and duration of exposure are systematically varied.
7. Development and testing of correlations for the depth of calcination.

8. Development of a stand-alone user-friendly executable for the prediction of depth of calcination.
9. Online workshops/webinars engaging fire investigators to understand the requirements of the fire investigators and to explain the prediction and analysis of the depth of calcination using the stand-alone application.

1.2: Research questions

Gypsum plasterboard (also known as Drywall, plasterboard, wallboard, sheetrock, gyprock, gypsum board, or gypsum panel) is a safe, efficient, easy-to-use, and fire-resistant product that suits the US construction market. The global gypsum production capacity is estimated to be 12.87 billion m^2 per year. The US has some of the largest high-quality gypsum reserves in the world and the US represents around 28% of the world's gypsum wallboard production capacity (www.globalgypsum.com, 2013). Gypsum (Calcium Sulfate Dihydrate) forms naturally when calcium sulfate is hydrated by groundwater and as a by-product of many desulphurization processes. Gypsum is the primary component of gypsum plaster boards. Gypsum undergoes calcination when heated. This endothermic dehydration improves fire safety. The process of gypsum calcination is governed by the coupled heat transfer, rate of dehydration, and the transport of water vapor produced during dehydration (Kozhumal, Hicks, & Sezer, 2019). However, current understanding of gypsum calcination is limited to simplified numerical models and limited experimental measurements with multiple uncontrolled variables.

Since the beginning of organized fire investigation in the late 1940s, fire investigators have relied on fire patterns as their basis for determining the fire origin (Rethoret, 1945). Fire patterns are defined as the “visible or measurable physical changes, or identifiable shapes, formed by a fire

effect or group of fire effects" (NFPA, 2021, p. 12). Absent the testimony of reliable eyewitnesses to the fire's inception, the investigator determines the origin in part by observation and analysis of the physical evidence (fire patterns) relative to fire science to reconstruct the fire. As such, fire origin determination is largely a matter of fire pattern recognition and analysis (NFPA, 2021). Gypsum loses its chemically bound water molecules and undergoes calcination when heated. During exposure to fire (i.e. heat flux), gypsum dehydrates leaving a measurable depth of calcination, which is used by fire investigators.

Currently, fire investigators identify fire patterns by visible observation or through depth measurements of materials affected by fire. This analysis demands the coupling of the physical laws of fire dynamics with the investigator's inference regarding the damage. The standard of care in the fire investigation profession is the 2021 edition of NFPA 921 *Guide for Fire and Explosion Investigations*, as espoused by the National Fire Protection Association (NFPA). Since its inception in 1992, NFPA 921 represents the current "state-of-the-art" and industry "standard of care" for fire and explosion investigations. With the introduction of NFPA 921, the fire investigation profession began a movement toward the implementation of science-based principles in fire investigation. Even though historic and current treatises espouse the use of fire patterns for fire investigations, only limited research has been conducted to study the scientific foundation of fire patterns. The National Institute of Standards and Technology (NIST), National Institute of Justice (NIJ), and the United States Fire Administration (USFA) have completed full-scale fire research specifically to address fire patterns (McGarry & Milke, 1997) (Shanley, Kennedy, & Ward, 1997) (Mealy, Wolfe, & Gottuk, 2013) (Mealy, 2013). Due to the numerous parameters

associated with full-scale fire tests and the limited number of studies conducted, there are still many questions unanswered.

The legal and science professions are currently scrutinizing forensic science, which is forcing the nation to question the scientific foundation of all forensics (National Academy of Science, 2009). The National Academy of Sciences released a cautionary report regarding this type of analysis. In this document, the authors outlined the need to improve the scientific foundations of the forensic disciplines, particularly those that are dependent on qualitative analyses and expert interpretation of observed patterns, including fire investigations (National Academy of Science, 2009). Availability of reliable and accurate quantitative measurements like depth of calcination and its relationship with the history of fire spread would help in addressing the problem.

Earliest research into gypsum exposed to fire was reported in the 1960s (Ryan, 1962). Many researchers explored the behavior of gypsum boards exposed to fire using experimental (King, Beretka, & Ridge, 1971), theoretical (Andesson & Jansson, 1987), and numerical methods (Mehaffey, Cuerrier, & Carisse, 1994; Sultan, 1996). These studies focused on testing the behavior of walls made with gypsum board, wood or steel studs when exposed to fire to predict failure. The limited theoretical and numerical studies used many simplifying assumptions on heat transfer, convection, and material properties. Further numerical studies attempted at exploring the process of gypsum calcination (Axenenko & Thorpe, 1996; Ang & Wang, 2004). Thermal behavior of commercially widespread gypsum board exposed to fire was analyzed by Wakili et al. (Wakili, Hugi, Wullschleger, & Frank, 2007). The study resulted in material properties of gypsum board at different temperatures. Following them, heat and mass transfer mechanisms occurring in a gypsum

board exposed to fire was analyzed numerically by Kontogeorgos and Founti (Kontogeorgos & Founti, 2010).

Numerical models have been developed and tested to reasonably predict fire spread, even though they employ many engineering approximations (McGrattanan, et al., 2012). Simultaneous Thermogravimetric Analysis (TGA) and Differential Scanning Calorimetry (DSC) results of gypsum boards available in the literature are significantly different. Also, there is up to 20% difference in the value of endothermic energy needed for dehydration among different experimental measurements. The mass loss during the gypsum calcination is largely due to the dehydration of gypsum releasing water vapor and a small part is due to the decomposition of calcium carbonate releasing carbon dioxide (Wakili, Hugi, Wullschleger, & Frank, 2007). Recent numerical studies on the gypsum thermo-chemistry (Kozhumal, Hicks, & Sezer, 2019) and the position of fire on the depth of calcination (Fowlie, Sezer, Gorbett, & Kozhumal, 2020) have quantitatively analyzed depth of calcination when exposed to fire. However, quantitative characterization of the fraction of calcium carbonate present in the gypsum board and the factors affecting its rate of decomposition are not sufficiently established for it to be included in a numerical model. In addition, the experimental measurements and TGA results in the literature suggest significant differences in the material properties of different gypsum boards available in the market. To develop a reliable predictive tool, gypsum calcination needs to be sufficiently characterized by Thermogravimetry Analysis (TGA), Differential Scanning Calorimetry (DSC), and Fourier Transform Infrared Spectroscopy (FTIR) of gypsum boards from different manufacturers. The reproducibility of the measurements and standard error need to be established.

The macroscopic fire experiments are not sufficient to understand the microscale properties of the gypsum board. The verification of the relationship between the history of fire spread and the depth of calcination requires a detailed understanding of the process of gypsum calcination. In this context, the present study explores the process of gypsum calcination using comprehensive three-dimensional unsteady computational model capable of solving the mass, species, momentum, and energy conservation equations. This allows us to develop correlations between material properties of the fuel, dimensions of the compartment and ventilation, and measurable depth of calcination on the compartment lining by performing systematic and reproducible fire experiments. Computational investigations help to understand the heat and mass transfer mechanisms that govern the gypsum calcination and to predict the depth of calcination. The experimental measurements can be used to validate and improve the numerical model. The correlations and criteria developed from the study will be tested for real life fire scenarios.

1.3: Research design and methods

1.3.1: Phase 1: Development and validation of gypsum calcination models

During a fire, the fire temperatures, heat release rates, heat fluxes to the walls, wall temperatures, and species concentrations change drastically. This makes it very difficult to reproduce and develop correlations for depth of calcination. As there are many variables due to the unsteady fire dynamics, a repeatable and reproducible characterization of the gypsum calcination requires simplification of the number of uncontrolled variables. In this project, experimental and numerical investigations with a uniform heat flux were carried out in the first phase.

1.3.1.1: Task 1.A: Development of a comprehensive 1D model

A one-dimensional model was developed by improving the methodology described in preliminary results. The previous studies on gypsum calcination directly used experimental mass loss rate

measured with a fixed heating rate for the numerical model (Kontogeorgos & Founti, 2010). This method might give misleading results when the heating rate (increase in temperature per unit time) of the gypsum board during fire exposure is significantly different from the value used for TGA analysis. In our model, we solved this problem by developing reaction rate equation as a function of temperature, and the remaining water that can be dehydrated based on the TGA results available in the literature (Wakili, Hugi, Wullschleger, & Frank, 2007).

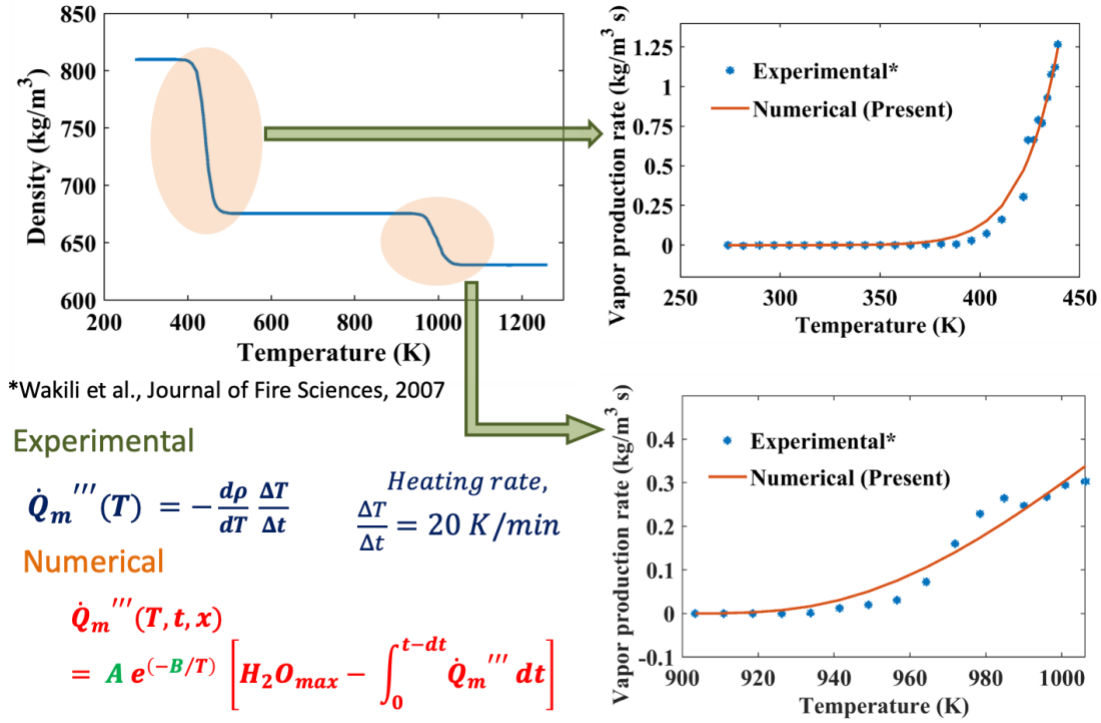

Figure 1: Modeling of rate of vapor production. The mass loss curve reproduced from the experimental results (Wakili, Hugi, Wullschleger, & Frank, 2007) is shown on top left, and comparison of numerical predictions with experimental measurements (right).

The rate of dehydration ($\dot{Q}_m'''$) was calculated numerically as in the equation given in Figure 1. The rate of dehydration ($\dot{Q}_m'''$), estimated for the numerical model was then compared to the calculated rate of dehydration from the experimental measurement (Figure 1, left top) for the two

stages of the gypsum calcination process as shown in Figure 1, right. Thus, converting the TGA results into just two sets of coefficients, A and B. Even though the agreement with exponential relationship seems acceptable for the first stage, it needed to be verified for different gypsum board and a wide range of heating rate. This was performed in Task 1.B and the results were used to improve the chemistry model. Combined TGA-DSC and FTIR studies were performed to get the release of water vapor and CO_2 during the gypsum calcination at different heating rates and a generalized chemistry model was developed.

1.3.1.2: Task 1.B: TGA, DSC, and FTIR

To strengthen the modeling of rate of dehydration, combined TGA and FTIR experiments were required. The slight underprediction of temperature in the initial stages and the overprediction of the temperature during peak dehydration rates might be because of the assumption of a fixed heat of dehydration throughout the process. It is very likely that different stages of the dehydration have deferent heats of dehydration. Characterization of the heat of dehydration required further TGA-DSC and FTIR investigations were performed on different gypsum wallboards for a range of heating rates.

In addition, the remaining water content in a gypsum board after fire exposure needs to be characterized to correlate the percentage of dehydration with the depth of calcination. TGA-DSC studies were conducted for gypsum boards from different locations and manufacturers and the results were tabulated. A total of 5-7 sets of experiments (15-21 in total) were required.

1.3.1.3: Task 1.C: Experiments with controlled heat flux and duration of exposure

As there are too many variables due to unsteady fire dynamics, varying temperatures, heat fluxes, and species concentrations, a repeatable and reproducible characterization of the gypsum calcination requires simplification of the number of uncontrolled variables. In experimental phase,

experiments were conducted with controlled uniform heat flux and duration of exposure. The temperature inside the gypsum board was measured along with the depth of calcination. The experimental series included a radiant burner for a uniform heat flux, a propane burner with a uniform fuel supply to closely mimic the concentration of water vapor in the fire (i.e., influence the species transport inside the gypsum board), and a larger diffusion burner. An array of nine thermocouples with four heat flux gauges was used to assure uniform heat flux in the entire experimental region. Gypsum boards with dimensions 0.6 m x 0.6 m were used for the experiments to avoid boundary effects on lateral heat and mass transfer and ensure one-dimensionality. Experiments were conducted by varying the heat fluxes in the range 0-100 kW/m^2 and durations of exposure from 0-30 minutes. These tests assisted in the development and testing of the numerical models.

1.3.1.4: Task 1.D: Sensitivity and reproducibility analysis

As there are significant differences in the material properties between different gypsum boards available in the market. This leads to differences in the heats of dehydration, density, moisture content, calcium carbonate content, porosity, and specific heat. The heat flux was verified numerically up to 200 kW/m^2. A systematic sensitivity study was completed to quantify the impact of these variations on the gypsum calcination and the prediction of depth of calcination. Systematic sensitivity studies on the effects of heats of dehydration, density, moisture content, calcium carbonate content, porosity, and specific heat capacity of gypsum boards on the depth of calcination were carried out by varying one property at a time. The sensitivity of the initial and boundary conditions was also analyzed. Methods including Monte-Carlo techniques were used to identify highly sensitive parameters and characterize them. The impact of small incremental

changes in an input parameter on output parameters like depth of calcination were statistically assessed.

1.3.1.5: Task 1.E: Validation of the 1D model

Even though the preliminary one-dimensional model is validated against experimental measurements in the available literature, a few key areas needed improvement and further validation. The modeling of gypsum thermo-chemistry, rate of dehydration, heat of dehydration, and variable porosity was improved as described in Task 1.A based on the TGA, DSC, and FTIR results from Task 1.B. The experimental results with controlled heat flux and duration of exposure from Task 1.C. was used to validate the numerical model.

1.3.2: Phase 2: Development and testing of 3D gypsum calcination models

1.3.2.1: Task 2.A: Development of a comprehensive 3D model

A three-dimensional computational model was developed following the mathematic formulation used in Phase 1, however, considering lateral heat and mass transfer. The model solved for the species transport equations and momentum equations in all three directions. The spatial gradients in heat flux and surface temperature were considered. The model was able to predict the depth of calcination in the entire compartment envelope even with the unsteady non-uniform heat flux from the fire. In addition to the source terms in the species transport equations, and energy equation as described in Phase 1, the gravity was accounted for using a source term in the y-momentum equation.

1.3.2.2: Task 2.B: Experiments with controlled variables

Due to the turbulent combustion, irregularities in the fuel, mixing, and reaction rates, most fires possess significant gradients in the temperature and local heat release rate. This leads to non-

uniform heat flux to the wall or gypsum board exposed to fire. There can be significant spatial gradients in temperature, rate of dehydration, and species concentration inside the gypsum board. The species transport of water vapor inside the gypsum board was not shown to be influenced by these lateral gradients. Precise gradients in heat flux were obtained by placing the gypsum board at different angles with a propane burner. By varying the distance and angle of inclination, different heat flux values and gradients in heat flux was obtained in both the lateral directions. Four heat flux gauges were used to ensure steady spatial gradients in heat flux and record them. The internal temperatures, depth of calcination, and the heat fluxes were measured.

1.3.2.3: Task 2.C: Comparing with the available full-scale compartment fire measurements

Verification of the developed correlations was completed through re-evaluating previous compartment fire tests conducted at EKU. Previously documented and published full-scale compartment fire tests performed at EKU for research into fire pattern reproducibility, usage, reliability, and persistence of fire patterns for fire investigation was re-evaluated. The fuel position, ignition time, surface temperature, and depth of calcination were measured. However, the heat flux or internal temperatures were not measured at the time of the original fire test. The experimental conditions were simulated numerically using Fire Dynamics Simulator (FDS) and the heat flux data was used to predict the depth of calcination using the developed model. The predicted depth of calcination was compared to the measured depth of calcination for selected cases. This assisted in analyzing the reliability of the correlation and trends in the predicted depth measurements. The correlations compared well with the FDS identified heat fluxes and the actual depth measurements taken at the time of the experiment.

1.3.2.4: Task 2.D: Verification and validation of the 3D model

The numerical predictions from the comprehensive 3D unsteady model (from Task 2.A.) were compared with the experimental measurements with non-uniform heat flux with controlled spatial gradients and duration of exposure (from Task 2.B.). Temperature profiles inside the gypsum board and depth of calcination at all locations was used for validation.

1.3.2.5: Task 2.E: Development of correlations

Verification of the developed correlations was completed by re-evaluating previous compartment fire tests conducted at EKU. A user-friendly application was developed that would help the fire investigators predict the depth of calcination based on either the heat fluxes to the gypsum board or the temperatures. The correlation is a simple calculation allowing investigators to input depth measurements to predict heat flux exposed to this area of the wall surface.

1.4: Expected applicability of the research

Currently, there is no guidance in any authoritative treatise on how to address the uncertainty and reliability related to comparing depth of calcination with characteristics of fire dynamics. Developing new correlations between fire history and depth of calcination will assist in standardizing the interpretation of damage. It is expected that the correlations and criteria developed from this study will provide the fire investigator with a better method to interpreting the measured depth of calcination and determining the fire dynamics that caused the damage.

2. PARTICIPANTS & OTHER COLLABORATING ORGANIZATIONS

2.1: Participants

Project Director

Shijin P. Kozhumal, Ph.D.

Co-Project Directors

Gregory E. Gorbett, Ph.D.

Hayri Sezer, Ph.D.

Investigator/Lab Coordinator

Trevor Borth

Graduate Students

Taylor Edwards

Muhammad Hasnain

Shehzad Kahn

Tejaswini Nallamothu

Jaclyn Nuckels

Vyshnavi Moparthi

Venkatesh Vankayalapati

Undergraduate Students

Ethan Fowlie

Carter Geist

Christopher Heavren

Molly Morrow

Rylan Paye

Sophia Sulzer

External Reviewer

Daniel Gottuk, Ph.D.

2.2: Collaborating organizations

Eastern Kentucky University (Primary applicant)

Georgia Southern University

3. OUTCOMES

3.1: Accomplishments

The major accomplishments from the project are,

1. Development and validation of a one-dimensional computational model for gypsum calcination.
2. Design, fabrication, and testing of a gas diffusion burner experimental setup.
3. TGA, DSC, and FTIR analysis of gypsum plasterboards under varying heating rates.
4. Development of a significantly improved chemistry model that accounts for variable heating rates.
5. Design, fabrication, and testing of a gas diffusion burner experimental setup and a radiant burner experimental setup for controlled non-uniform heat flux.
6. Experimental investigation of gypsum calcination when exposed to a gas diffusion burner.
7. Detailed sensitivity analysis of the parameters affecting gypsum calcination.
8. Development and validation of the three-dimensional computational model.
9. Online workshops/webinars engaging fire investigators.
10. Two stand alone applications, one for the prediction of depth of calcination and another for plotting the transients in temperature and water vapor density at certain locations inside the gypsum board.

A comprehensive one-dimensional unsteady computational model was developed to solve the mass, species, momentum, and energy conservation equations assuming local thermodynamic

equilibrium in the homogeneous porous material. The dehydration of the gypsum board, coupled with the heat and mass transport through it, was modeled. As the species transport inside the porous gypsum board is extremely difficult to measure experimentally, the transport of water vapor was analyzed numerically by considering the diffusion due to the concentration gradients, convection due to the pressure gradient, the water vapor generation during calcination, and its removal due to re-condensation. The internal temperature profile from the experiments was compared to the temperature profile predicted by the model.

An experimental setup was designed, fabricated, and tested with a diffusion burner and radiant panel. Validation tests and troubleshooting of the test apparatus construction were conducted. Experiments were conducted with different propane flow rates and the heat flux and internal temperature were measured. Experiments were also conducted with uniform heat fluxes from a radiant panel, as well as being modified for experiments with controlled non-uniform heat flux. Repeatability of the experimental measurements have also been analyzed. Water cooled heat flux gauges were used to measure the heat flux gradients. Internal temperatures and depth of calcination were also recorded.

Thermogravimetric Analysis (TGA), Differential Scanning Calorimetry (DSC), and Fourier-Transform Infrared Spectroscopy (FTIR) were performed to characterize the calcination of gypsum boards. The mass loss rate of commercially available gypsum boards was investigated in this study using TGA at various heating rates. The differences in the dehydration characteristics of different ages and types of gypsum boards were investigated.

A significantly improved chemistry model that accounts for variable heating rates was developed and added to the one-dimensional unsteady computational model which was developed prior to the reporting period. Thermogravimetric data, with a wide range of heating rates from 10 ^{o}C/min to 100 ^{o}C/min, were analyzed to develop Arrhenius type dehydration rate equations based on temperature, heating rate, and remaining water content. The one-dimensional computational model with the varying heating rate chemistry model is validated with experimental measurements of internal temperatures.

Detailed sensitivity analysis was carried for the one-dimensional gypsum calcination model. Sensitivity of the model output to the key properties and constants was assessed quantitatively. Both global and local sensitivity were estimated and reported.

A three-dimensional computational model based on a finite volume method was developed to predict the calcination of gypsum boards. The 3D gypsum calcination model solves for the species transport equations, momentum equations, and heat transfer in all three directions. The model can predict the depth of calcination in the entire compartment envelope even with the unsteady non-uniform heat flux from the fire. The 3D model was verified and validated against experimental measurements.

3.2: Results and findings

3.2.1: Summary of findings

The present study has investigated exposure of gypsum board to known heat fluxes over varying durations to evaluate the relationship between calcination depth measurements and its potential quantitative application to fire investigations. Controlled laboratory-scale experiments were

conducted with gypsum board exposed to a uniform heat flux. During this exposure, the internal temperature profile is recorded using an array of 12 thermocouples, placed at different depths inside the gypsum board, and the depth of calcination is measured. This process is repeated for several different heat fluxes from a radiant burner, a premixed burner, and a diffusion burner. The relationship between internal temperatures and depth of calcination was established. The effects of heat flux and the duration of exposure on the depth of calcination were analyzed. The radiant burner provided a more uniform heat flux. The diffusion and premixed burners mimicked fire scenarios better. Measurement uncertainty was evaluated throughout the experimental series and demonstrated graphically.

TGA, DSC, and FTIR Spectroscopy were performed to characterize the calcination of gypsum boards. For all types of commercially available gypsum boards, the TGA data demonstrated a clear dependency of heating rate on mass loss rate. Multiple non-linear dehydrations steps were identified and analyzed. The heat flow through the gypsum board was analyzed using DSC for different heating rates and the effective heat transfer coefficient was calculated. The stretching and bending vibrations of H_2O were analyzed using FTIR Spectroscopy during different stages of gypsum dehydration.

A comprehensive one-dimensional unsteady computational model was developed to solve the mass, species, momentum, and energy conservation equations assuming local thermodynamic equilibrium in the homogeneous porous material. The model helps to explore the phenomenon of gypsum calcination and systematically identify fire patterns. TGA data, with a wide range of heating rates from 10 ^{o}C/min to 100 ^{o}C/min, were analyzed to develop Arrhenius type dehydration

rate equations based on temperature, heating rate, and remaining water content. The model calculates the dehydration rates for each computational cell, for every iteration, based on the temperature and heating rate of the computational cell. Hence, the model can analyze situations when different parts of the gypsum boards are undergoing different heating rates which is very common when exposed to fire. The computational model was validated by comparing the predictions with experimental measurements of internal temperatures.

Comprehensive sensitivity study has provided significant qualitative insight into the dominant effects of the gypsum board calcination and dehydration process. It was shown through both derivative-based local sensitivity analysis, and variance-based global sensitivity analysis that the porosity and initial density are the dominant parameters.

A 3D computational model was developed to simulate the dehydration of gypsum board using the conservations of mass, species, momentum, and energy equations. The results of the 3D model are consistent with the 1D model in both cases of uniform and variable heat fluxes. The calcination of gypsum wallboards exposed to fire can be analyzed as a one-dimensional problem as the pressure and concentration gradients along the thickness of the gypsum board during calcination are significantly higher than the gradients along the other two directions.

Approximate correlations were developed connecting depth of calcination and incident heat flux, and duration of exposure based on numerical predictions and experimental measurements.

3.2.2: Experimental methods and Procedure

3.2.2.1: Radiant burner experiments

The experiments conducted in this study focused on controlling variables with focused temperature and heat flux measurements to better analyze the heat and mass transfer through the gypsum wallboard when exposed to uniform heat fluxes. Sections of gypsum boards 2-ft x 2-ft (0.61m x 0.61m) in size of ½-inch (12.7 mm) thickness were placed in a pre-built apparatus. The apparatus was a steel track with an affixed radiant burner (Dayton Model 3E462, commercial radiant heater) and a sliding steel frame that housed the gypsum board (Figure 2). Three trials were conducted for each heat flux value: 10 kW/m^2, 20 kW/m^2, and 30 kW/m^2. An array of 12 type-K thermocouples (Omega Engineering GG-K-20-SLE) placed through the ambient-side progressing at 1mm depth increments starting from 1mm from the surface exposed to the heat flux to the backside of the surface (12mm) and at the surface of the gypsum (fire-side) (Figure 3 and Figure 4). A cold-water heat flux gauge (Medtherm model 64, rated for up to 50 kW/m^2) was placed at the surface of the gypsum board (fire-side). While under constant exposure from the heat source, depth of calcination measurements were taken using a spring-loaded, digital depth probe developed at EKU (Figure 2 and Figure 3). The design and resultant pressure for the depth probe are consistent with previous research by Mealy et. al (Mealy, Wolfe, & Gottuk, 2013). These depth measurements were taken and recorded every minute up to 30 minutes or until the calcination measurement exceeded the full thickness of the gypsum board (12.7 mm).

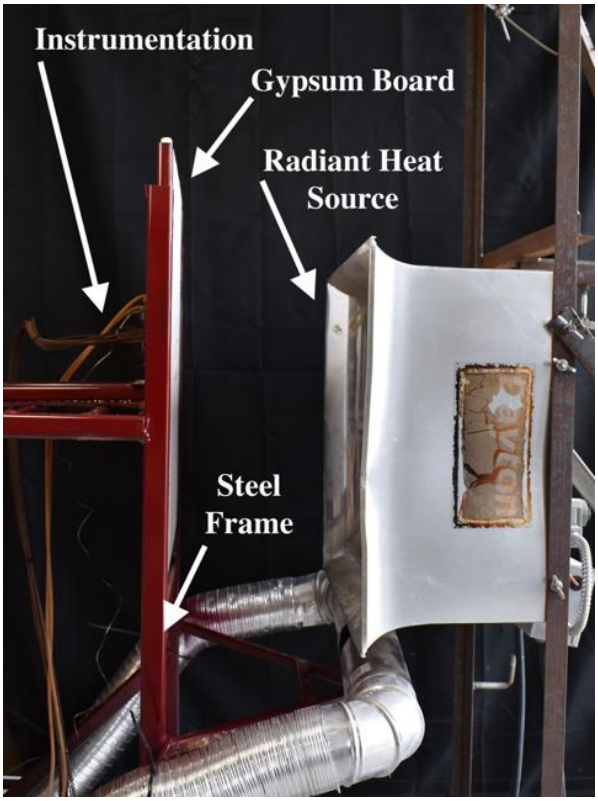

Figure 2: Experimental setup (annotated photograph).

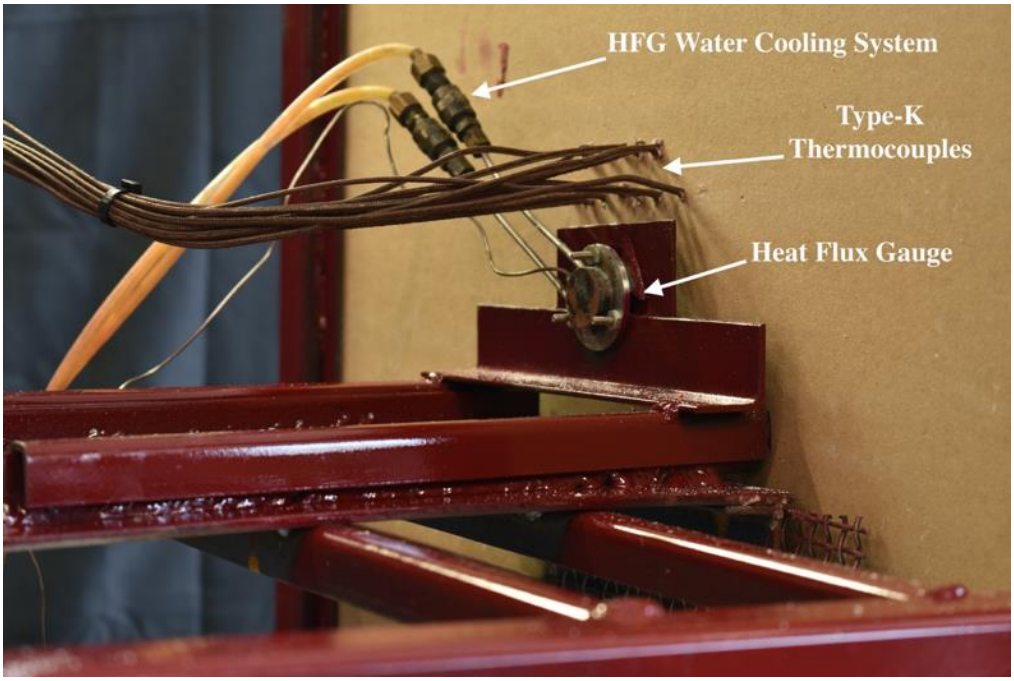

Figure 3: Experimental setup – Close-up photograph of experiment instrumentation.

Validation tests were conducted to determine the placement of thermocouples and where the depth measurements should be taken to best match the radiant heat flux measurements. Three tests per heat flux were completed to assure repeatability and validation. The validation tests revealed that the most consistent temperatures were found within a 12-inch wide by 6-inch high area near-center of the wallboard. The heat flux gauge was placed in the center of this area and the thermocouples in proximity (<4 inches). This is the location where all depth measurements were taken and where the thermocouples were located for each test (Figure 3). Furthermore, before each trial the heat flux gauge was tested to maintain the proper heat flux average (+/- 1 kW/m^2), propane tanks were adequately filled and the thermocouples were tested for general functionality. No other variables were changed and consistent conditions were preserved.

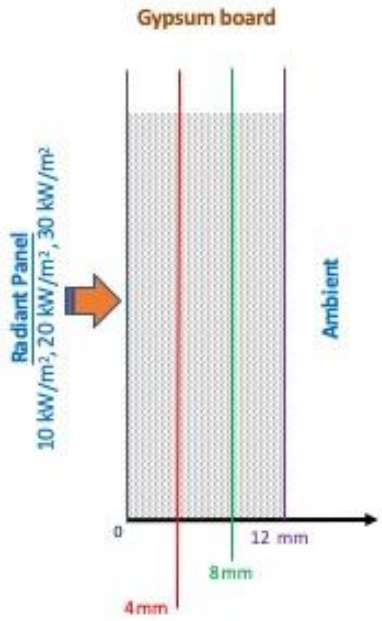

Figure 4: Experimental setup – Illustration of the drywall cross-section of drywall.

Three separate experiments were conducted at heat fluxes of 10 kW/m^2, 20 kW/m^2, and 30 kW/m^2. During the exposure to 10 kW/m^2, 20 kW/m^2, and 30 kW/m^2, the board remained at the same distance during the entirety of its exposure.

3.2.2.2: Premixed burner experiments

A series of experiments were conducted using a premixed propane torch (Harris Products model KH825-03) to provide high heat fluxes: ~100+ kw/m^2. Due to the high heat fluxes involved it was determined that introducing the depth probe to direct flame impingement would be detrimental to both the researcher and the instrument, so an alternate method of collecting temperature, heat flux, and calcination depth data was devised. A sample would be instrumented with a radiometer and exposed to direct impingement for one minute. The sample would be probed for depth and then replaced with a fresh sample. The sample would be heated for 2 minutes and tested, followed by 3 minutes, 4 minutes and so on until the gypsum calcination caused the probe to penetrate the entire thickness (blow-through). This entire process was repeated two more times. Then a fresh sample would be fully instrumented with thermocouples and a radiometer as described in the diffusion burner section and subjected to the full duration of heating that caused the blow-through. The data from these experiments are combined and are treated analytically as a single result. Three trials each of 50 kw/m^2, 60 kw/m^2, 70 kw/m^2, 80 kw/m^2, 100 kw/m^2, and 140 kw/m^2 were conducted, with 9 trials at 90 kw/m^2, conducted to perform a sensitivity analysis.

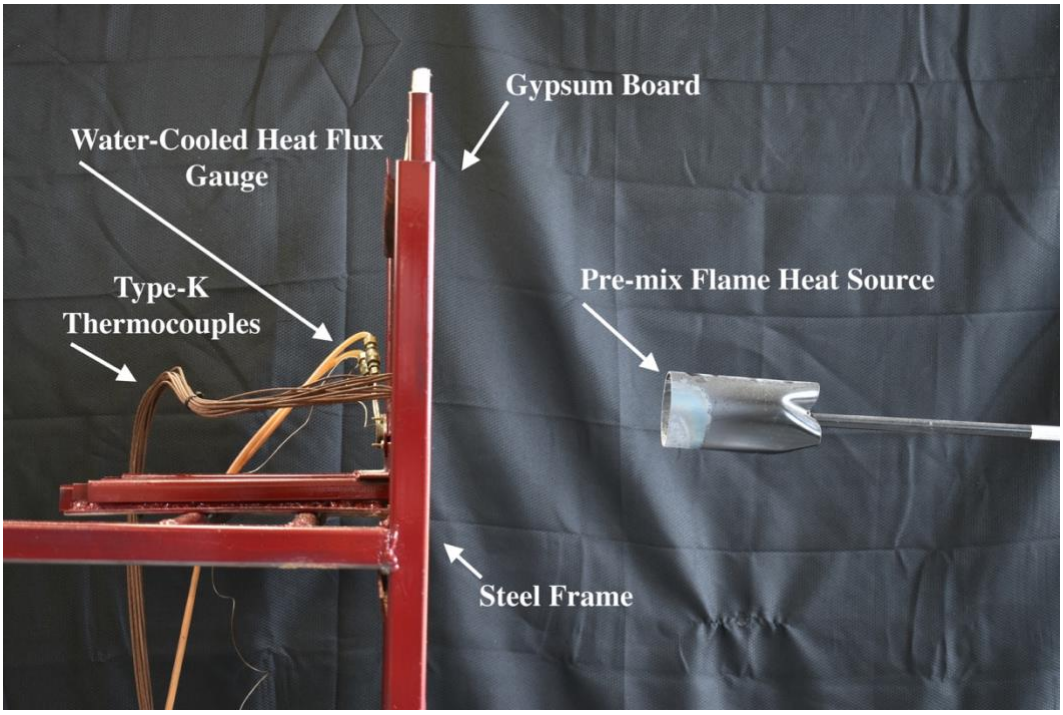

Figure 5: Annotated photograph of the experimental set up of a premix flame trial

3.2.2.3: Diffusion burner experiments

The test apparatus was constructed of commercially available 2x4 lumber, separated into the burner section and the testing section. The sections are vertically isolated from each other with a layer of high-density ceramic fiber board. The burner section houses the diffusion burner itself and the mass flow controller. The diffusion burner is 30cm x 30cm (11.8" x 11.8") in size and controlled with an Omega digital mass flow controller beginning at 10 L/min and increases to 40 L/min. The burner is constructed of 14-ga mild steel, welded along all seams with a penetration for gas introduction approximately 2 inches from the bottom. Ceramic wool, sandwiched between stainless steel wire mesh was used as the diffusing barrier. The test section measures approximately 0.914 m x 1.22m x 1.22m (3' x 4' x 4') in size (Figure 6 and Figure 7) with an open top. The rear wall of the apparatus is lined with the test specimen, a 1.22m x 1.22m (4' x 4') section of gypsum wallboard. The side and front walls of the apparatus are lined with 22 gauge perforated galvanized

steel mesh with a 40% open area due to the 0.318cm (0.125”) openings. The metal mesh was added as a diffuser to mitigate the influences of environmental airflow on the plume. A radiometer is mounted along the centerline of the test specimen approximately 40.64cm (16”) above the floor of the apparatus. The array of thermocouples is mounted into the gypsum wallboard from the rear of the test specimen approximately 40.64-50.8cm (16-20”) above the floor of the apparatus near in a 10cm grid near the radiometer (Figure 6 and Figure 7). A door is provided to allow access to the specimen for depth probing.

Figure 6: Test apparatus constructed for the diffusion burner tests

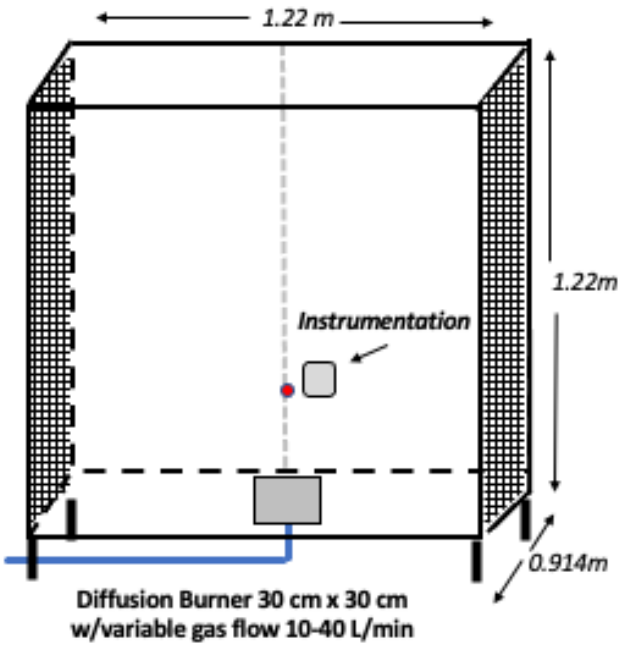

Figure 7: Schematic of diffusion burner test apparatus

Validation tests of the design were conducted for reproducibility purposes. The validation tests measured temperature values along the center line of the burner at 10 cm vertical intervals, and in two parallel columns 10 cm to the left and the right of the centerline. The thermocouple measurements were averaged by position and arrayed in a plane graph. The area of highest consistent temperature was 20CM to 40CM from the base of the flame at the centerline. Figure 4 indicates that the best height for radiometer placement and the thermocouple array for testing is 40cm (16”). The area from 30-40cm and within 10cm of the centerline was determined to be the best location for conducting depth of calcination measurements primarily due to the consistency of temperature and the visual location of the flame during this examination. When the burner is increased through the projected flow ranges, this area was consistently within the steady plume exposure instead of within the intermittent upper region of the fire plume.

Instrumentation in the testing area included a Medtherm series 64 radiometer located 40cm from the bottom of the specimen. Temperature was measured at +1cm from the surface, the surface

temperature (depth 0) and then by 1mm increments through the specimen using Omega Engineering GG-K-20-SLE K-type thermocouples. Test depths were penetrated from the back of the board using probes calibrated to specific depths for consistent depth placement. Depth measurements were taken every 60 seconds using a spring-tensioned digital depth probe by reaching the protected probe directly into the testing area and taking a measurement during direct flame impingement. A series of experiments were conducted: 8 experiments at 20 SLPM for testing and a sensitivity analysis, plus 4 trials each of 60, 80, and 120 SLPM.

3.2.2.2: TGA, DSC, and FTIR analysis

A TGA Q50 from TA Instruments was used to perform TGA measurements. The TGA instrument can be seen in Figure *8*. The mass loss measurements were performed with new samples and heating rates ranging from 10 $^oC/\ min$ up to 100 $^oC/\ min$ with a step size of 10 $^oC/\ min$. The TGA analysis was then performed on the 40-year-old sample, with heating rates of 10, 20, 50, 80, 90, and 100 $^oC/\ min$. In both the new and old gypsum board measurements, the temperature was carried up to approximately 950 ^oC.

Figure 8: TA Instruments TGA Q50 device utilized to perform Thermogravimetric Analysis.

The DSC analysis was performed using the TA Instruments DSC250 device shown in Figure *9* . The DSC measurements were performed at three different heating rates (20, 50, and 100 $^{o}C/\ min$) and were carried out to 250 ^{o}C to ensure coverage of the peak energy absorption. From the DSC measurements, we examined the specific energy absorption of the gypsum board.

Figure 9: TA Instruments DSC250 device utilized to perform Differential Scanning Calorimetry.

To perform FTIR spectroscopy, a Thermofisher Scientific Nicolet iS10 device was used, with a Smart iTX accessory; shown in Figure *10*. The FTIR spectroscopy was performed for wavelengths ranging from 16 μm to 251 μm (corresponding to approximate wavenumbers of 4000 cm^{-1} and 250 cm^{-1}). FTIR data was initially collected for a gypsum board sample exposed to a uniform heat flux, with 4/5 of the layers being analyzed for H_2O bending and stretching, where layer 1 was directly exposed to the flame, and layer 5 was on the ambient side of the gypsum.

Figure 10: Thermo Scientific Nicolet iS10 FTIR device with Smart iTX accessory.

3.2.3: Experimental results

3.2.3.1: Experiments with radiant burner

Internal temperatures were measured using the embedded thermocouple array. Comparison and analysis of these internal temperature profiles are critical, since temperature is one of the driving factors of gypsum calcination (Kozhumal, Hicks, & Sezer, 2019) (Ang & Wang, 2004).

Measured time histories of temperature, at different depths inside the gypsum board, when exposed to 10 kW/m^2 is shown in Figure 4. Temperatures on the surface of the gypsum board exposed to the heat flux, are also shown. In the presence of 10 kW/m^2 heat flux, the surface temperature reaches a value of around 300 ^{o}C. As the surface is heated up, the gypsum board dehydrates and the heat transfer from the surface exposed to the heat flux to the inside of the gypsum board causes the internal temperatures to increase. As the heat flux is relatively small, the rate of heat transfer

is relatively slow with temperatures reaching a nearly steady state after around 33 minutes (*Figure 11*). The gas-phase temperature, on the exposed gypsum board surface, is higher than that of the porous gypsum board.

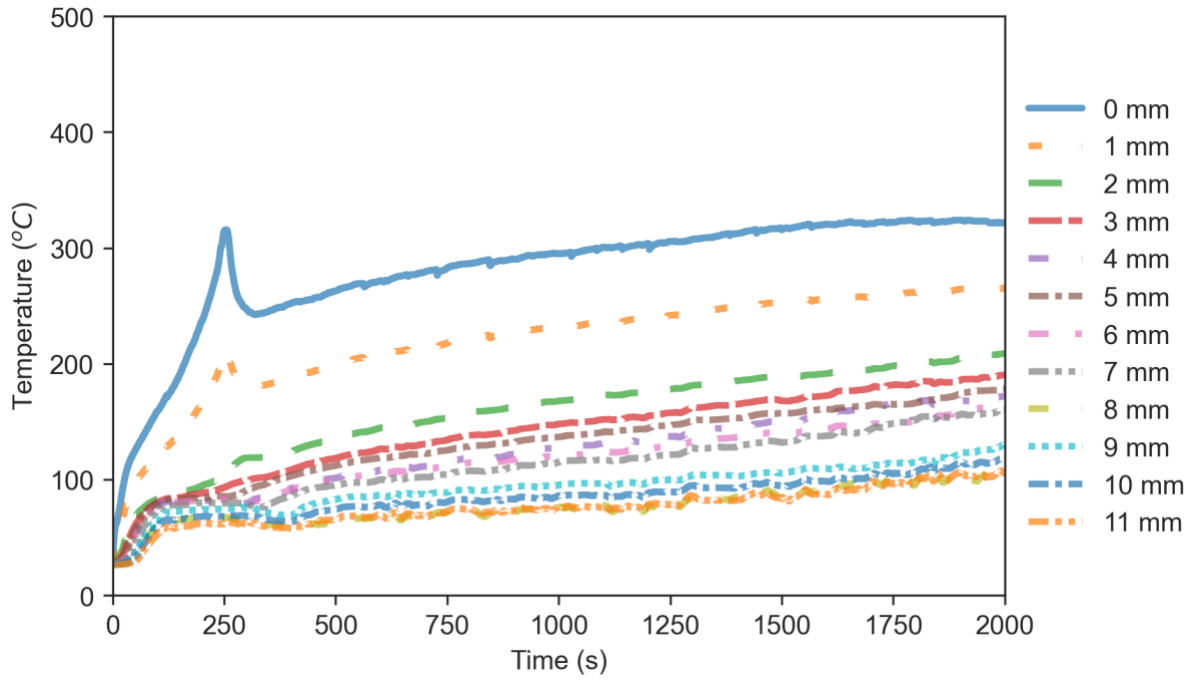

Figure 11: Time histories of temperature at different depths inside the gypsum board when exposed to a uniform heat flux of 10 kW/m^2 from the radiant burner. The depth is measured from the side exposed to the heat source. Depth = 0mm represents gas-phase temperature on the surface of the exposed side.

When the heat flux is increased to 20 kW/m^2, the surface temperature increased to around 400 °C. Steady state temperatures internally begin to occur around 30 minutes (*Figure 12*). Finally, when the heat flux is increased to 30 kW/m^2, the surface temperature increased to around 450 °C. With the increased heat flux of 30 kW/m^2, the temperatures reach a nearly steady state in approximately 25 minutes of exposure (*Figure 13*). In all three series of tests there are significant periodic oscillations observed in the history of surface temperatures. This is most likely due to the

unsteadiness in the gas-phase caused by the movement of hot gasses driven by buoyancy. The internal temperatures for the higher heat fluxes are also observed to be higher when compared to the case with 10 kW/m^2 heat flux. A clear spike in temperatures near the side exposed to the heat source is observed for the 10 kW/m^2, 20 kW/m^2, and 30 kW/m^2 experiments around similar temperatures. The commercial gypsum boards used in the study have thin paper layers. The spike in temperature is most likely related to the endothermic pyrolysis of the paper layer at the surface, the diffusion of hot gases produced during the pyrolysis into the gypsum board, and the burning of the thin paper layer.

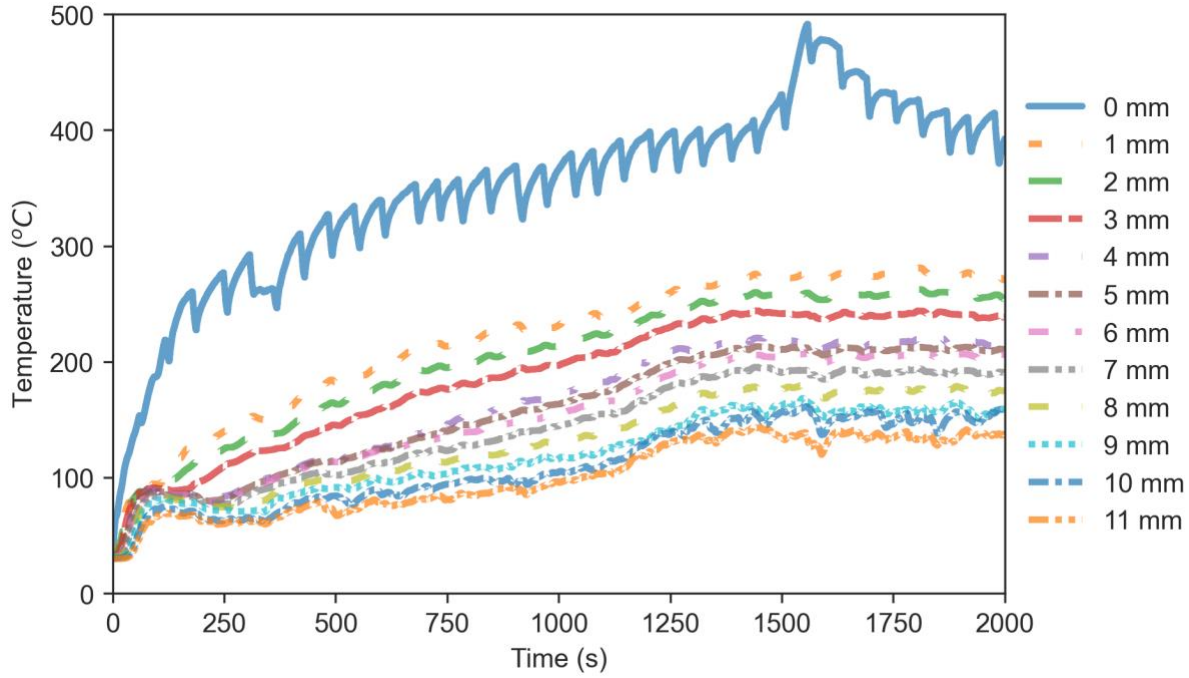

Figure 12: Time histories of temperature at different depths inside the gypsum board when exposed to a uniform heat flux of 20 kW/m^2 from the radiant burner. The depth is measured from the side exposed to the heat source. Depth = 0mm represents gas-phase temperature on the surface of the exposed side.

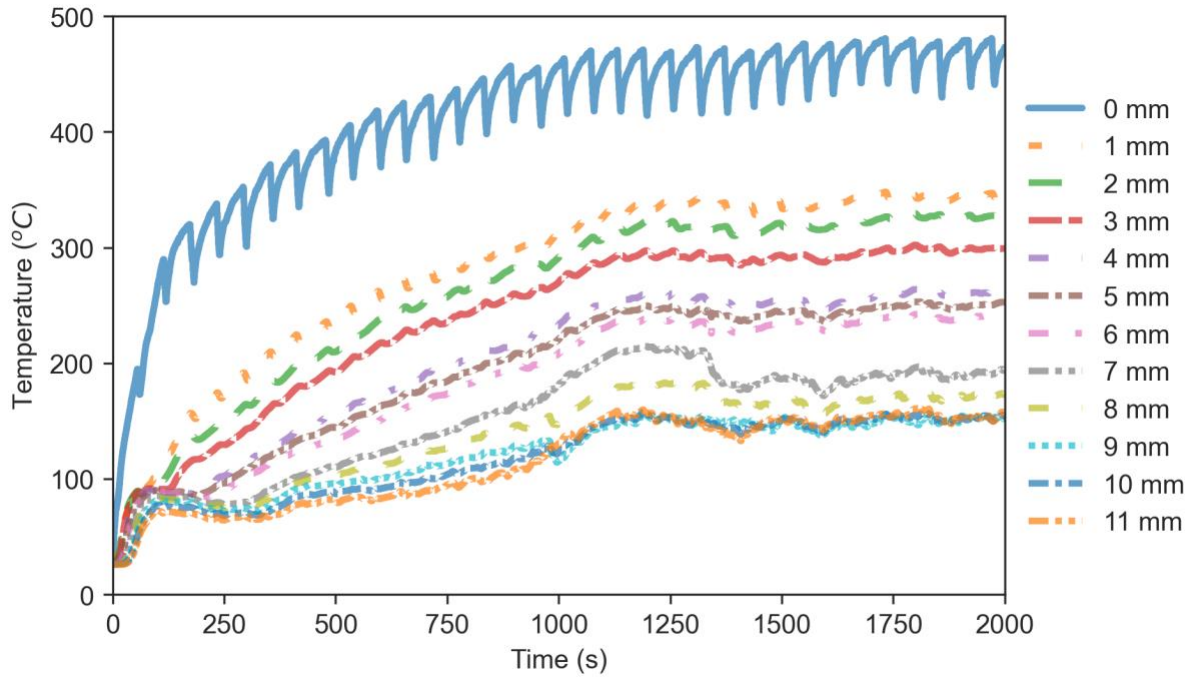

Figure 13: Time histories of temperature at different depths inside the gypsum board when exposed to a uniform heat flux of 30 kW/m^2 from the radiant burner. The depth is measured from the side exposed to the heat source. Depth = 0mm represents gas-phase temperature on the surface of the exposed side.

The internal temperatures for the higher heat fluxes are also observed to be higher when compared to the case with 10 kW/m^2 heat flux. A clear spike in temperatures near the side exposed to the heat source is observed for the 10 kW/m^2, 20 kW/m^2, and 30 kW/m^2 experiments around similar temperatures. The commercial gypsum boards used in the study have thin paper layers. The spike in temperature is most likely related to the endothermic pyrolysis of the paper layer at the surface, the diffusion of hot gases produced during the pyrolysis into the gypsum board, and the burning of the thin paper layer.

3.2.3.1.1: Depth of calcination: Radiant panel experiments

The depth of calcination measurements and their rate of change for all three heat fluxes and the various trials are analyzed graphically. The depth of calcination of the gypsum board is also recorded every minute of the experiment when exposed to each uniform heat flux. The measurements of the depth of calcination are superimposed with the internal temperatures to analyze their relationship (Figure *14*). The maximum depth of calcination is found to be between 5-6 mm for the case with 10 kW/m^2 heat flux, ~6 mm for the 20 kW/m^2 heat flux, and ~7mm for the case with 30 kW/m^2 heat flux. Mean depth values after a near steady state, after 10 minutes are found to be 4.1 mm, 4.65 mm, and 5.97 mm with heat fluxes 10, 20, 30 kW/m^2 respectively. As expected, the depth of calcination increases with an increase in heat flux. However, the relationship is found to be non-linear. Also, fluctuations are observed in the measurement of the depth of calcination. This is likely due to the local irregularities in the composition of the commercially available gypsum boards.

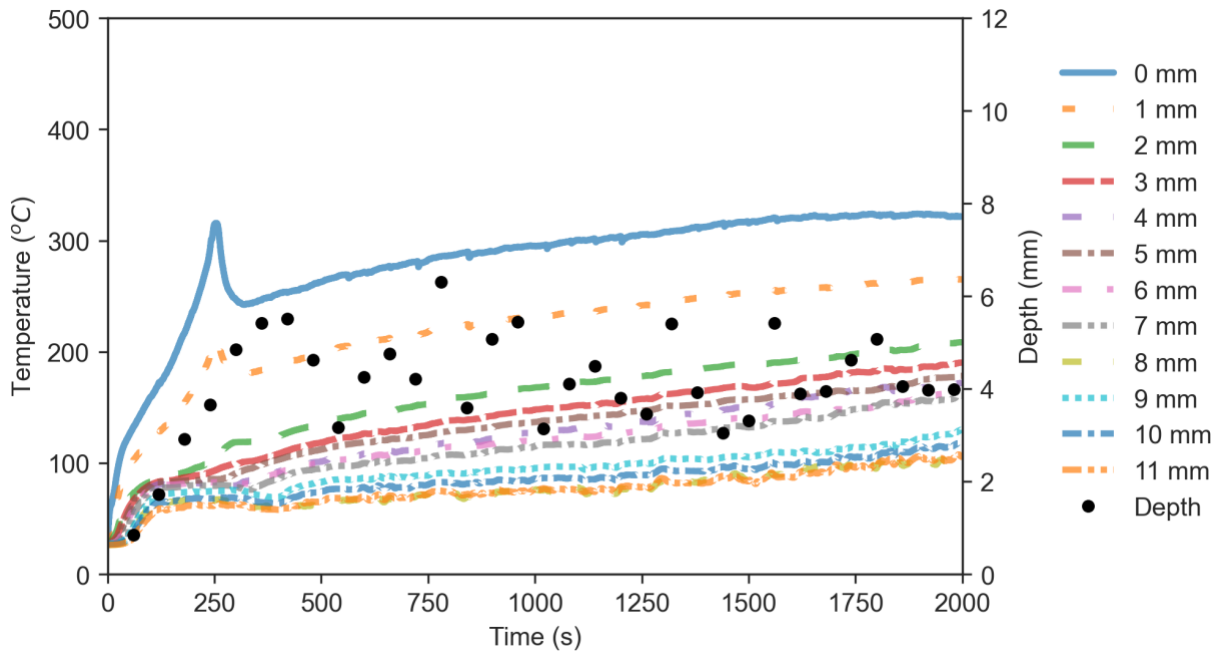

Figure 14: Temperatures at different depths inside the gypsum board with depth measurements superimposed when exposed to a uniform heat flux of 10 kW/m^2 from the radiant burner. The depth is measured from the side exposed to the heat source.

The rate of change of the measured depth of calcination is not constant over time. Small fluctuations could be due to the experimental uncertainties. As expected, the rate of change of the measured depth of calcination is highest at the higher heat fluxes. For 10 kW/m^2 and 30 kW/m^2, the measurements appear to plateau at a maximum value 4 mm for 10kW/m^2 and 6 mm for 30 kW/m^2. The 20 kW/m^2 measurements fluctuated between 4-6 mm. Taking the mean of the depth measurements for each uniform heat flux graphically demonstrates these differences (Figure *15*). The experimental measurements show the velocity of propagation of the dehydration front is highly non-linear as observed in the numerical predictions of Kozhumal et al. (Kozhumal, Hicks, & Sezer, 2019).

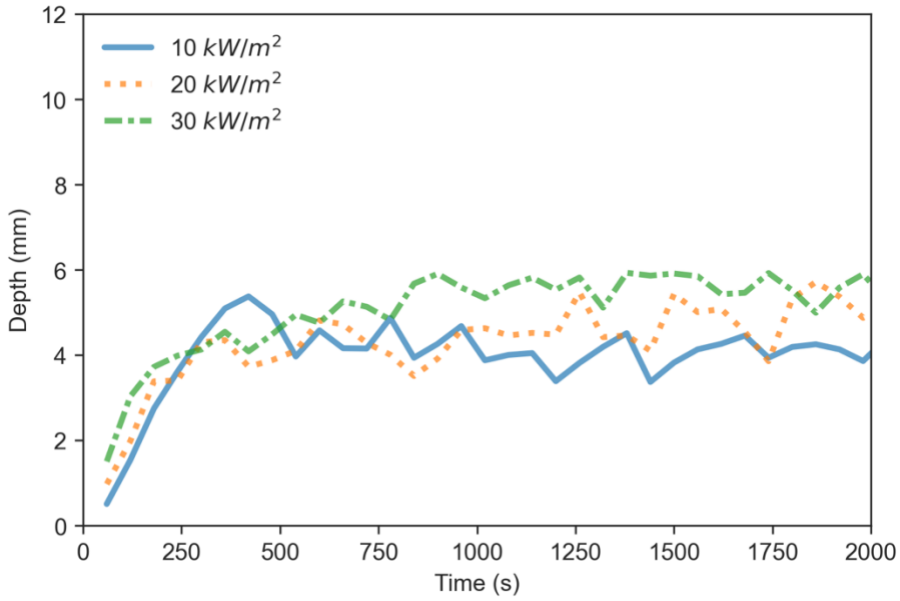

Figure 15: Comparison of mean of depth of calcination measurements when exposed to different uniform heat fluxes from 10 kW/m^2 to 30 kW/m^2. 12mm is completely through the gypsum board.

A different technique to view the data is to use contour plots to illustrate the internal temperatures (Figure *16*). The contour plots provide a better depiction of how the temperature profile moves internally through the gypsum board given the various heat fluxes and durations.

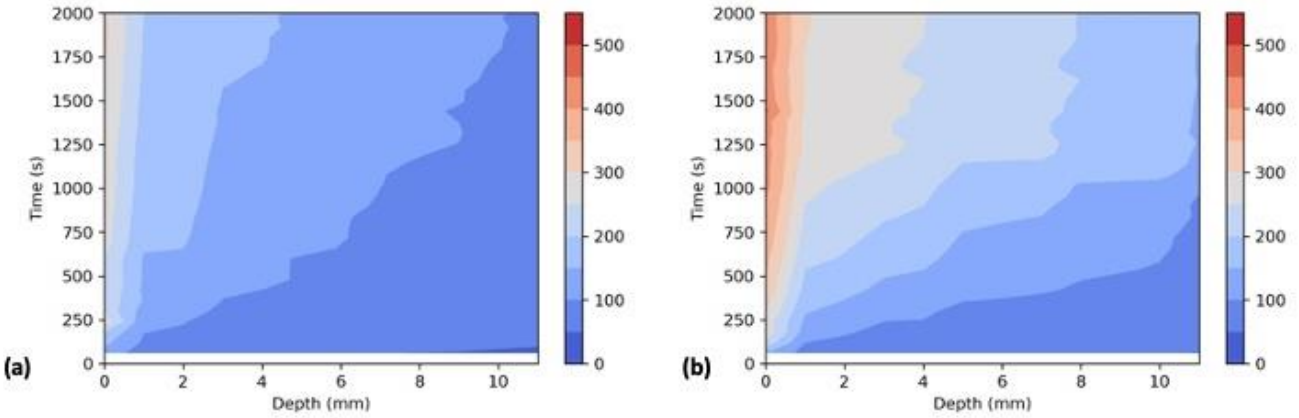

Figure 16: Contour plot of temperatures (°C) inside the gypsum board when exposed to a uniform heat flux from a radiant burner (a) 10 kW/m^2, (b) 30 kW/m^2.

3.2.3.1.2: Measurement uncertainty: Radiant panel experiments

Experimental work is always accompanied with measurement uncertainty. Mean temperatures for each thermocouple depth were determined and the uncertainty expressed as a standard deviation. The standard deviation for 10 kW/m^2 was approximately 10-15% after the initial spike in temperatures (Figures 15-16). The standard deviation for 20 kW/m^2 is approximately 5-15%. The standard deviation for 30 kW/m^2 was on the order of ~40%. The surface temperature had the greatest standard deviation for all three heat fluxes, most likely due to the pyrolysis and combustion of the surface paper.

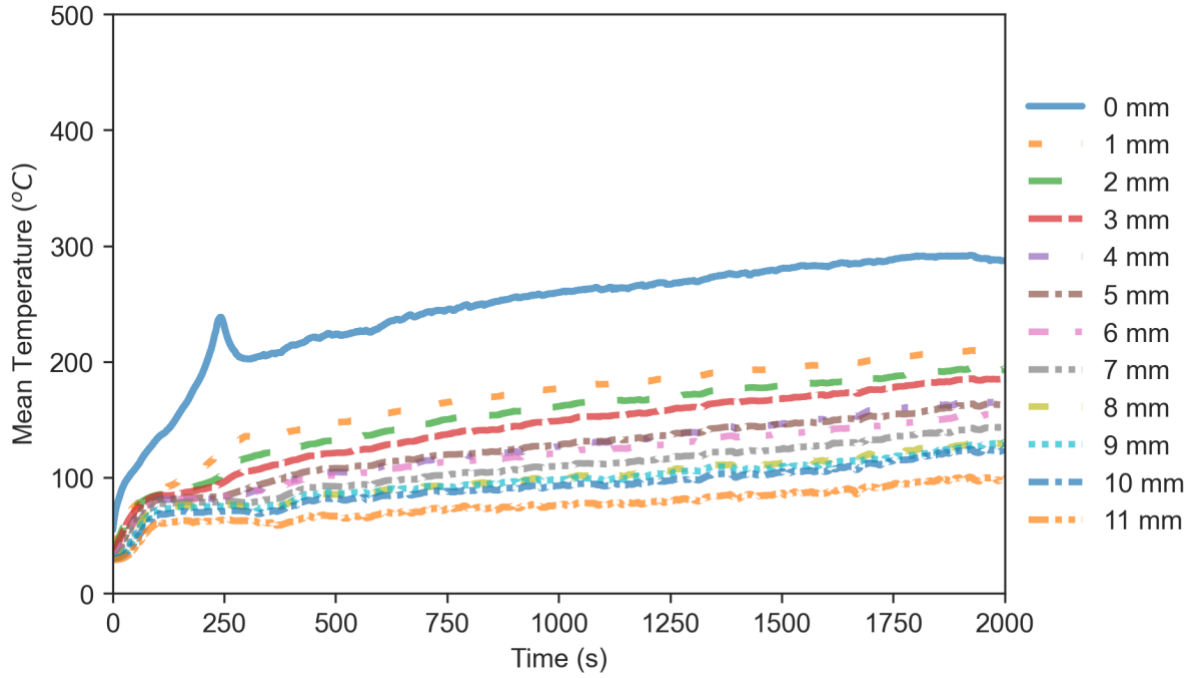

Figure 17: Mean temperatures at different depths inside the gypsum board when exposed to a uniform heat flux of 10 kW/m^2 from the radiant burner.

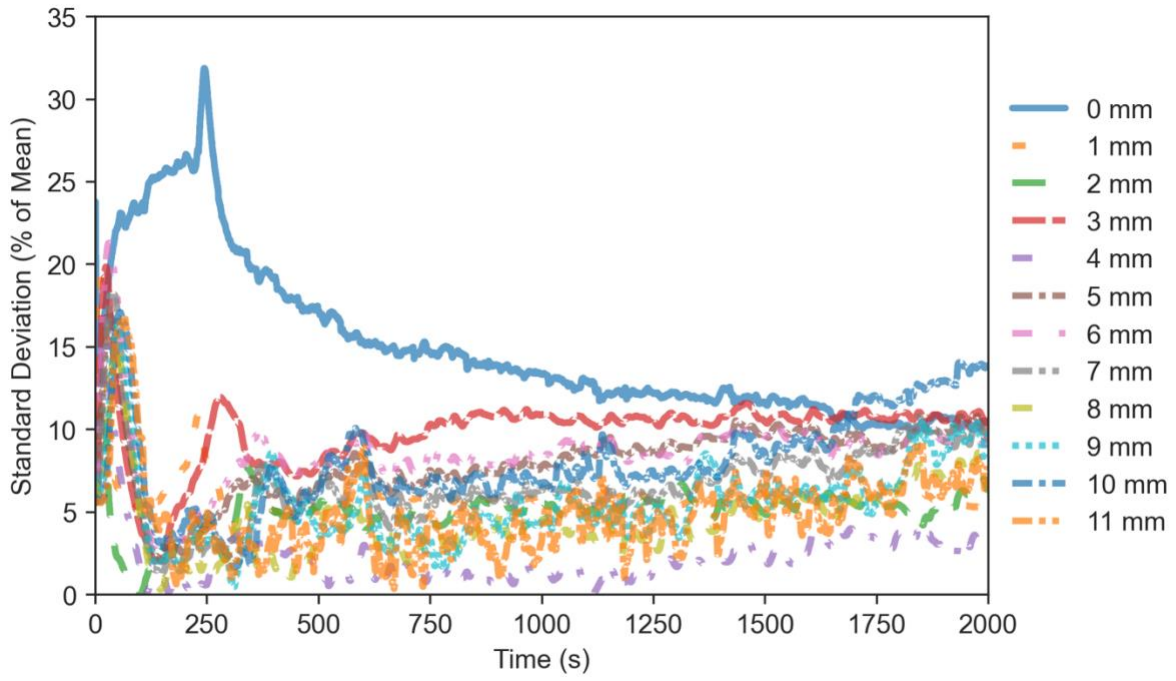

Figure 18: Percentage of the standard deviation for temperature measurement uncertainty when exposed to a uniform heat flux of 10 kW/m^2 from the radiant burner

3.2.3.1.3: Experimental Temperature at Depth of Calcination

As the calcination process is dictated by internal temperatures, analysis of the temperature of the dehydration front during gypsum calcination when exposed to different heat fluxes could help in understanding the process. However, direct experimental measurement of the temperature of the dehydration front is challenging inside the opaque and porous gypsum board. In the present study, the depth of calcination was measured every minute to track the history of the propagation of the dehydration front. However, this data has significant noise due to local irregularities in the gypsum board and experimental uncertainties (Figure *19* a). Hence, a suitable polynomial curve fit is used to reduce the fluctuations (Figure *19* and Figure *20*). The temperature at the location of the dehydration front, obtained from the depth of calcination measurement, was calculated using

interpolation of the temperature data on both sides of the location. This gives the temperature of the dehydration front for each minute during the gypsum calcination (Figure *19* and Figure *20*).

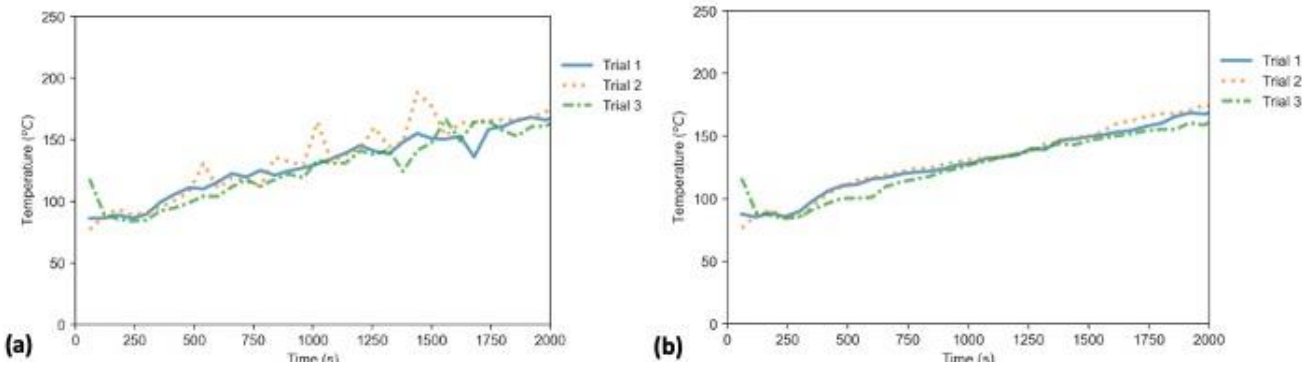

Figure 19: Temperature at the depth of calcination when exposed to a uniform heat flux of 10 kW/m^2 from the radiant burner, obtained using interpolation. (a) This graph demonstrates the data plotted for three trials before applying the polynomial curve fit for the depth measurements, (b) This graph demonstrates the data plotted for three trials after applying the polynomial curve fit for the depth measurements.

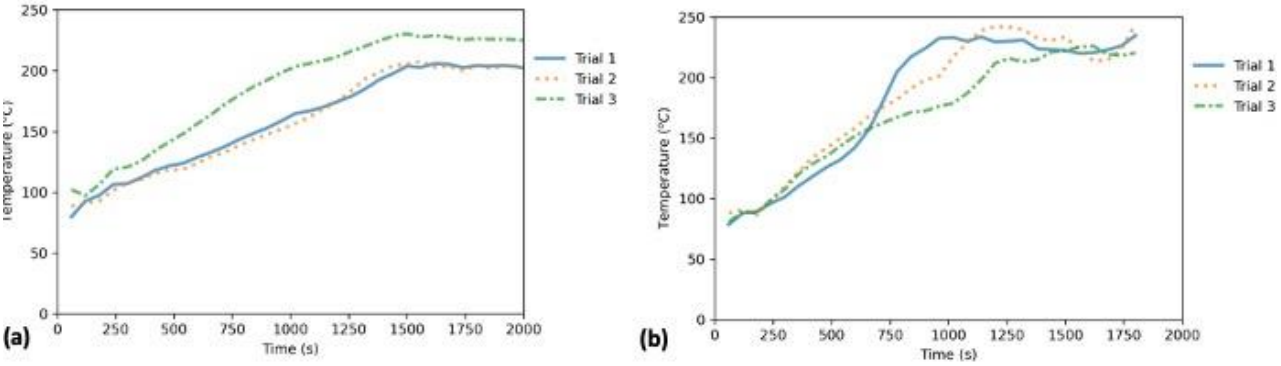

Figure 20: Temperature at the depth of calcination when exposed to a uniform heat flux of (a) 20 kW/m^2 from the radiant burner (b) 30 kW/m^2. This graph demonstrates the data plotted for three trials obtained using interpolation after applying the polynomial curve fit for the depth measurements.

At a low heat flux of 10 kW/m^2, the temperature at the depth of calcination reaches peaks around 160 ^{o}C. This increases to around 210 ^{o}C with a heat flux of 20 kW/m^2 and further increases to around 230 ^{o}C with 30 kW/m^2 heat flux. As the heat flux increases, the heating rate increases and the time available for a unit change in temperature decreases thereby requiring a higher temperature for the same degree of calcination. This is consistent with the thermogravimetric measurement of gypsum samples with constant (Wakili, Hugi, Wullschleger, & Frank, 2007) and varying heating rates (Section 3.2.3.4). This shows that gypsum calcination is dictated primarily by internal temperatures and heating rates. In the early stages, a thin paper layer present in commercially available gypsum boards gets ignited and this influences the depth of calcination and temperatures at and very close to the surface. Once, the board reaches a near steady state, even though the local heating rate approaches zero, the depth of calcination and the temperature at the location stays nearly the same. This causes the differences in the temperature at the depth of calcination with different heat fluxes after reaching near steady state even though the heating rate is not different afterward. However, as the parts of the board get preheated before it gets sufficiently calcinated, the history of the heat flux and duration of exposure could also influence the temperature at the depth of calcination. This shows the depth of calcination depends on the internal temperatures, heating rates, and the history of heating.

Experiments were also carried out with controlled non-uniform heat flux from the radiant burner to investigate any three-dimensional effects. However, the effect of the three-dimensionality of gypsum calcination was found to be well within the experimental uncertainties. Hence, the effect of three-dimensionality was only studied numerically, and the findings are reported in Section 3.2.6.4.

3.2.3.2: Experiments with premixed burner

Even though radiant burners can reliably produce uniform heat flux, it is challenging to produce high heat fluxes from radiant burners. Premixed burners were used to achieve high heat fluxes in a more reliable and safer manner. The temperatures and the depth of calcination are measured like the experiments with the radiant burner. Measured time histories of temperature at different depths inside the gypsum board when exposed to different uniform heat fluxes.

Mean temperatures for each thermocouple depth were determined for 90 kW/m^2 heat flux (Figure 21) and the uncertainty expressed as a standard deviation (*Figure 22*). The standard deviation for 90 kW/m^2 was comparable to the measurement itself during the early stages and reduces to around 30% of the mean values after a minute.

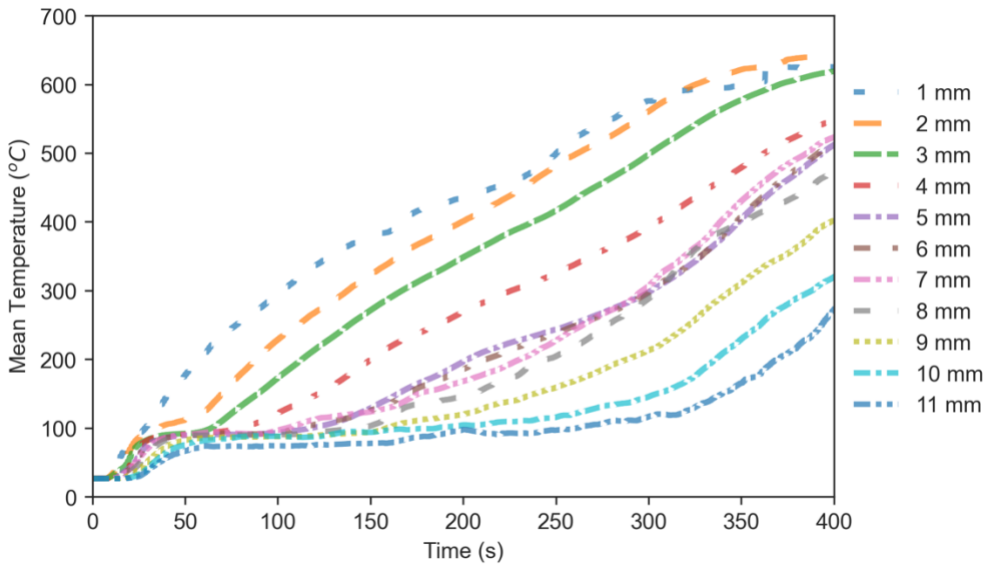

Figure 21: Time histories of temperature at different depths inside the gypsum board when exposed to a uniform heat flux of 90 kW/m^2 from the premixed burner. The depth is measured from the side exposed to the heat source.

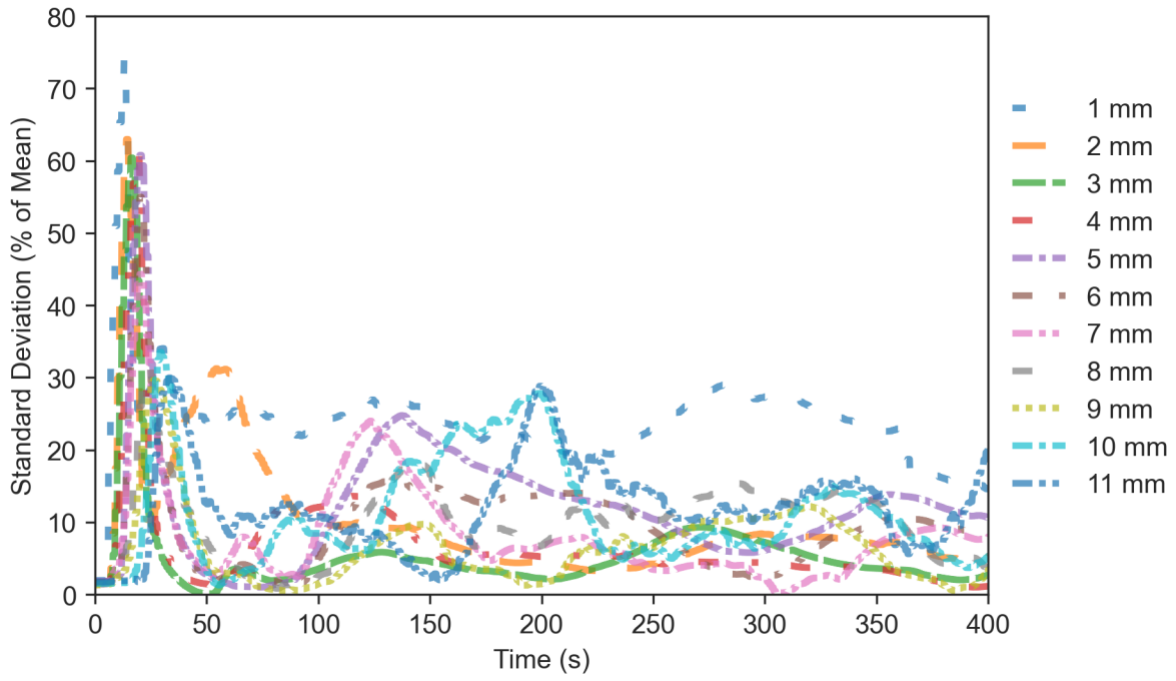

Figure 22: Percentage of the mean for measurement uncertainty when exposed to a uniform heat flux of 90 kW/m^2 from the premixed burner

Even though such high heat fluxes are observed during compartment fires, they lead to the entire gypsum board getting calcinated within a few minutes (Figure 31). Because of this, measurement of the depth of calcination might not provide much useful additional information to the fire investigators.

The depth of calcination of the gypsum board is also recorded every minute of the experiment when exposed to each uniform heat flux from the premixed burner. The measurements of the depth of calcination are compared for different heat fluxes (Figure 23). The entire gypsum board gets calcinated under these high heat fluxes. However, the duration of exposure needed for the gypsum board to dehydrate varies with the heat flux applied. Significant fluctuations are observed in the

measurement of depth of calcination. This is likely due to the local irregularities in the composition of the commercially available gypsum board. Certain outliers are also noted in the measurements.

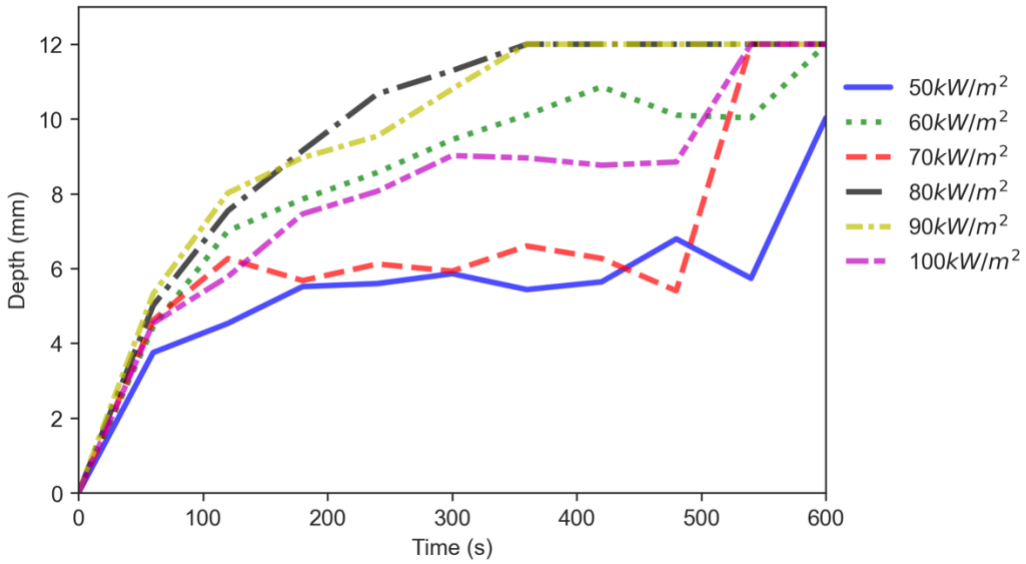

Figure 23: Comparison of depth of calcination measurements when exposed to different uniform heat fluxes from 50 kW/m^2 to 100 kW/m^2 using the premixed burner. 12mm is completely through the gypsum board.

3.2.3.3: Experiments with diffusion burner

3.2.3.3.1 Temperature measurements

Measured time histories of temperature, at different depths inside the gypsum board, when exposed to flames from the diffusion burner with propane flow rates of 60 SLPM, 80 SLPM, and 120 SLPM have been shown in Figure 24, Figure 25, and Figure 26 respectively. As it is very difficult to control the heat flux to a point from the turbulent flame, multiple experiments were conducted. With 60 SLPM flowrate, the surface temperature reaches a value of around 225 ^{o}C. As the surface heats up, the gypsum board dehydrates and the heat transfer from the exposed surface to the inside of the gypsum board causes the internal temperatures to increase. Significant fluctuations are

observed in the history of surface temperature and internal temperatures due to the highly turbulent flame.

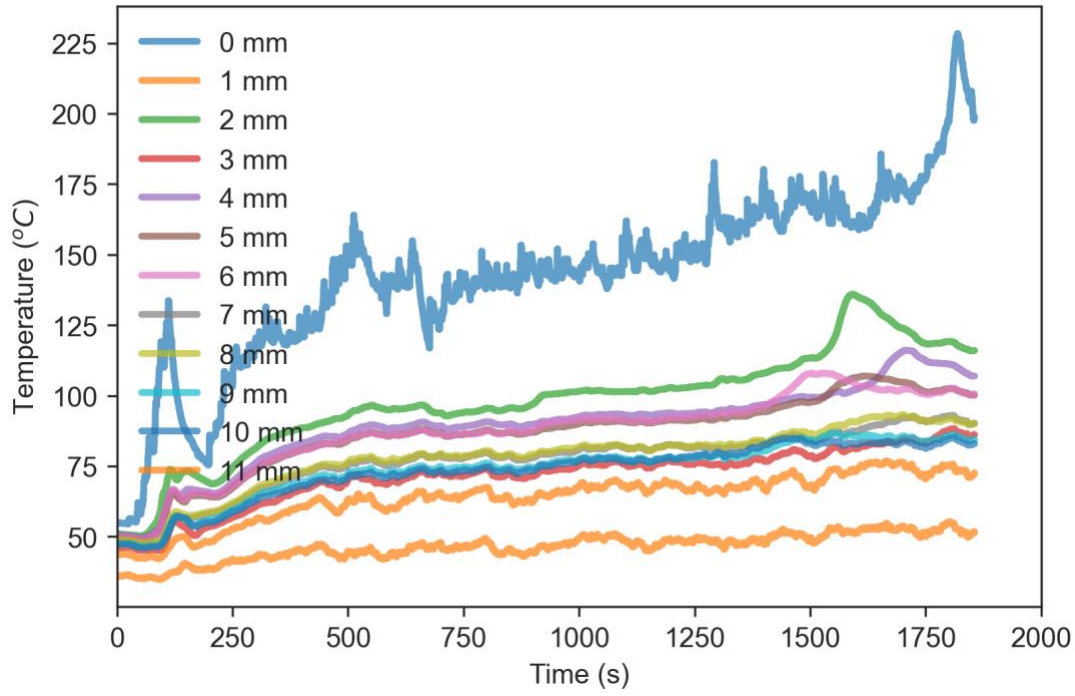

Figure 24: Time histories of temperature at different depths inside the gypsum board when exposed to flames from the diffusion burner with a flow rate of 60 SLPM. The depth is measured from the side exposed to the heat source.

When the flow rate is increased to 80 SLPM, the peak surface temperature is slightly increased to approximately 250 °C with fluctuations observed in the history of temperatures. This could be due to the unsteadiness and randomness associated with the turbulent flame. The internal temperatures are also observed to be slightly higher when compared to the case with 60 SLPM flow rate.

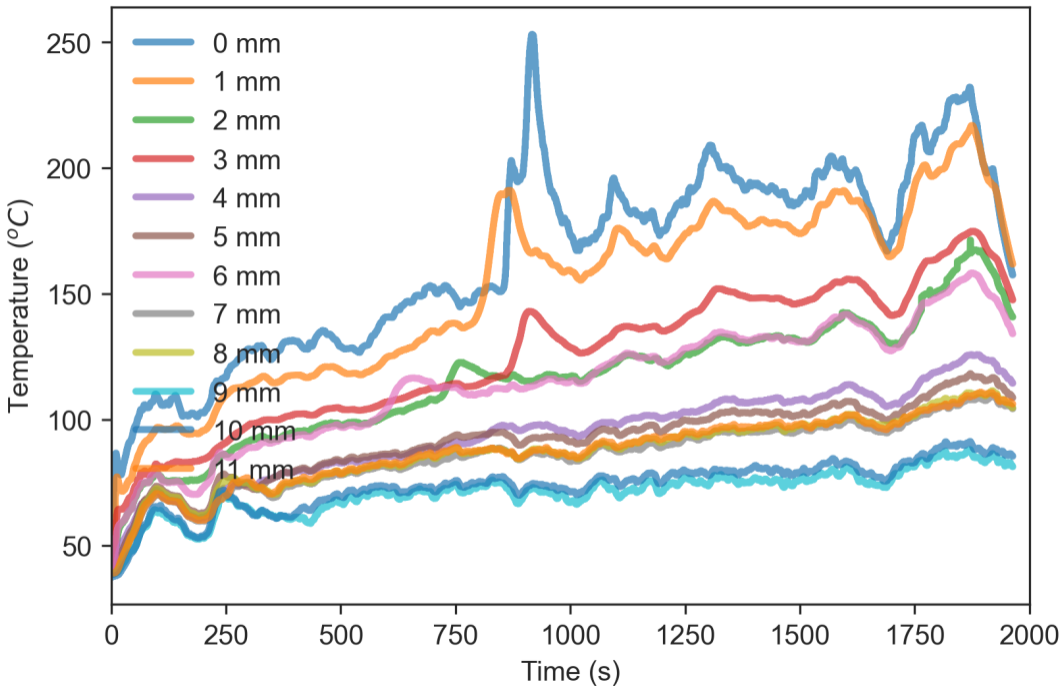

Figure 25: Time histories of temperature at different depths inside the gypsum board when exposed to flames from the diffusion burner with a flow rate of 80 SLPM. The depth is measured from the side exposed to the heat source.

When the flow rate is further increased to 120 SLPM, the surface temperature increased to approximately 440 °C. More fluctuations are observed in the surface temperature than the internal temperatures. This could be due to the increased response time inside the gypsum board and the endothermic dehydration of the gypsum board.

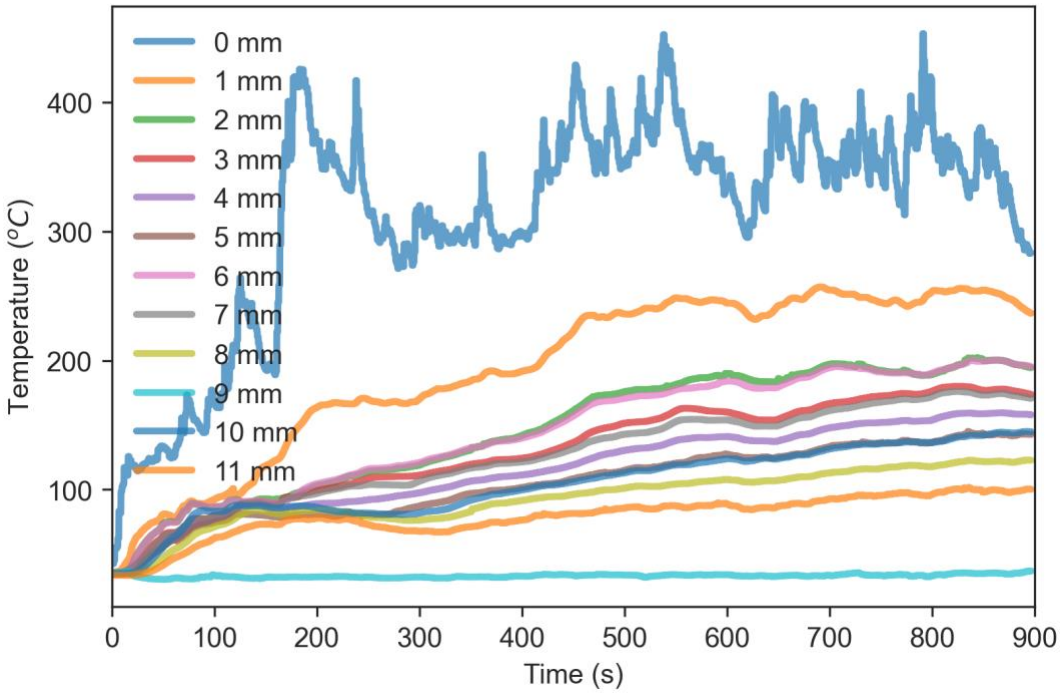

Figure 26: Time histories of temperature at different depths inside the gypsum board when exposed to flames from the diffusion burner with a flow rate of 120 SLPM. The depth is measured from the side exposed to the heat source.

3.2.3.2.2: Depth of calcination measurements

The depth of calcination of the gypsum board was also recorded every minute of the experiment for each flow rate. The measurements of the depth of calcination are compared for repeat trials for each flow rate. The depth of calcination recorded during the experiments with propane flow rates of 60 SLPM, 80 SLPM, and 120 SLPM are shown in Figure 27, Figure 28, and Figure 29 respectively.

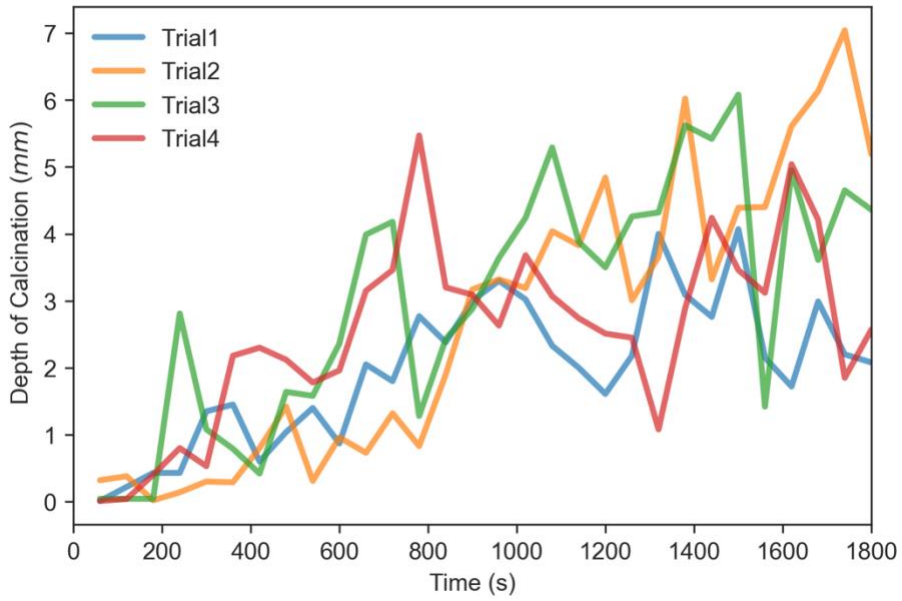

Figure 27: Comparison of the depth of calcination measurements when exposed to flames from the diffusion burner with a flow rate of 60 SLPM. 12mm is completely through the gypsum board.

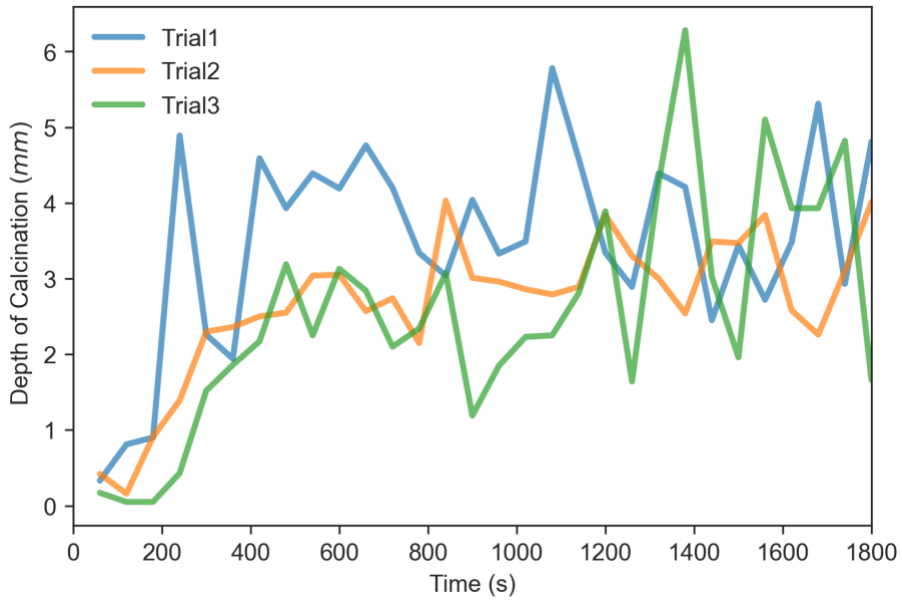

Figure 28: Comparison of the depth of calcination measurements when exposed to flames from the diffusion burner with a flow rate of 80 SLPM. 12mm is completely through the gypsum board.

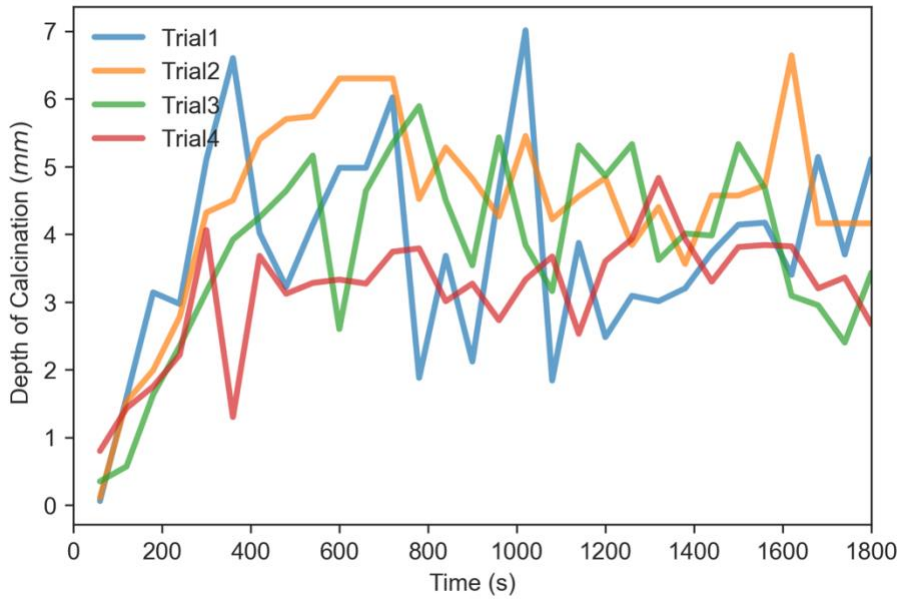

Figure 29: Comparison of the depth of calcination measurements when exposed to flames from the diffusion burner with a flow rate of 120 SLPM. 12mm is completely through the gypsum board.

Fluctuations are observed in the measurement of the depth of calcination even for repeat experiments conducted at identical conditions. This is primarily due to the randomness of turbulent flames. Possible local irregularities in the composition of the commercially available gypsum boards and experimental uncertainties might also play a role.

Even though it would be difficult to arrive at reliable correlations based on the results from the diffusion burner experiments, these experiments more closely represent realistic fires than controlled heat flux from radiant burners. The time histories of heat flux recorded from the experiments was used as a boundary condition for the numerical model. The experimental measurements of the internal temperatures and the depth of calcination are compared to the corresponding numerical predictions. These experimental measurements were also used in verifying the reliability of correlations that were developed.

3.2.3.2.3: Repeatability analysis

In addition to the repeatability analyses for the radiant burner and the premixed burner, repeatability analyses have also been carried out for the experimental measurements with the diffusion burner. Repeatability analysis was carried out to understand whether the measurements of temperature and depth of calcination, are repeatable. The mean and standard deviation of the depth of calcination recorded during the multiple trials with propane flow rates of 60 SLPM, 80 SLPM, and 120 SLPM have been shown in Figure 30, Figure 31, and Figure 32 respectively.

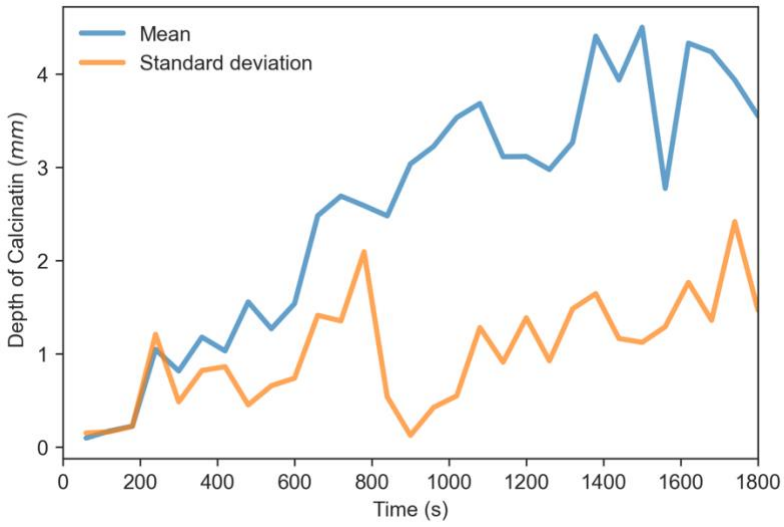

Figure 30: Comparison of the mean and standard deviations of the depth of calcination measurements when exposed to flames from the diffusion burner with a flow rate of 60 SLPM. 12mm is considered through. The depth is measured from the side exposed to the heat source.

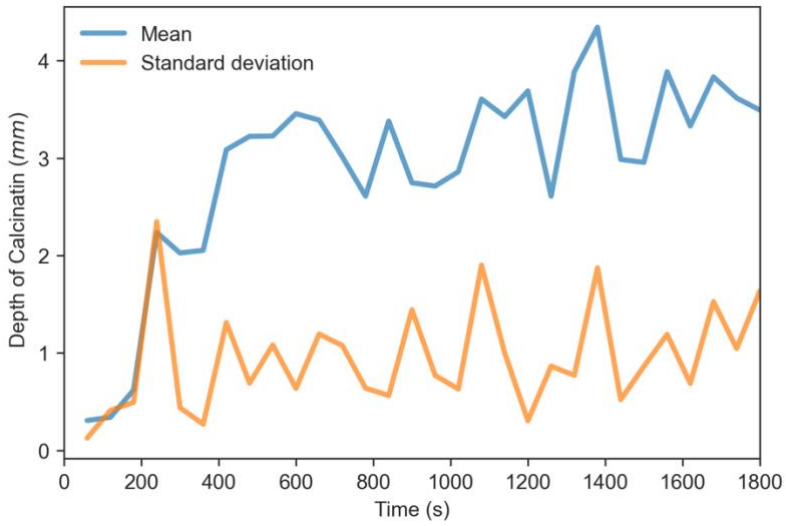

Figure 31: Comparison of the mean and standard deviations of the depth of calcination measurements when exposed to flames from the diffusion burner with a flow rate of 80 SLPM. 12mm is considered through. The depth is measured from the side exposed to the heat source.

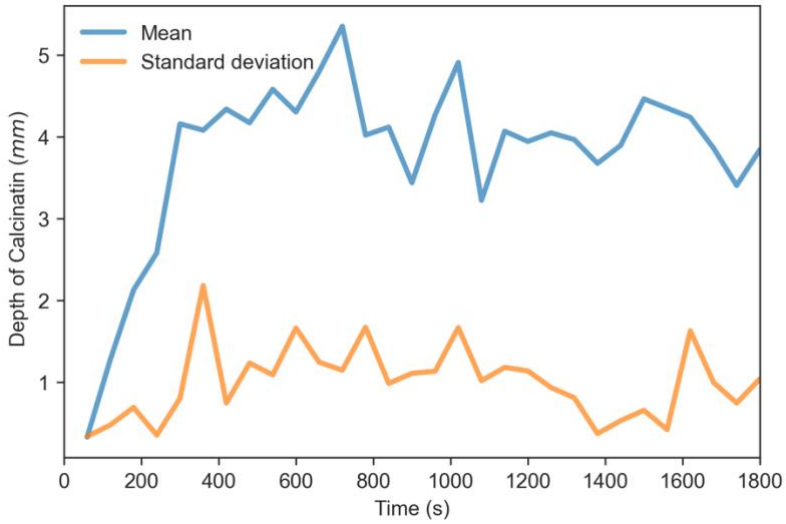

Figure 32: Comparison of the mean and standard deviations of the depth of calcination measurements when exposed to flames from the diffusion burner with a flow rate of 120 SLPM. 12mm is considered through. The depth is measured from the side exposed to the heat source.

Commercially available gypsum boards are expected to have minor differences in composition and local irregularities based on the repeatability analyses for the experiments with the radiant burner. In addition to this, the turbulent flames are expected to significantly affect the repeatability. Experiments were conducted in a wire mesh cage to minimize the effects of external wind.

The differences between experiments increase as the depth of calcination increases. The uncertainty in the depth of calcination measurement is observed to reach up to 2 mm. Similar studies with radiant burner showed a standard deviation of depth measurements of only around 1 mm. Even though there are fluctuations in the depth of calcination measurements, the peak values are not significantly affected by the propane flowrate through the diffusion burner.

3.2.3.4: TGA, DSC, and FTIR analysis

Previous studies, such as that done by Wakili et al (Ghazi Wakili, K., Hugi, E., Wullschleger, L. and Frank, T.H., 2007), attempted to characterize the thermo-physical properties of the gypsum board through both experimental and numerical studies, such as the thermal conductivity and specific heat capacity. Similarly, a study performed by Zehfuß, Sander (Zehfuß, J. and Sander, L., 2021) sought to determine the specific heat capacity, thermal conductivity, and density of gypsum board subject to different heating and cooling rates. Other studies, such as that done by Jeong et al (Jeong, S.G., Chang, S.J., Wi, S., Lee, J. and Kim, S., 2017), have utilized FTIR spectroscopy, DSC analysis, and TGA to study the latent heat of gypsum board. Other studies, such as that done by Kontogeorgos and Founti fit an Arrhenius-type reaction rate through DSC experimental data (Kontogeorgos, D.A. and Founti, M.A., 2012). Various other studies have utilized experimental

and numerical methods to characterize the heat and mass transfer within the gypsum board when exposed to high temperatures or flames (Kontogeorgos, D. and Founti, M., 2010).

The quantification of dehydration depth in the gypsum board is an important characteristic in fire intensity investigations. This study seeks to utilize TGA, DSC, and FTIR to determine the effects of the heating rate on the temperature-dependent mass-loss proportion. An additional study is presented to show the effects of aging on the gypsum board mass-loss through comparison of a newly manufactured sheet, and a 40-year-old sheet of gypsum.

The results from the TGA study are compared with the results presented by Wakili et al (Ghazi Wakili, K., Hugi, E., Wullschleger, L. and Frank, T.H., 2007) at 20 $^{o}C/\ min$ shown in Figure *33*. The results of the study performed by Wakili et al. show an average deviation of approximately 2% mass loss for a given temperature. Despite the 2% difference, present results qualitatively agree with that presented by Wakili et al. The first decrease in the mass, which occurs at approximately 150 ^{o}C corresponds to the water released in equations 1 and 2. At significantly higher temperatures (around $750^{o}C$) reactions other than dehydration can occur including decomposition of calcium carbonate (Sanders & Gallagher, 2002).

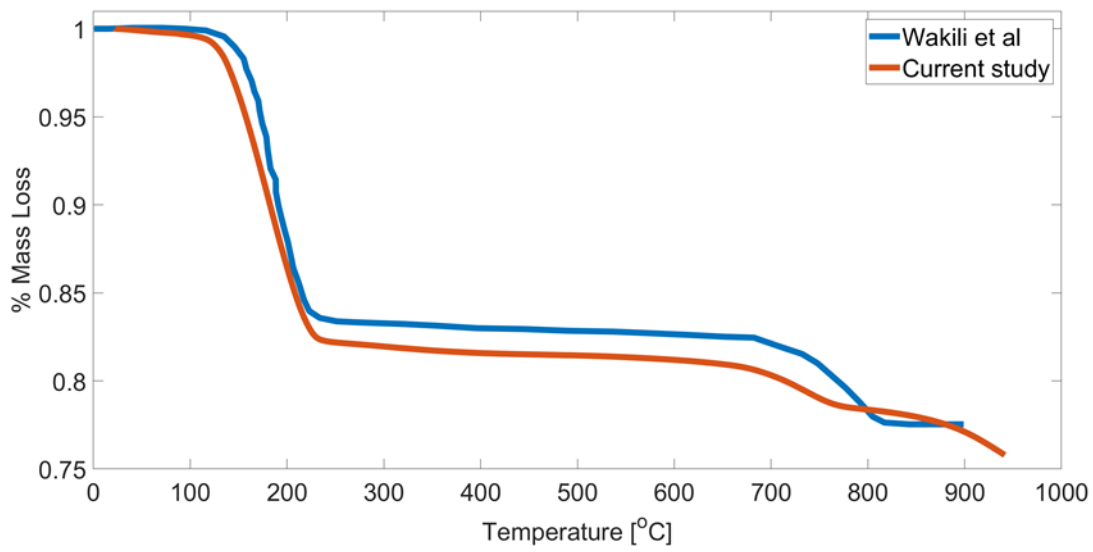

Figure 33: Comparison of TGA from Wakili et al.

The TGA results for the effects of heating rates ranging between 10 °C/min and 100 °C/min are shown below in Figure 34. When studied at different heating rates, the temperature derivative of the calcination reaction peaks at the lowest heating rate of 10 °C/min as this allows a longer time for the dehydration process. The temperature derivative of the calcination reaction then decreases steadily. The location of the maximum temperature derivative of the calcination also shifts to high temperatures, with the peak for 10 °C/min appearing at about 150 °C, and the peak temperature derivative of the calcination reaction shifts to approximately $275^{o}C$ at high heating rates.

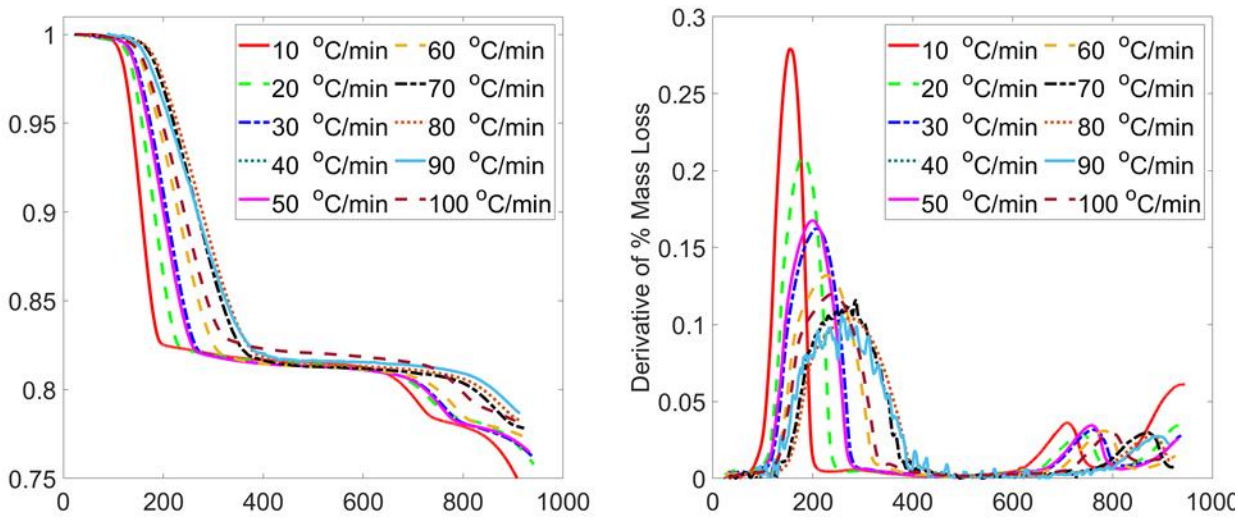

Figure 34: TGA of new gypsum board for heating rates between 10 and 100 °C/ min (left) mass loss from the sample (right) derivative of %mass loss.

Similarly, to the newly manufactured gypsum board, as seen in Figure *35*, the 40-year-old gypsum sample has shown that the maximum calcination rate occurs at a heating rate of 10 °C/min. The trends are similar to the new sample. Figure *36* displays a comparison for the TGA of the new and old gypsum board samples. The 40-year-old sample is found to have a slightly higher amount of absorbed free water than the newly manufactured sample. From the mass loss derivative, it is observed that the old gypsum board dehydrates at a higher rate when compared to the new counterpart. The maximum calcination rate for the old gypsum board occurs at a slightly higher temperature than that of the new gypsum board. However, the difference in TGA results even with a 40-years age difference is minimal. This is only one sample for an old board. There could be sufficient variation in old boards that the difference seen here is within the variation of multiple old boards.

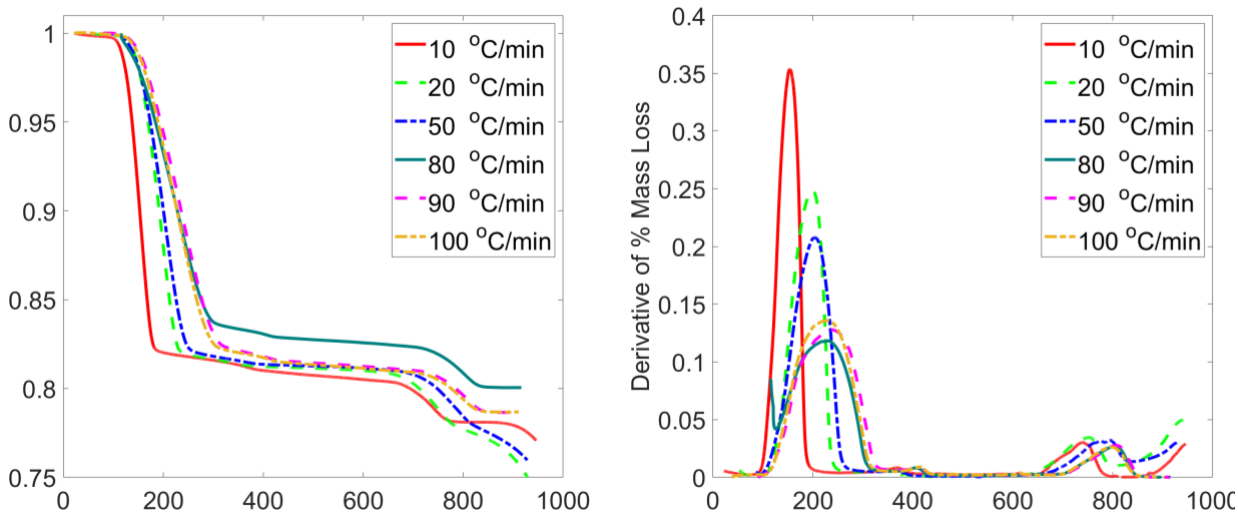

Figure 35: TGA of 40-year-old gypsum board at heating rates between 10 and 100 °C/min (left) mass loss from the sample (right) derivative of mass loss.

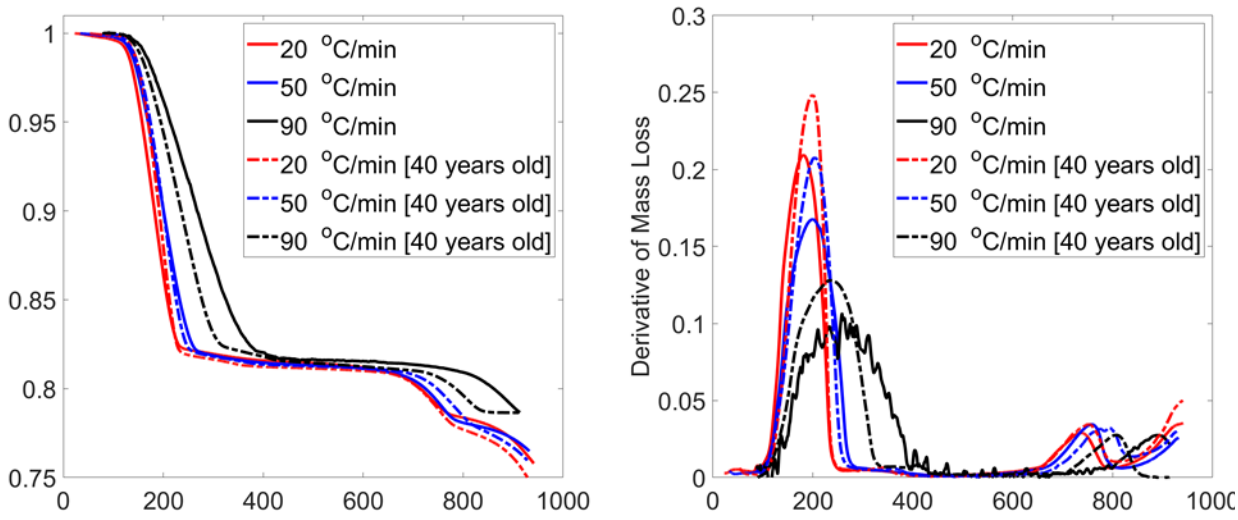

Figure 36: TGA comparison between new and old gypsum board at 20,50,90 °C/ min (left) % mass loss from the sample (right) derivative of mass loss.

Figure *37* shows the results of the DSC for the commercial gypsum board at a heating rate of 5 *°C/*min. CertainTeed regular drywall panel (model #640365) with a thickness of 0.5 inch (12.7 mm) was used for the study. At the low heating rate of 5 *°C/*min, the peaks of two dehydration steps are shown. These represent the two stages of the gypsum dehydration process as given in equations 1, and 2. However, we were not able to use the DSC device for high temperatures. The effective specific heat capacity can be obtained from the DSC data.

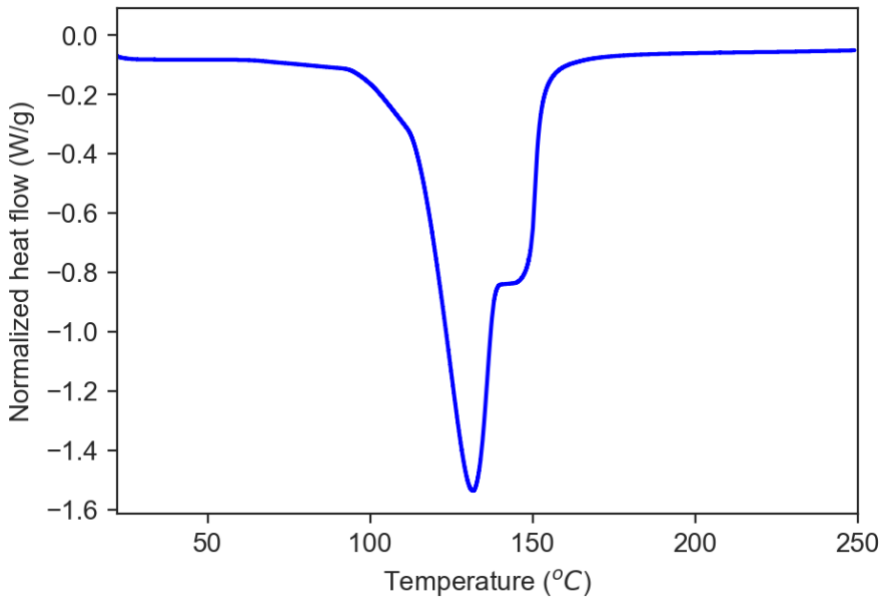

Figure 37: DSC of gypsum board at a heating rate of 5 °C/ min.

FTIR spectroscopy was performed on a gypsum board exposed to heating. Samples were taken from different layers along the depth of the gypsum board. The FTIR data shown in Figure *38* displays the effect of layer depth on water concentrations. The water concentration throughout the gypsum sample increases as the distance from the heat source increases (Figure *38* b and c). This is evident through the absorbance data for wavenumbers between 3200 and 3600 cm^{-1}, which corresponds to the H_2O stretching spectrum, as well as for wavenumbers between 1500 and 1750 cm^{-1}, which corresponds to the H_2O bending spectrum. From these ranges of the absorbance spectrum, we can see that the strength of the H_2O stretching and bending that the concentration of H_2O increases as we move away from the heat source, with the layer closest to the ambient side having the highest concentration of H_2O.

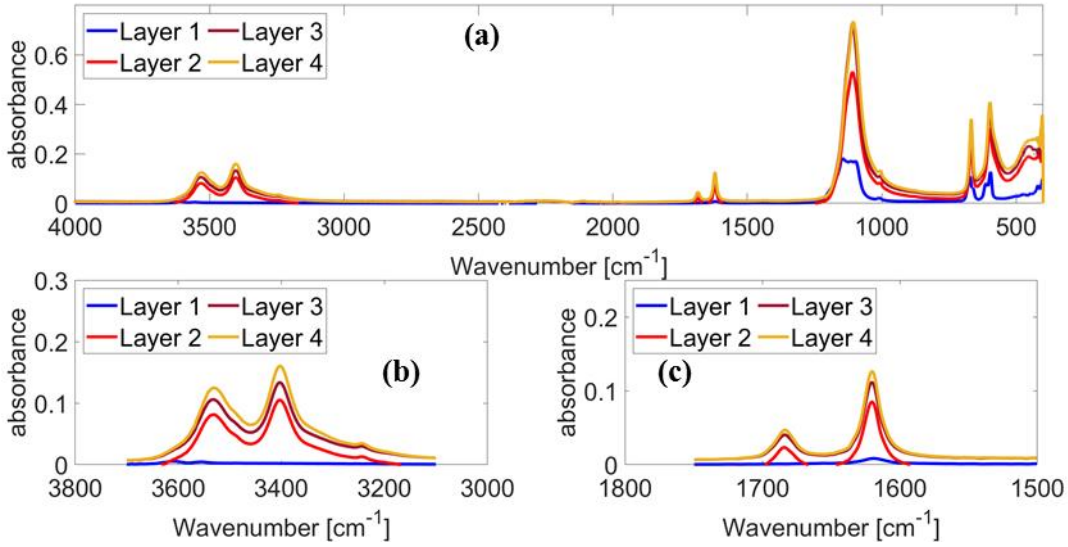

Figure 38: FTIR of gypsum board exposed to heat flux; layer (1) closest to heat source through layer (4) on the ambient side. (a) full FTIR spectrum (b) H_2O stretching spectrum (c) H_2O bending spectrum.

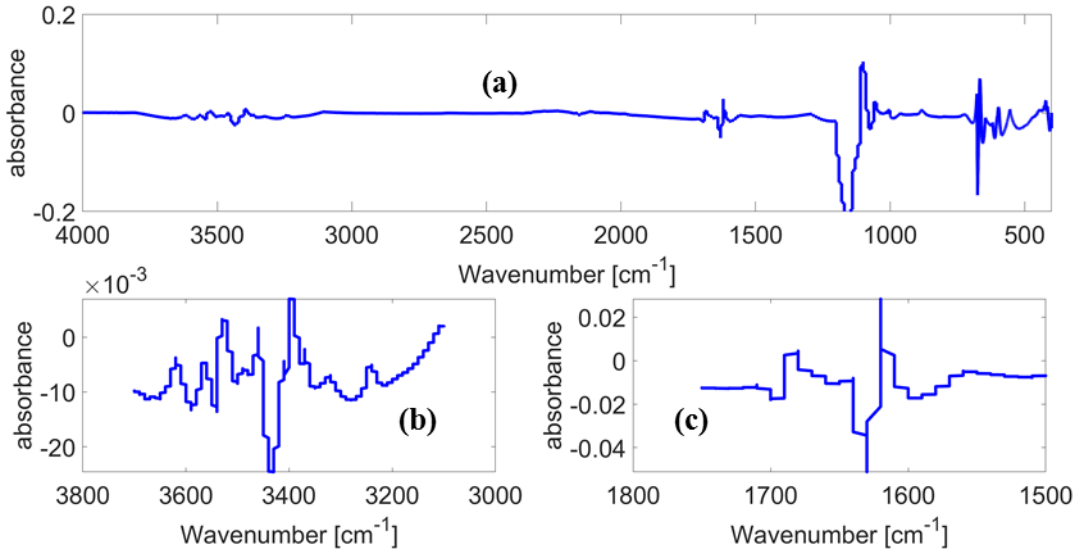

Figure 39: FTIR of gypsum board exposed to heat flux. Sample taken from the layer closest to the heat source after calcination. (a) full FTIR spectrum (b) H_2O stretching spectrum (c) H_2O bending spectrum.

Experimental results of the TGA, DSC, and FTIR spectroscopy on the heat-exposed gypsum board were presented to explain the calcination and dehydration of the gypsum board. TGA results were utilized to study the effects of heating rate on the dehydration of gypsum board. TGA results are also utilized to study the difference in heating rate effects between an aged gypsum board and a newly manufactured gypsum board. The results show that the calcination reaction rate varies non-linearly with the heating rate. DSC data was presented to study the effective heat capacity and effective latent heat of the gypsum board, to determine the thermal energy required for the endothermic dehydration/calcination reaction to occur. FTIR data was presented to study the dehydration depth within the layers of the gypsum sample. The FTIR data showed a clear increase in the water concentrations between each layer, as the distance from the heat source increased.

3.2.3.5: Scanning Electron Microscopy

To better explore the microscopic aspects of gypsum calcination, Scanning Electron Microscopy (SEM) of the gypsum board exposed to heat flux was performed. Hitachi FlexSEM 1000 II SEM fitted with a Bruker ESPIRIT compact energy dispersive X-ray spectrometer available at EKU was used for the study. Backscatter electron (BSE) mode was used with an accelerating voltage of 5 kV for visualization and 20 kV for elemental analysis. Gypsum boards exposed to heat have significant local irregularities up to several hundreds of microns. Elements like fiberglass used for support are also identified in the SEM images. Figure 40 (left) is of a location with fiberglass and Figure 40 (center) is of a location without it. Figure 40 (right) is a further magnified view. These local irregularities affect the reproducibility of experimental measurements.

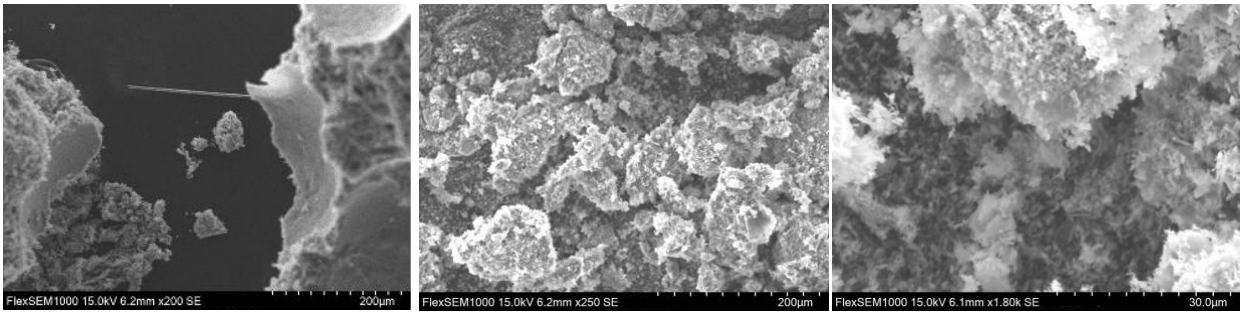

Figure 40: SEM images with different levels of magnification at different locations of a regular gypsum board exposed to heat.

3.2.4: Numerical Methods

3.2.4.1: Gypsum thermo-chemistry

Gypsum ($CaSO_4 \cdot 2H_2O$) contains 21% by mass chemically bound water in addition to a small amount of absorbed free water. The dissociation of chemically bound happens in two stages. In the first stage, the calcium sulfate dihydrate gets converted into calcium sulfate hemihydrate ($CaSO_4 \cdot ½\ H_2O$) and release 75% of the chemically bound water. In the second stage, which

requires a high temperature of around 700 ºC, calcium sulfate hemihydrate dehydrates to form calcium sulfate. The stages in gypsum calcination are shown in Equations 1 and 2.

$$CaSO_4 \cdot 2\ H_2O \rightarrow CaSO_4 \cdot \frac{1}{2} H_2O\ + \frac{3}{2} H_2O \quad (1)$$

$$CaSO_4 \cdot \frac{1}{2} H_2O\ \rightarrow CaSO_4 + \frac{1}{2} H_2O \quad (2)$$

3.2.4.2: Species conservation

The mass conservation of the gas-phase species in the porous medium is implemented as shown in the Equation 3, which considers the diffusion due to the concentration gradients, convection due to the pressure gradient, and the mass generation due to the production of water vapor.

$$\emptyset\ \frac{\partial {\rho_g}^k}{\partial t} = \nabla \cdot \left(D_{eff}\ \nabla {\rho_g}^k\right) - \nabla \cdot \left({U_g}^D\ {\rho_g}^k\right) + {\dot{Q}_m}^{\prime\prime\prime\ k} \quad (3)$$

The diffusive mass transfer of water vapor due to the concentration gradients is calculated using Fick's law. The mass transfer of water vapor due to the pressure gradients, caused by the increased vapor concentration during the evaporation, is calculated using Darcy's law.

3.2.4.3: Momentum conservation

The gas phase in the porous medium is considered to be a mixture of ideal gases. The pressure is calculated as the sum of the partial pressures of individual gases. The mean filtration velocity vector (Darcy velocity vector) of the gas mixture is obtained from the pressure gradients as shown in Equation (4).

$${U_g}^D = -\frac{K}{\mu_g} \nabla P_g \quad (4)$$

3.2.4.4: Energy conservation

The heat transfer through conduction, heat transfer caused by the mass transfer due to both diffusion and convection, heat absorption or production due to the pressure changes, and the heat

absorption due to the endothermic dehydration are calculated to obtain the energy conservation as shown in Equation 5.

$$\left\{\rho_s c_s + \emptyset \sum_{k=1}^{N^g} \left({\rho_g}^k {c_{p,g}}^k\right)\right\} \frac{\partial T}{\partial t} = \nabla \cdot \left(K_{eff}\, \nabla T\right) - \nabla \cdot \left[\sum_{k=1}^{N^g} \left\{{c_{p,g}}^k \left({j_{diff}}^k + {j_{pres}}^k\right)\right\}\right] T + \emptyset \frac{\partial P_g}{\partial t} + {\dot{Q}_T}''' \quad (5)$$

Here, ${j_{pres}}^k = {\rho_g}^k {U_g}^D$, and ${j_{diff}}^k = -D_{eff}\, \nabla {\rho_g}^k$.

3.2.4.5: Water vapor re-condensation

In the early stages of the gypsum dehydration, transport of water vapor released from the side of the gypsum board exposed to fire to the colder ambient side could result in re-condensation of a part of the transported water vapor. In the present model, the effect of water vapor re-condensation is accounted for by adding a negative component to the source terms in the species conservation equation (${\dot{Q}_m}'''$) for the water vapor and by adding a positive component to the source term in the energy conservation equation (${\dot{Q}_T}'''$). The source terms are applied in each computational cell during every time step using the saturation vapor pressure and the heat of condensation corresponding to the cell temperature. Therefore, the effect of water vapor condensation diminishes as the temperature inside the gypsum board increases and vanishes as the temperature exceeds the boiling point at the corresponding pressure of the computational cell.

3.2.4.6: Solution Methods

The governing equations are discretized using a finite volume method and the coefficient matrix for the system of differential equations is solved using the TDMA (tridiagonal matrix algorithm). A fully implicit Euler's method is used for the time integration. A 12 mm thick gypsum board with an initial density of 810 kg/m^3 is considered. The decrease in density of the porous material due to the dehydration is considered. A uniform grid spacing of 0.2 mm and a time step of 0.05 s are used. The predictions are ensured to be independent of the grid spacing and time step. Temperature-dependent thermo-physical properties are used for both the solid phase and the gas-phase. A central differencing scheme is used for the conductive and diffusive terms along with an upwind scheme, sensitive to the change in velocity direction, for the convection term.

3.2.4.7: Initial and boundary conditions

Gypsum board with a thickness of 12 mm was considered in the present study. One side of the gypsum board (x = 0 mm) is exposed to the ambient and the other side (x = 12 mm) is exposed to a fire (Figure 4). The total pressure at the outer surfaces of the gypsum board is assumed to be atmospheric pressure. The initial temperature is assumed to be 20 ^{o}C at the ambient side. The initial partial pressure of water vapor at the ambient side is estimated assuming a relative humidity of 40%. The initial partial pressure of water vapor at the 'fire side'- which here means the side of the gypsum board exposed to fire- is estimated assuming stoichiometric combustion products from methane-air mixture. A convection boundary condition is used for the mass and a convection-radiation boundary condition is used for the energy. A temperature of 1000 K is assumed for the gas-phase to calculate the convective heat transfer from between the gypsum board and the fire.

3.2.4.8: Properties

A porosity of 0.68 (Craft, Isgor, Hadjisophocleous, & Mehaffey, 2008) and permeability of 10^{-15} m^2 (Bear, 1972) were used based on the literature. The diffusion coefficient of water vapor in the air is taken as $D_{AB} = 2.56 \times 10^{-5}$ m^2 (Schwertz & Brow, 1951). The effective diffusion coefficient is calculated as $D_{eff} = \emptyset D_{AB}/\tau$. The tortuosity factor, τ, is assumed to be 1.869 (Blondeau, Tiffonnet, Damian, Amiri, & Molina, 2003). A convective heat transfer coefficient of 10 W/m^2 K, a convective mass transfer coefficient of 9.55×10^{-3} m/s, and an emissivity of 0.9 are assumed (Ahmed & Hurst, 1997). The endothermic gypsum dehydration significantly absorbs heat and produces water vapor. The present study has used the data from the thermogravimetric analysis (TGA) of Wakili et al. (Wakili, Hugi, Wullschleger, & Frank, 2007) for the mass generation and energy absorption source terms. The effective specific heat of the solid gypsum board, water vapor, and air (The Engineering Toolbox, n.d.) are evaluated as a function of temperature and were updated every time step. The effective thermal conductivity is calculated using the mass-weighted average.

3.2.4.9. Sensitivity Analysis

Sensitivity analysis allows for the study of the effects of variation in certain parameters on the output of a mathematical model. In general, sensitivity analysis can be broken into two distinct types: local sensitivity and global sensitivity. Local sensitivity studies look at the effect of a change in a parameter within a close vicinity of the model input values, while global sensitivity studies the effect of a change in the model input parameters over all the potential values. Variance-based sensitivity analysis is a form of global sensitivity analysis which studies the sensitivity of a model parameter through the fraction of the total model variance which that parameter is responsible for. This method, originally developed by I. M. Sobol (Sobol, Sensitivity Estimates for Nonlinear

Mathematical Models, 1993) (Sobol, 2001), is most easily calculated through a Monte Carlo approximation.

3.2.4.9.1: Local Sensitivity Analysis

Local sensitivity analysis seeks to study the effects of parameters close to the nominal or average value. Most commonly, a normalized derivative definition is used for local sensitivity analysis. Let y be the model output and let k be a parameter. The local sensitivity of y to parameter k is given as

$$l_k = \frac{k}{y}\frac{dy}{dk} \qquad (6)$$

For models without explicit formulas for the model output, it is most common to use numerical differentiation, with k varying by 1%. Rewriting eq. 6 with numerical differentiation yields

$$l_k \approx \frac{y(1.01k)-y(k)}{0.01y} \qquad (7)$$

3.2.4.9.2: Global Sensitivity Analysis

Global sensitivity analysis allows for sensitivity studies to be conducted across all parameter values within a specified tolerance (e.g. 5%, 10%, etc.). Let $\vec{x} \in \mathbb{R}^n$ represent the vector of input parameters for the model. Let the function $f(\vec{x})$: $\mathbb{R}^{\boldsymbol{n}} \rightarrow \mathbb{R}$ represent the model output. From the analysis of variances, we can represent the model output in terms of the contributions of individual parameters, with constant f_0, the analysis of variances (ANOVA) decomposition up to second order terms is given as

$$f(\vec{x}) = f_0 + \sum_{i=1}^{n} f_i(x_i) + \sum_{i<j} f_{ij}(x_i, x_j) + o(x_i, x_j, x_k) \qquad (8)$$

Where $x_i \in \vec{x}$, and $f_i(x_i)$ is a function only of x_i, and $o(x_i, x_j, x_k)$ represents all the functions of three or more parameters. The details of the mathematical model were reported in (Paye, Hancock, Khan, Kozhumal, & Sezer, 2023)

3.2.5: Validation

3.2.5.1: Based on surface temperature

The temperature history inside the gypsum board is plotted at three locations, x = 4 mm, 8 mm, and 12 mm where the experimental measurements are available (Wakili, Hugi, Wullschleger, & Frank, 2007). The temperature of the surface exposed to the heat flux was reported. However, the heat flux values were not reported in the study. Hence, the available surface temperature was used as a boundary condition for the numerical model. The numerical predictions are compared with the experimental measurements as shown in Figure 41.

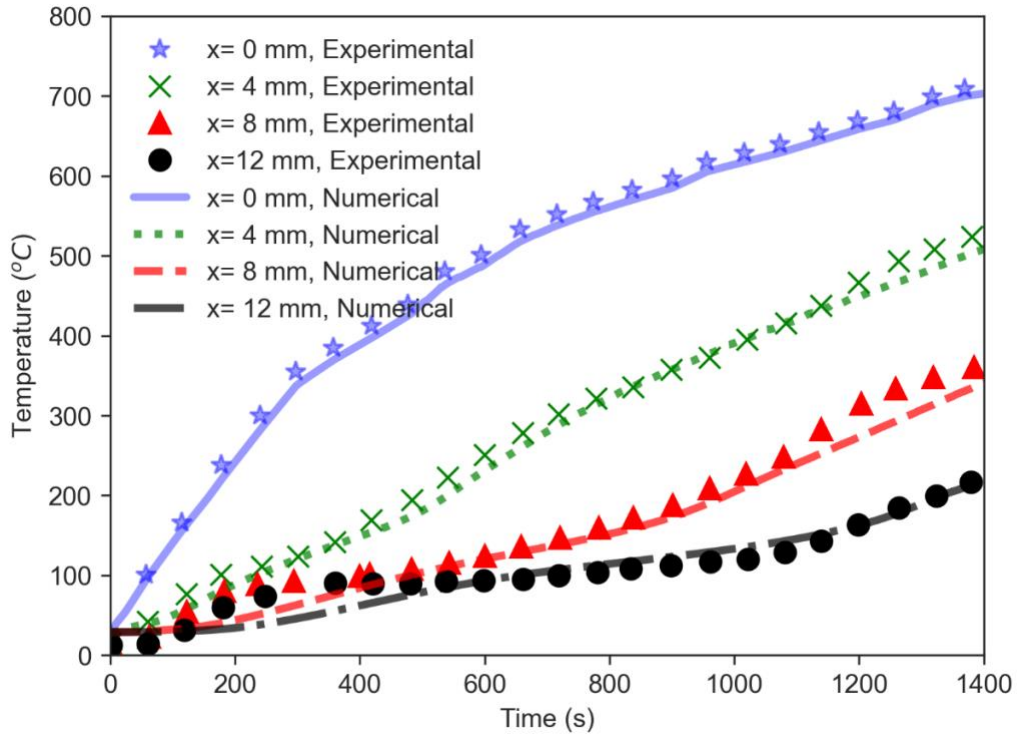

*Figure 41: Comparison of the time histories of temperature at different locations inside the gypsum board between the experimental measurements * (Wakili, Hugi, Wullschleger, & Frank, 2007) and the present numerical predictions. Depth is measured from the side exposed to the heat source.*

The trends in the temperature evolution are captured well. However, differences are observed between the measured and predicted temperatures, especially in the early stages of gypsum calcination and during the peak rate of dehydration. After around 20 minutes, the predictions match closely with the experimental observations.

3.2.5.3: Based on exposed heat flux

The numerical predictions from the one-dimensional model with varying heating rate chemistry were compared with the current experimental measurements. The temperature history inside the gypsum board is plotted at four locations, x = 0 mm, 4 mm, 8 mm, and x = 12 mm. The numerical predictions are compared with the experimental measurements when exposed to a heat flux of 10 kW/m^2 as shown in Figure 42. Experimental measurements from the initial trial were used for comparison as mean values distort some of the unsteadiness observed in the temperature measurements.

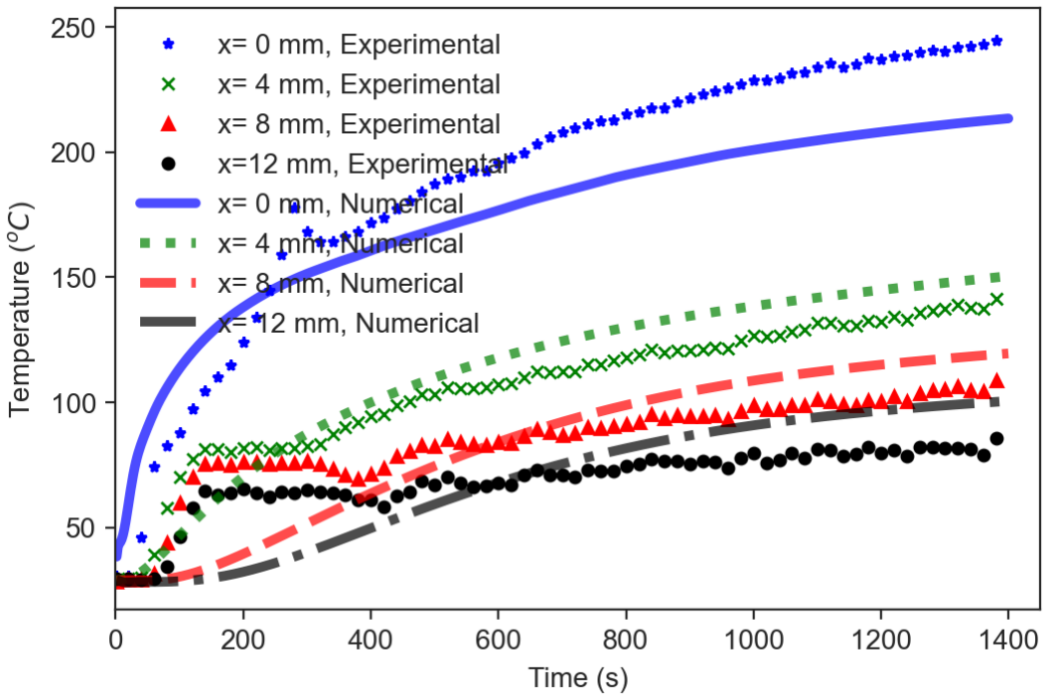

Figure 42: Comparison of time histories of temperature at different depths inside the gypsum board between the experimental measurements and the numerical predictions when exposed to a heat flux of 10 kW/m^2 from the radiant burner. Depth is measured from the side exposed to the heat source.

The model reasonably predicts the temperature of the gypsum board, except in the initial stages. The trends in the temperature history are well predicted. For the most part, the numerical predictions are within the experimental uncertainty. The predictions appear to have improved with the improvement in the chemistry model. The thin paper layer present in commercially available gypsum boards could be the reason for the differences in the early stages of exposure to heat flux. When the heat flux is increased to 20 kW/m^2, the temperature values also increased substantially. The surface temperature is predicted accurately (Figure *43*).

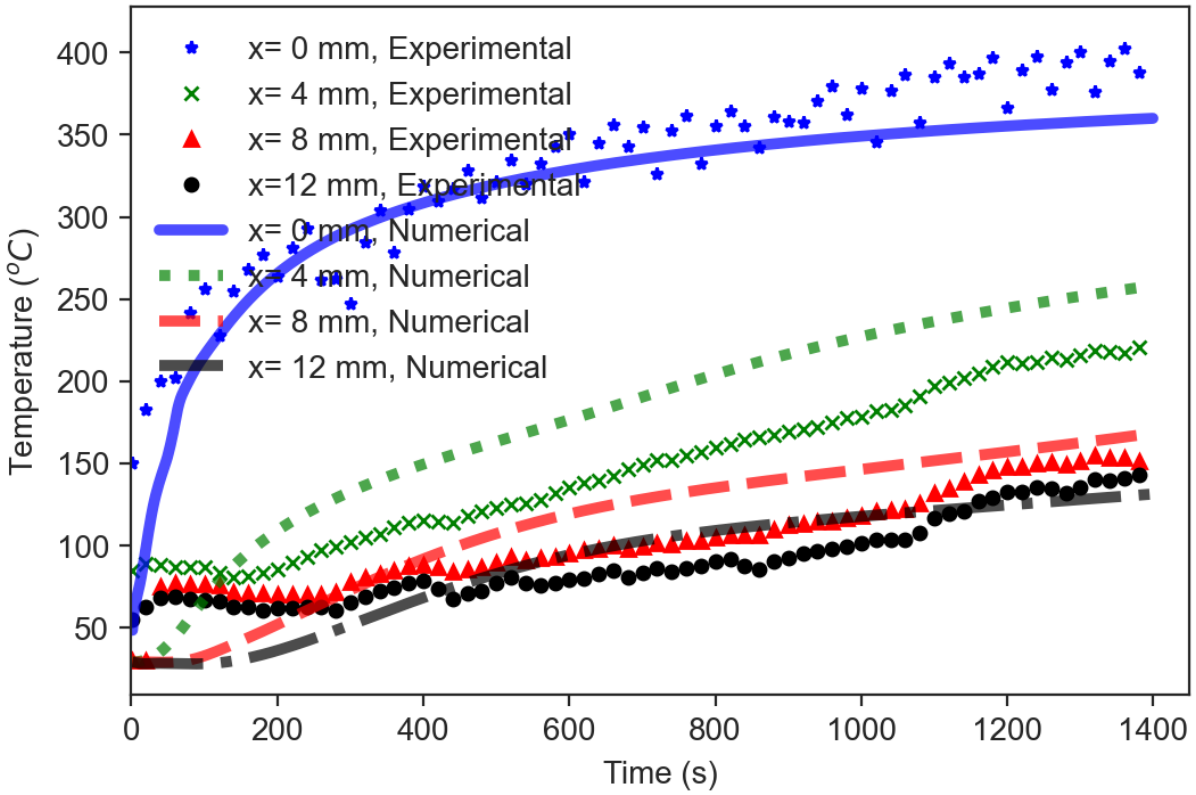

Figure 43: Comparison of time histories of temperature at different depths inside the gypsum board between the experimental measurements and the numerical predictions when exposed to a heat flux of 20 kW/m^2 from the radiant burner. Depth is measured from the side exposed to the heat source.

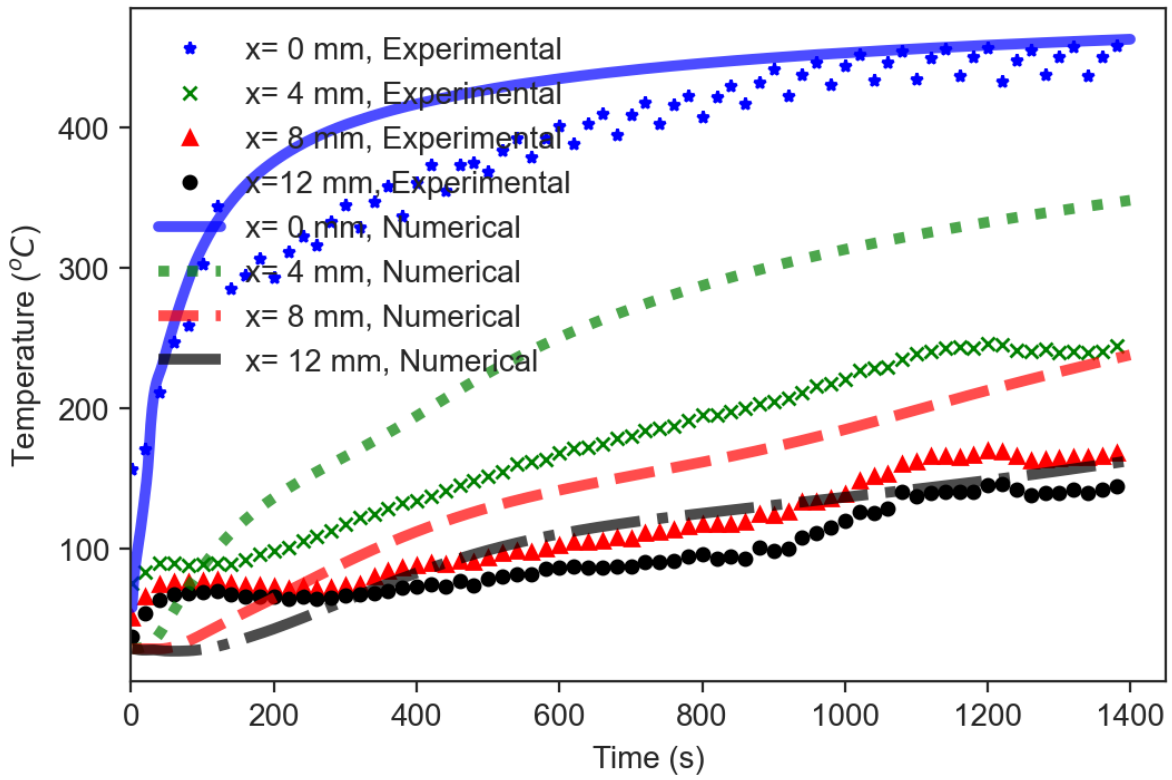

Figure 44: Comparison of time histories of temperature at different depths inside the gypsum board between the experimental measurements and the numerical predictions when exposed to a heat flux of 30 kW/m^2 from the radiant burner. Depth is measured from the side exposed to the heat source.

With a heat flux of 50 kW/m^2, the trends in the surface temperature rise are predicted within one standard deviation of experimental uncertainty. However, the internal values are overpredicted towards the end of dehydration process.

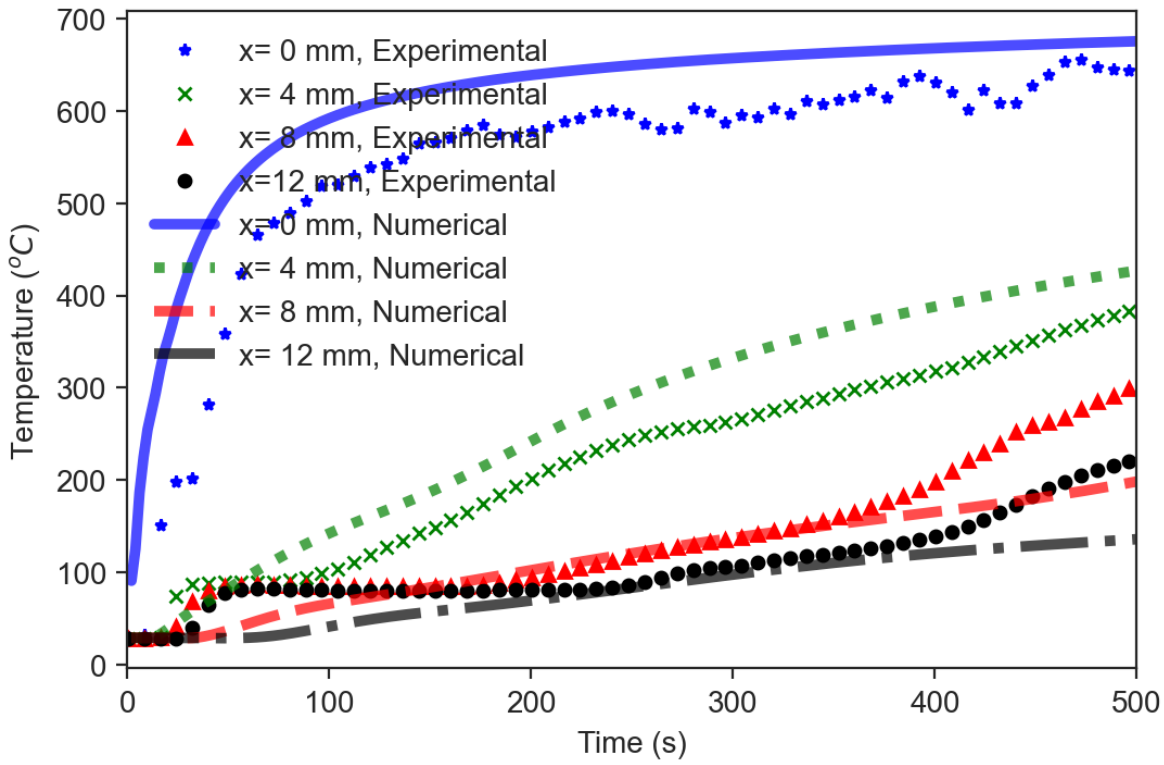

Figure 45: Comparison of time histories of temperature at different depths inside the gypsum board between the experimental measurements and the numerical predictions when exposed to a heat flux of 50 kW/m^2 from the premixed burner. Depth is measured from the side exposed to the heat source.

When the heat flux is further increased to 70 kW/m^2, the peak surface temperature is predicted within one standard deviation of experimental uncertainty. However, internal temperatures are underpredicted by the model, especially towards the ambient side, as the gypsum board gets completely calcinated.

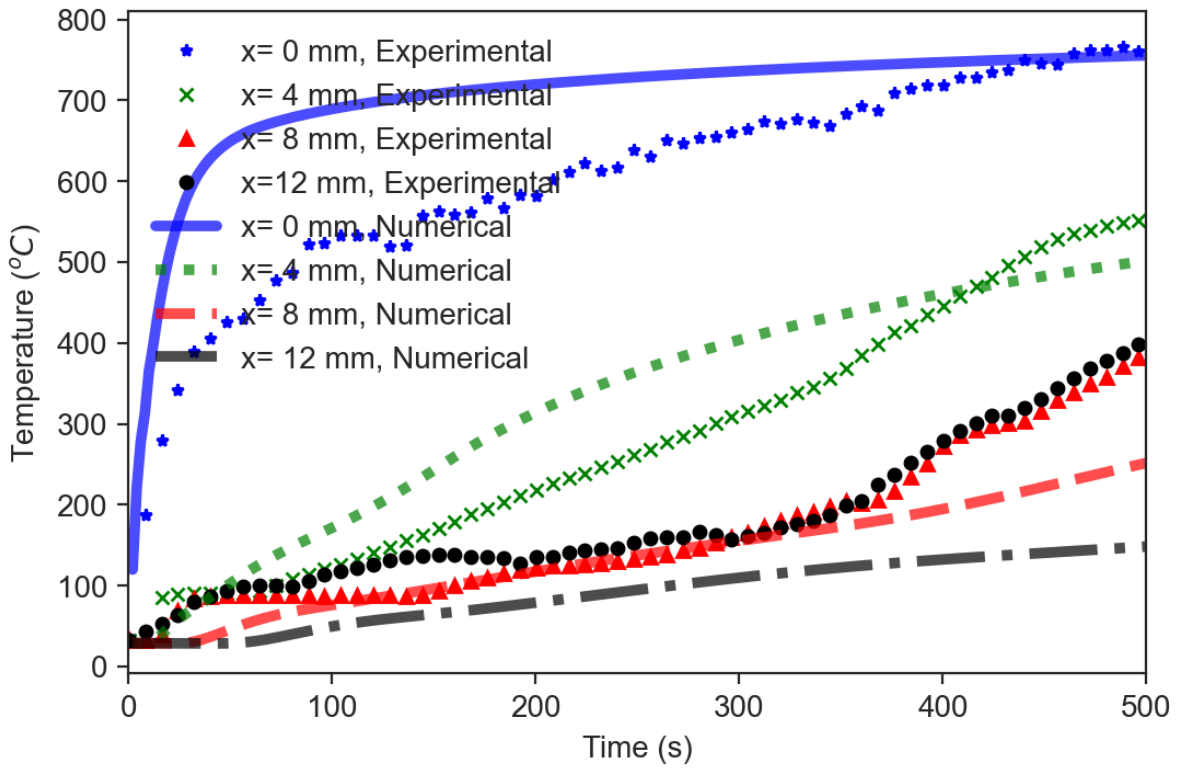

Figure 46: Comparison of time histories of temperature at different depths inside the gypsum board between the experimental measurements and the numerical predictions when exposed to a heat flux of 70 kW/m^2. Depth is measured from the side exposed to the heat source.

At a very high heat flux of 90 kW/m^2 (Figure 47), the temperature of the surface exposed to heat flux increases rapidly. However, as the endothermic dehydration process absorbs most of the heat supplied, the increase in the internal temperatures is much slower. This trend is well captured by the numerical model. At high heat fluxes the paper layer at the back of the gypsum board can also burn causing a rapid increase in the temperatures.

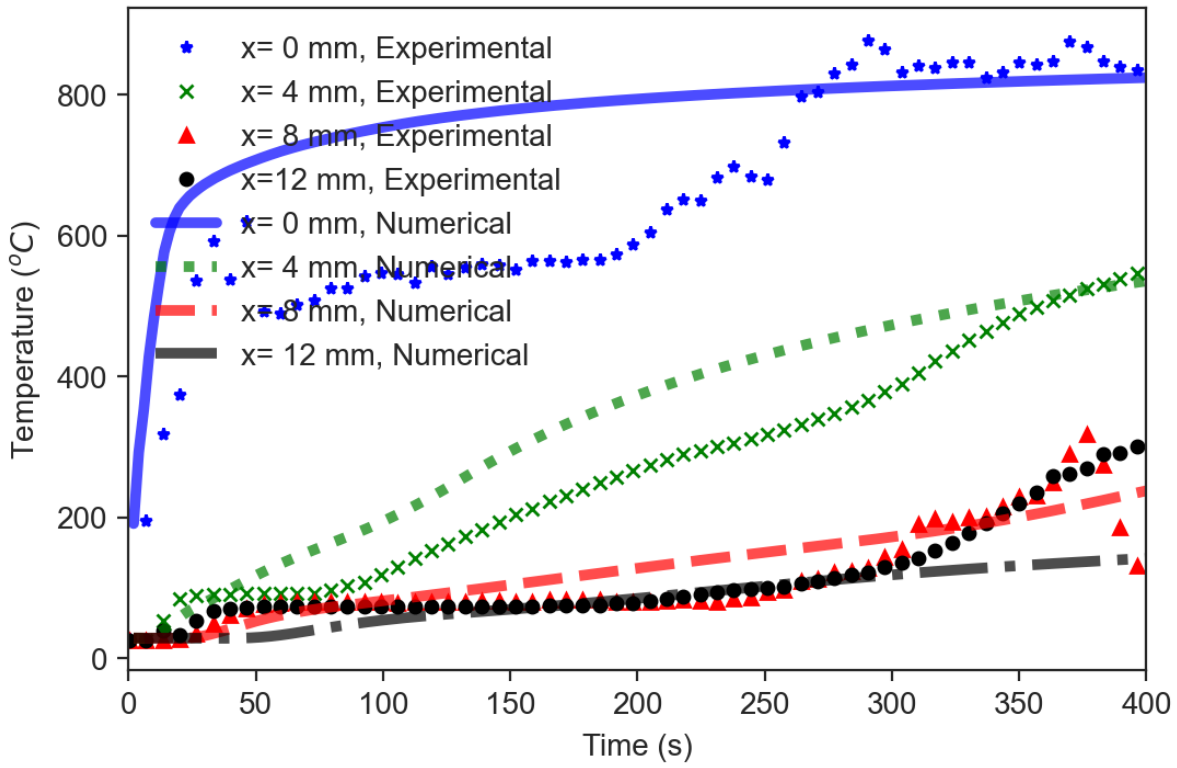

Figure 47: Comparison of time histories of temperature at different depths inside the gypsum board between the experimental measurements and the numerical predictions when exposed to a heat flux of 90 kW/m2. Depth is measured from the side exposed to the heat source.

As noted in Section 3.2.3: Experimental results, the experimental uncertainties increase with increase in heat flux and temperatures. This could be amongst the reasons for increased deviation between numerical predictions and experimental measurements for higher heat fluxes.

3.2.6: Numerical Results

3.2.6.2: Development of varying heating rate gypsum thermo-chemistry model

3.2.6.2.1: Development of reaction rate equations

The governing equations are discretized using a finite volume method and the coefficient matrix for the system of differential equations is solved using the TDMA (tridiagonal matrix algorithm). A fully implicit Euler's method is used for the time integration. The predictions are ensured to be

independent of the grid spacing and time step. Temperature-dependent thermophysical properties are used for both the solid phase and the gas phase. A central differencing scheme is used for the conductive and diffusive terms along with an upwind scheme, sensitive to the change in velocity direction, for the convection term.

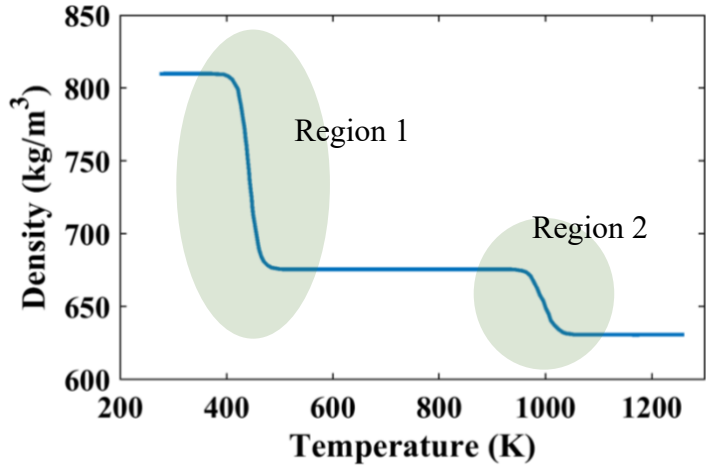

Experimental

$$\dot{Q}_m{}'''(T) = -\frac{d\rho}{dT}\frac{\Delta T}{\Delta t}$$

Heating rate,

$$\frac{\Delta T}{\Delta t} = 10 - 100\ K/min$$

Numerical

$$\dot{Q}_m{}'''(T,\ t,\ x) = A\, e^{(-B/T)}\left[H_2O_{max} - \int_0^{t-dt} \dot{Q}_m{}'''\, dt\right]$$

Figure 48: Modeling of rate mass loss rate. The mass loss curve produced from the TGA data and the method to calculate the mass loss rate (or vapor production rate numerically.

Numerically, the rate of dehydration ($\dot{Q}_m{}'''$) required in Equation 4 needs to be calculated as in the equation given in Figure *48*. This requires the total water content and time integration of the rate of water production, the temperature, and two coefficient values. Based on the normalized TGA data (*Figure 34*), the derivative of mass loss of the gypsum with respect to temperature is

calculated. This value is multiplied by the density and the heating rate to find the mass loss rate per unit volume of gypsum.

The rate of dehydration ($\dot{Q}_m{}'''$), estimated for the numerical model is then compared to the calculated rate of dehydration (mass loss rate) from the experimental measurement (Figure *34*) for the two stages of the gypsum calcination process as shown in Figure *48*. The coefficients for the reaction rate equations for each heating rate are then estimated. The reaction rates (mass loss rates) are calculated from these reaction rate equations. Thus, converting the TGA results into just two sets of coefficients, A and B. The coefficients depend on the temperature range and the heating rate. Effective heat capacity, which is required for the numerical model is calculated based on DSC results.

3.2.6.2.2: Comparison of experimental and numerical mass loss rates

The numerical and experimental mass loss rates are compared in Figure 49 -Figure 50. Experimental mass loss rates were obtained from TGA studies (Figure *34*) following the method shown in Figure 48. Numerical mass loss rate is calculated from the developed reaction rate equations following the method shown in Figure 48. The results are in good agreement at low temperatures and heating rates. The agreement with exponential relationship is acceptable, despite the complex dehydration process involved during the release of chemically bound water. The first range (the low-temperature range) represents vapor production. The second region is more complex. At higher temperatures reactions other than dehydration can occur including decomposition of calcium carbonate (Sanders & Gallagher, 2002). Also, higher heating rates could result in more experimental noise. Despite all these factors, the developed chemistry model is capable of closely predicting the reaction rates over a wide range of heating rates.

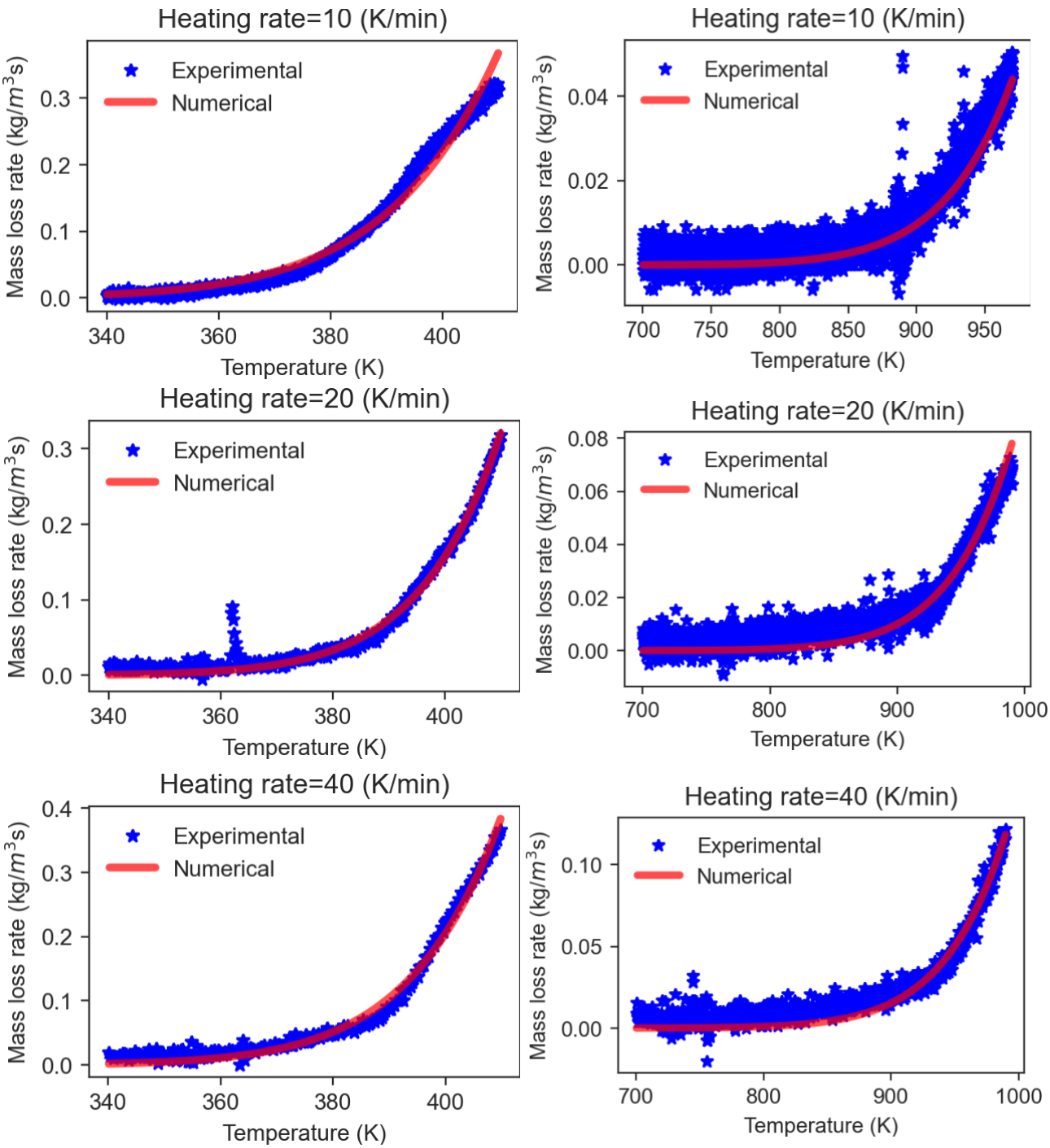

Figure 49: The mass loss rate per unit volume from the experimental TGA data and comparison of numerical predictions from the developed reaction rate equations in two regions- the low-temperature region (left) and the high-temperature region (right)- during the gypsum dehydration under heating rates, 10 K/min, 20 K/min, and 40 K/min.

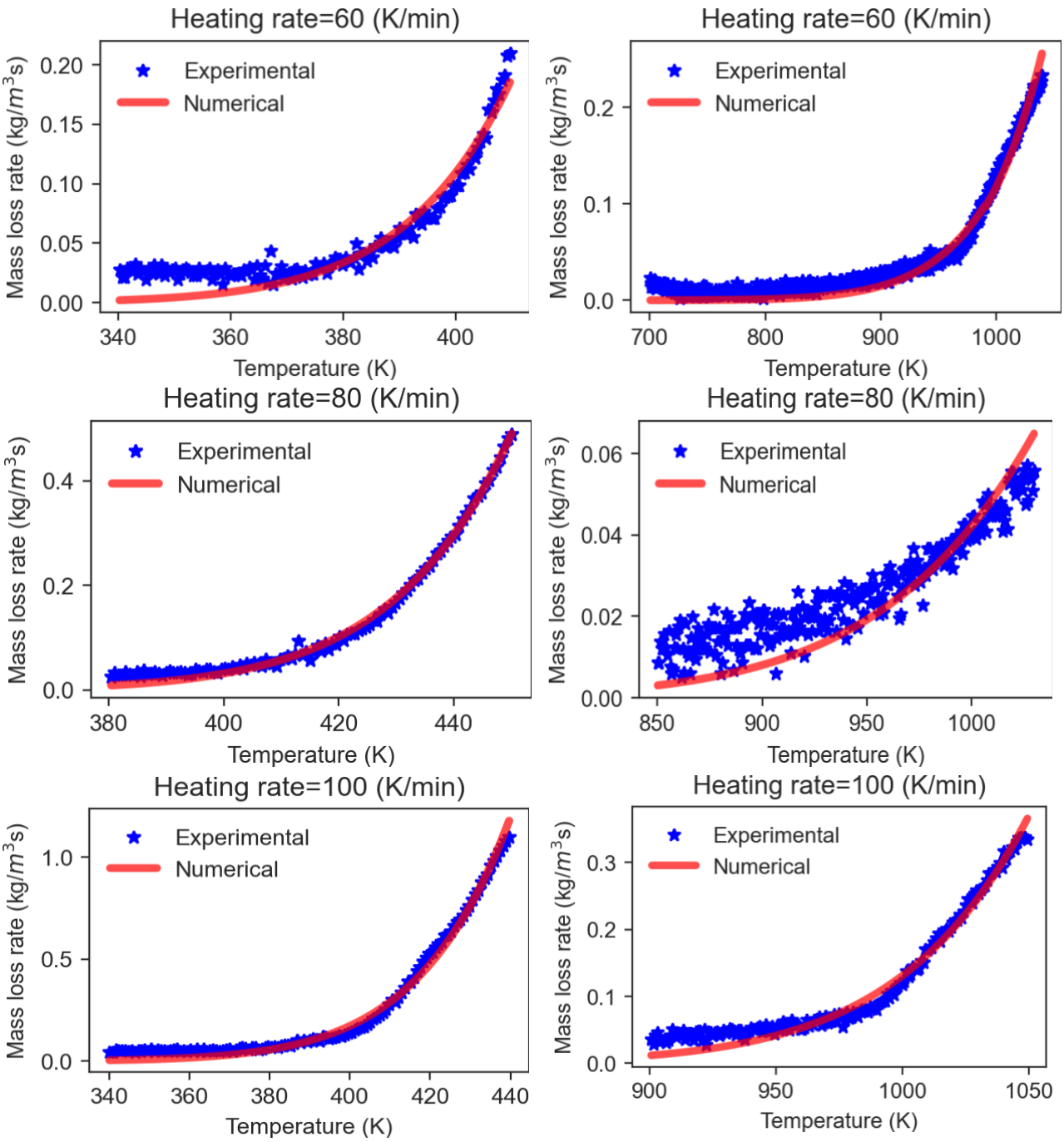

Figure 50: The mass loss rate per unit volume from the experimental TGA data and comparison of numerical predictions from the developed reaction rate equations in two regions- the low-temperature region (left) and the high-temperature region (right)- during the gypsum dehydration under heating rates, 60 K/min, 80 K/min, and 100 K/min.

3.2.6.2: Results from the 1D model with variable heating rate

As too many variables are changing simultaneously, an in-depth analysis of the process of gypsum calcination is challenging. As heat flux is the most critical measurable parameter that influences the gypsum calcination, a controlled numerical study by varying the heat flux alone was performed. To understand the relationships between the depth of calcination and cumulative heat flux, the temperature history, and the propagation of dehydration front inside the gypsum board were analyzed. Two heat flux values, 10 kW/m^2, and 70 kW/m^2, are used for comparison. As expected, the temperature inside the gypsum board increases with the increase in heat flux as explained in the validation section. The relationship is found to be nonlinear due to the complex heat and mass transfer during the dehydration process.

The propagation of the dehydration front is analyzed using the profiles of vapor density at different time instants. Figure 51 and Figure 52 show the evolution of the dehydration front through the thickness of the porous gypsum board when exposed to heat fluxes of 10 kW/m^2 and 70 kW/m^2. The location of maximum vapor density gives the location of dehydration front at that instant. In the initial stages, for 10 kW/m^2 heat flux, the region of the maximum vapor density is close to the side exposed to the heat flux. The rate of vapor production is very small at this stage. The internal temperature and the rate of dehydration increase during exposure to the heat flux. When the gypsum board is exposed to the heat flux for longer durations, the region of maximum vapor density moves farther inside the porous material. This process continues either till the entire board is dehydrated or till the depth of calcination reaches a plateau.

When the heat flux is increased to 70 kW/m^2, the propagation of the dehydration front becomes faster with increased values of vapor density. As the gypsum board gets dehydrated at high

temperatures, steam is generated, and it leaves the porous medium through both sides. This causes a decrease in the vapor density towards the end of the dehydration process.

The propagation velocity of the dehydration front varies even with constant heat flux. The propagation velocity is found to be relatively small at the early stages due to low temperatures and low rates of dehydration. As the temperature inside the porous medium increases, the speed of propagation of the dehydration front also increases. However, as the first stage of gypsum calcination nears its completion, the rate of dehydration and the speed of propagation of the dehydration front decrease. As the dehydration front moves closer to the ambient side, the propagation velocity decreases due to the increased heat losses at the ambient side.

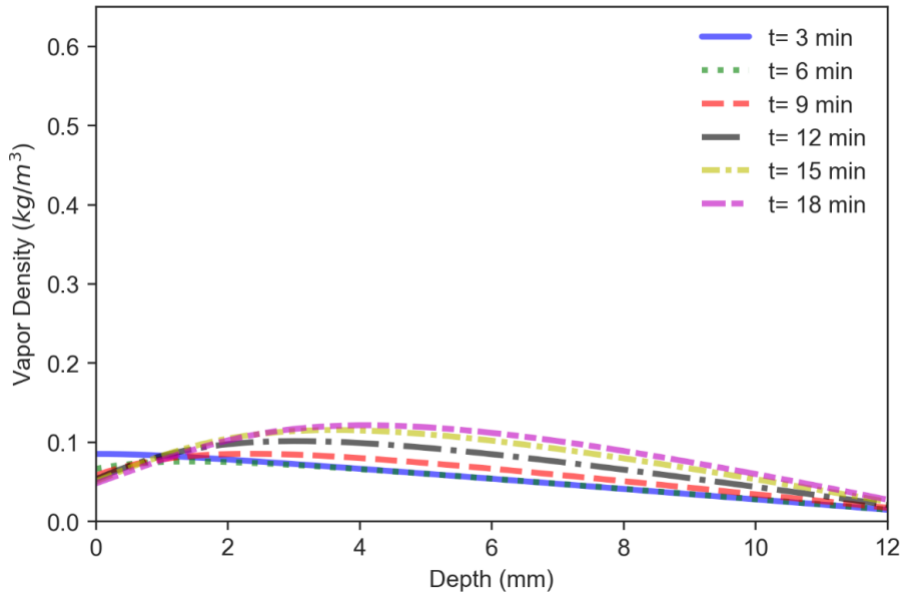

Figure 51: Profiles of vapor density at different time instants in the gypsum board when exposed to incident radiative heat fluxes of 10 kW/m^2. The distance is measured from the side exposed to the heat source.

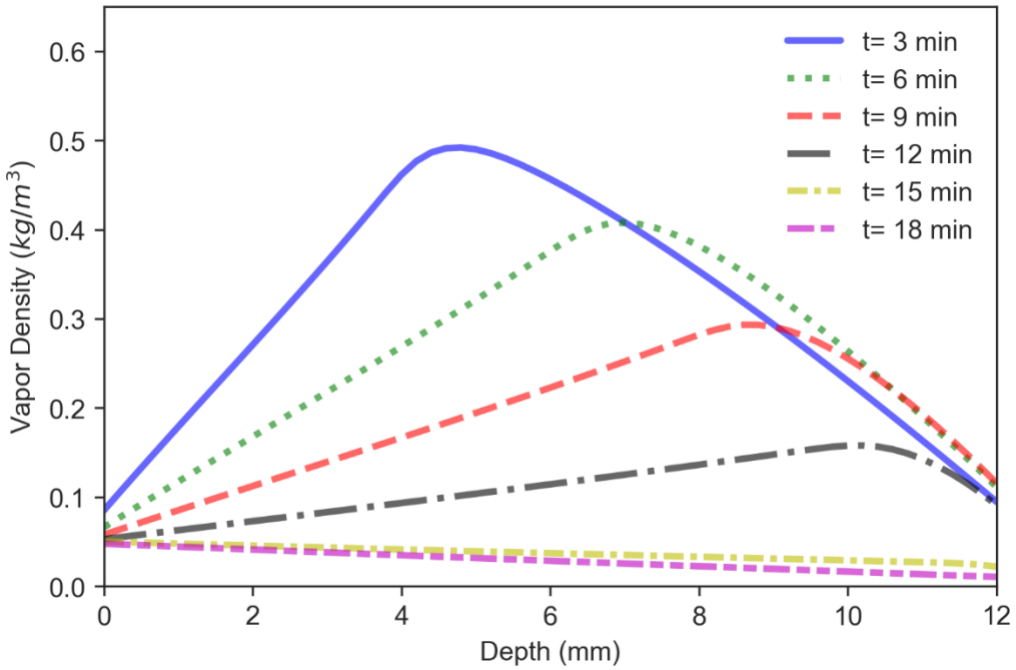

Figure 52: Profiles of vapor density at different time instants in the gypsum board when exposed to incident radiative heat fluxes of 70 kW/m^2. The distance is measured from the side exposed to the heat source.

3.2.6.3: Sensitivity Analysis

The Monte Carlo simulations were performed with $N = 150000$ trials. The Monte Carlo integration also utilized Sobol sequences to reduce the required number of trials through quasi-Monte Carlo integration.

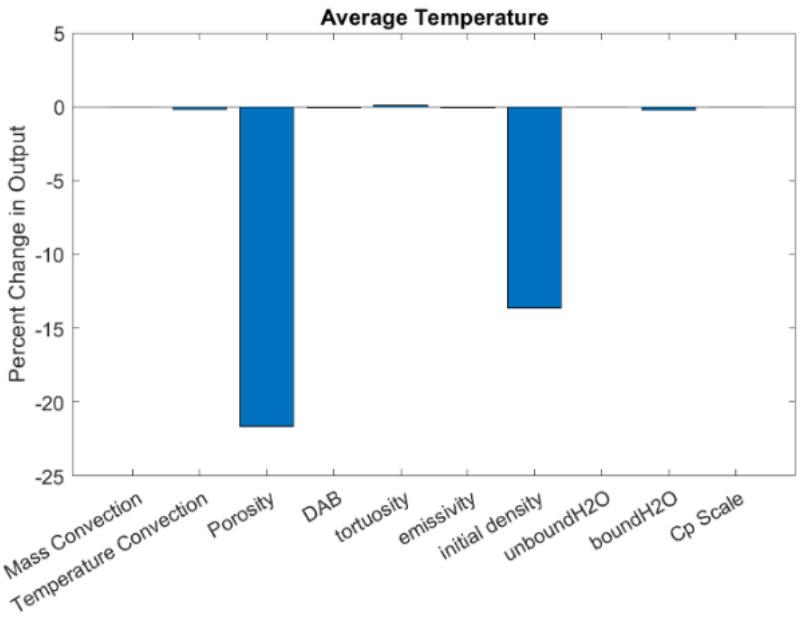

Figure 53: Local sensitivity analysis results for the average temperature profile.

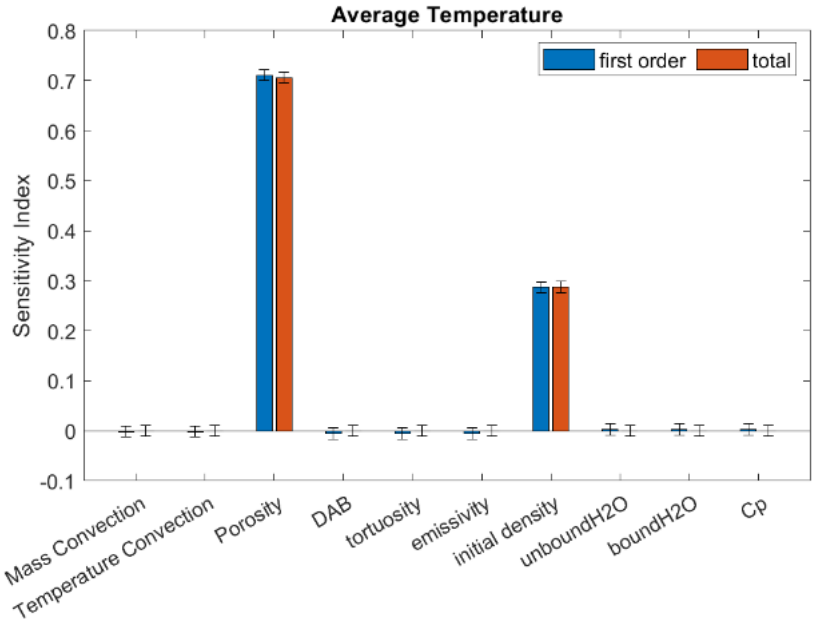

Figure 54: Global sensitivity indices for average temperature.

Throughout the temperature studies, significant effects caused by the porosity of the gypsum board were observed. In general, the porosity most directly determines the makeup of the gypsum board, that is the fraction of the board that is made up of air/water vapor and the fraction made up of

calcium sulfate. This gives a direct dependence for all the thermal properties, such as specific heat, thermal conductivity, and total density. In the global sensitivity analysis, the porosity accounts for approximately 70% of the total variance, while the initial density accounts for approximately 27%. The remaining 3% is distributed amongst the remaining variables. Even thermal convection coefficient and the emissivity had very small effects in comparison with density and porosity.

It is also important to note that the global sensitivity study and the local sensitivity study produce the same ordering of the variables. The highest contributions come from the porosity and initial density. In the study on the minimum water vapor fractions, the mass convection coefficient showed the highest contribution, with similar contributions coming from the porosity and initial density, as well as comparable contributions from the binary diffusion coefficient and the tortuosity. Both studies also showed a small but significant contribution from the bound water fraction as well.

Although there are some aspects of the study which were affected by statistical noise in the Monte Carlo estimate, the global sensitivity analysis is still in qualitative agreement with the local sensitivity analysis. This statistical noise still puts the feasible values of the variance fraction well within the error bounds given by a 90% confidence interval as well. Despite the statistical effects from the Monte Carlo simulations, the global sensitivity analysis still predicted physically reasonable values for the variance fractions.

3.2.6.4: Results from the 3D model

A controlled study was conducted to examine the relationship between the depth of calcination and cumulative heat flux in gypsum board by comparing the results of a 3D heat and mass transfer

model with those previously obtained from the 1D model. Three heat flux values of 10 kW/m^2, 25 kW/m^2, and 40 kW/m^2 were applied at the fire side and the internal temperature of the gypsum board was monitored.

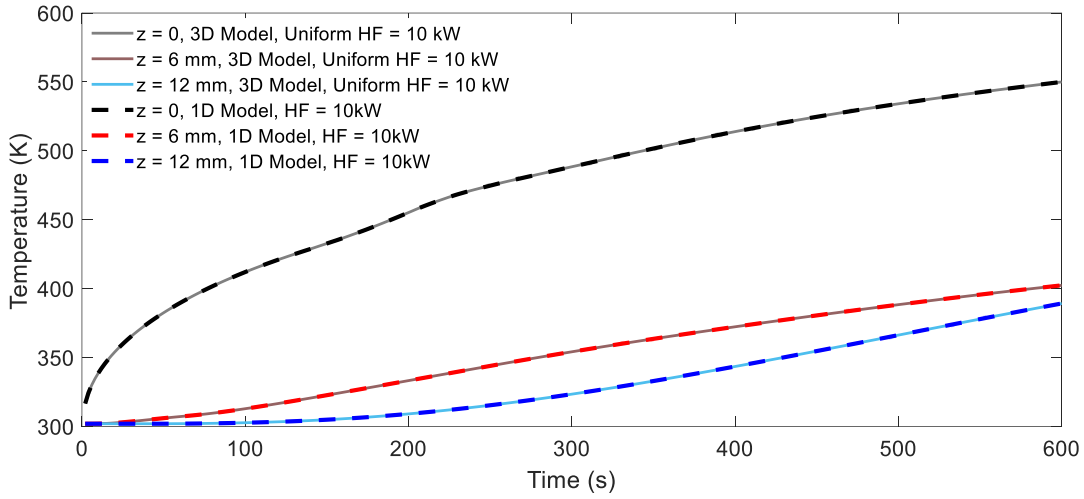

Figure 55: Comparison of 1D and 3D heat and mass transfer models for gypsum board calcination for uniform heat flux (HF) = 10 kW/m^2.

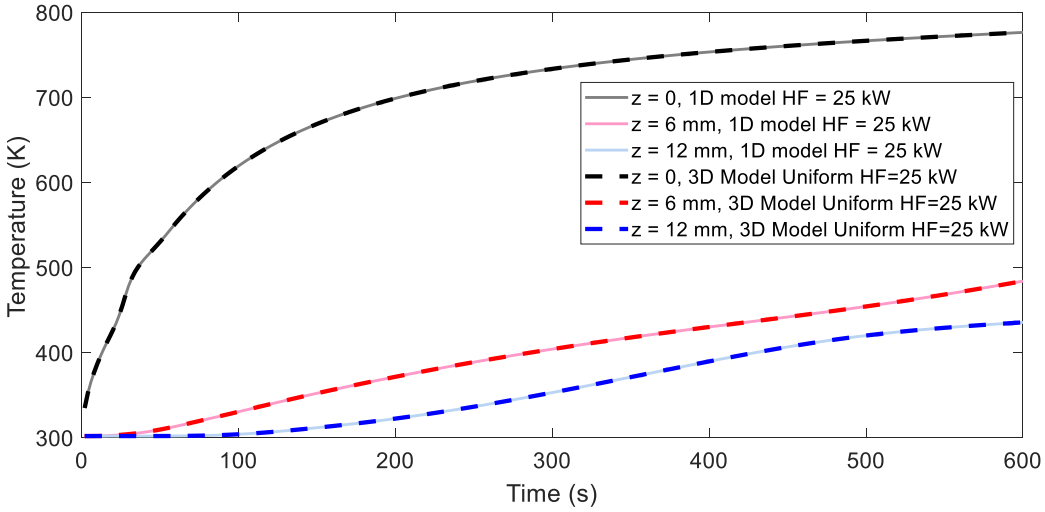

Figure 56: Comparison of 1D and 3D heat and mass transfer models for gypsum board calcination for uniform heat flux (HF) = 25 kW/m^2.

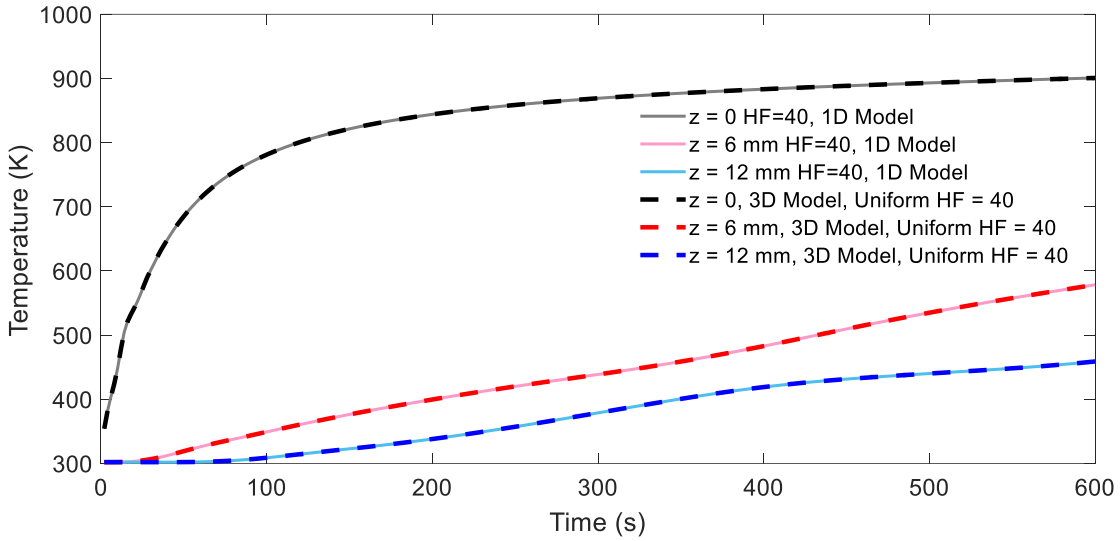

Figure 57: Comparison of 1D and 3D heat and mass transfer models for gypsum board calcination for uniform heat flux (HF) = 40 kW/m^2.

Similarly, it is illustrated in Figure 55 that a comparison of temperature results between the 3D and 1D models for a uniform heat flux of 10 kW/m^2 at z = 0 demonstrates complete overlap and agreement. Similarly, Figure 56 and Figure 57 demonstrate the variation of temperature with respect to time at varying heat fluxes of 25 kW/m^2 and 40 kW/m^2 respectively. It is observed that an increase in heat flux results in an increase in temperature, however, this relationship is nonlinear due to the complexity of heat and mass transfer and the dehydration process.

In actual fire incidents, the assumption of uniform heat flux is not mostly applicable. Therefore, to get a sense of temperature field more realistic situations, the 3D model is implemented for gypsum board configuration where the heat flux changes abruptly from 10 kW/m^2 to 40 kW/m^2. The schematic of such a configuration is demonstrated in Figure 58.

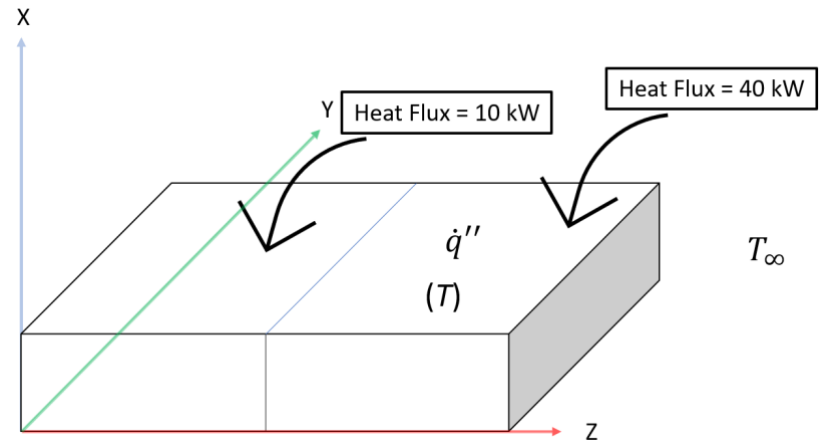

Figure 58: Two sections of the gypsum board with varying heat fluxes of 10 kW/m^2 and 40 kW/m^2.

After applying the model to the configuration given in Figure 58, the results are compared at three different locations along depth (X-axis) as shown in Figure 59. It can be noticed that there is a significant difference in the temperature profile at the surface exposed to the varying heat fluxes. The model can also be implemented and extended for more complex heat flux configurations.

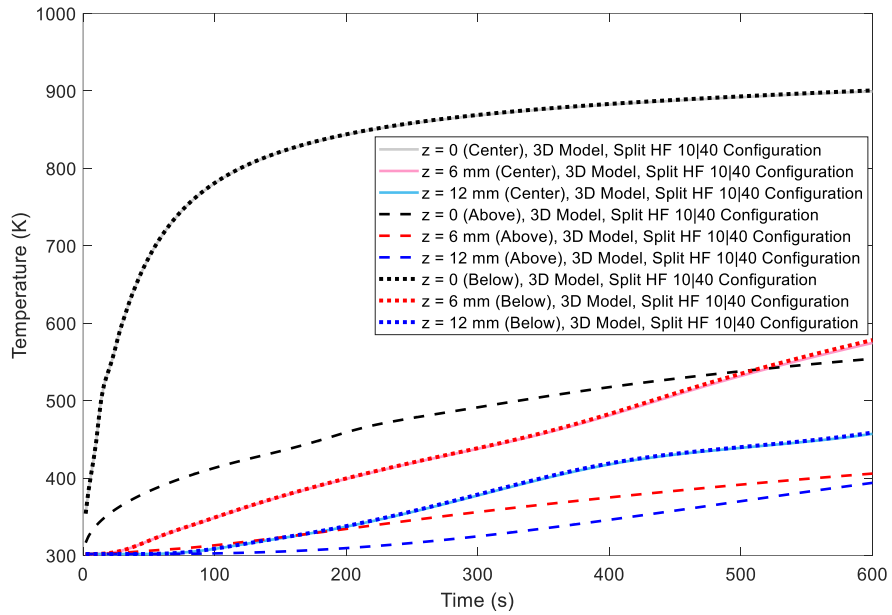

Figure 59: Temperature fields comparison for the configuration of gypsum board given with abrupt change in heat flux from 10 kW/m^2 to 40 kW/m^2.

3.2.6.5: Correlations for depth of calcination

The depth of calcination depends on the exposed heat flux, duration of exposure, heat losses, material, and thermo-physical properties of the gypsum board, etc. This makes it challenging to develop accurate correlations connecting depth of calcination. However, an approximate correlation quantitatively connecting depth of calcinations to exposed incident heat flux will be helpful to fire investigation. In this context, approximate correlations are developed based on numerical predictions and experimental measurements. A logarithmic fit is used to display the relationship between depth of calcination (in mm) and exposed incident heat flux (in kW/m^2) as shown in Figure 60.

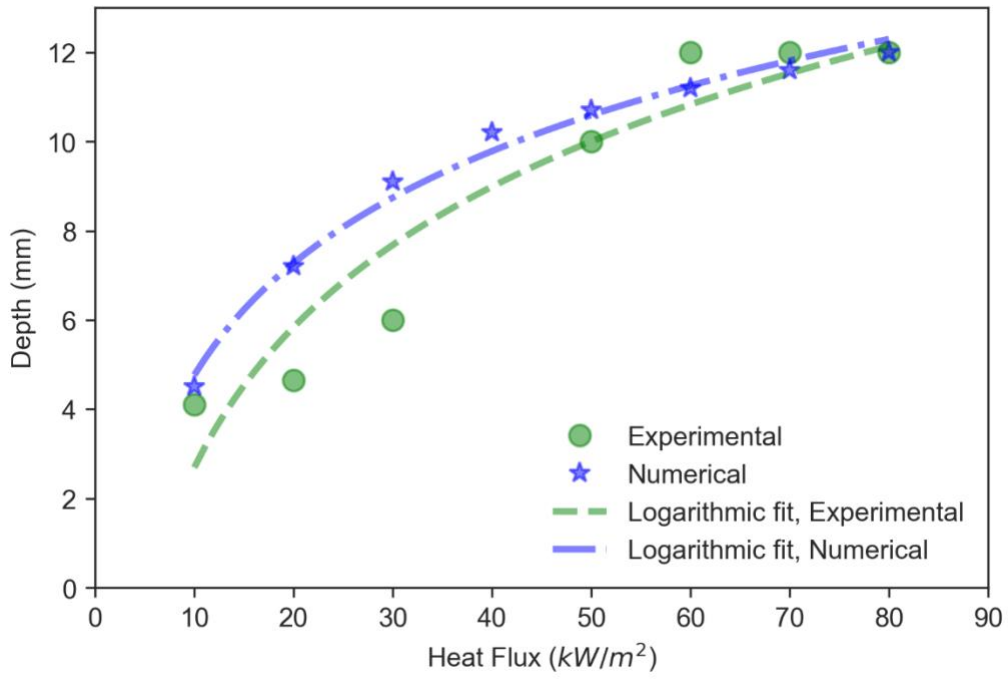

Figure 60: Relationship between depth of calcination and incident heat flux based on numerical predictions and experimental measurements.

Based on numerical predictions,

Depth of calcination ~ 3.62 * ln (Heat flux) - 3.57

Based on experimental measurements,

Depth of calcination ~ 4.54 * ln (Heat flux) – 7.76

Where, depth of calcination is in mm and incident heat flux is in kW/m^2.

Based on experimental measurements, mean depth of calcination after reaching a near steady state is considered. The depth measurements reach a near steady state or the entire 12 mm board gets calcinated by around 10 minutes. With high heat fluxes, above 60 kW/m^2 the entire board gets calcinated before reaching a steady state. Based on numerical predictions the location of peak vapor density with values above the initial value after reaching a near steady state is considered. This is a reliable estimate of the depth of calcination as it tracks the location of the dehydration

front inside the gypsum board. However, near the boundaries, as the vapor produced leaves the board immediately, this may not accurately show the depth of calcination. The coefficient of determination, denoted R^2, is found to be 0.9886 for the numerical correlation and 0.9011 for the experimental correlation.

If the duration of exposure with the peak heat flux is known, the correlations can be revised as below.

Based on numerical predictions,

$$\textbf{Depth of calcination} \sim (3.62 * \ln(\text{Heat flux}) - 3.57)\,(1-e^{(-t/100)})$$

Based on experimental measurements,

$$\textbf{Depth of calcination} \sim (4.54 * \ln(\text{Heat flux}) - 7.76)\,(1-e^{(-t/100)})$$

Here, depth of calcination is in mm, incident heat flux is in kW/m^2, and the duration of exposure to the heat flux, t, is in seconds. The part, $1-e^{(-t/100)}$, tends to unity as time increases and may be neglected if duration of exposure to the heat flux is greater than 8 minutes or 480 seconds.

Correlations available in the literature (Mealy, Wolfe, & Gottuk, 2013) connecting the depth of calcination to exposed heat flux used total heat flux (time-integrated or cumulative heat flux). This makes them unreliable to predict the non-linearity in the propagation of dehydration front observed even with a constant heat flux in both experimental and numerical studies from the project. During exposure to heat flux or fire, surface temperatures of the gypsum board increase leading to increased heat losses. When the heat losses are similar to the heat influx, the gypsum board reaches a near-steady state. After this stage, the depth of calcination remains nearly the same even with further exposure to heat flux as shown in *Figure* 15. For higher heat fluxes, the entire gypsum board gets calcinated before reaching the near-steady state as shown in Figure 23. The correlations developed in the study, even though approximate, are capable of addressing this effect.

3.2.6.6: Comparisons with full-scale compartment measurements

Previously documented full-scale compartment fire tests performed at EKU for research into fire pattern reproducibility was re-evaluated using the correlations given above. Depth of calcination was measured for compartment linings. However, heat flux data was not recorded experimentally. Fire Dynamics Simulator (FDS), developed by the National Institute of Standards and Technology (NIST), is used to simulate the compartment fire and calculate the heat fluxes to the compartment lining. These heat flux values are then fed into the developed correlations to predict depth of calcination. Visualization of the compartment and the heat flux from the FDS for a selected wall are shown in Figure 61.

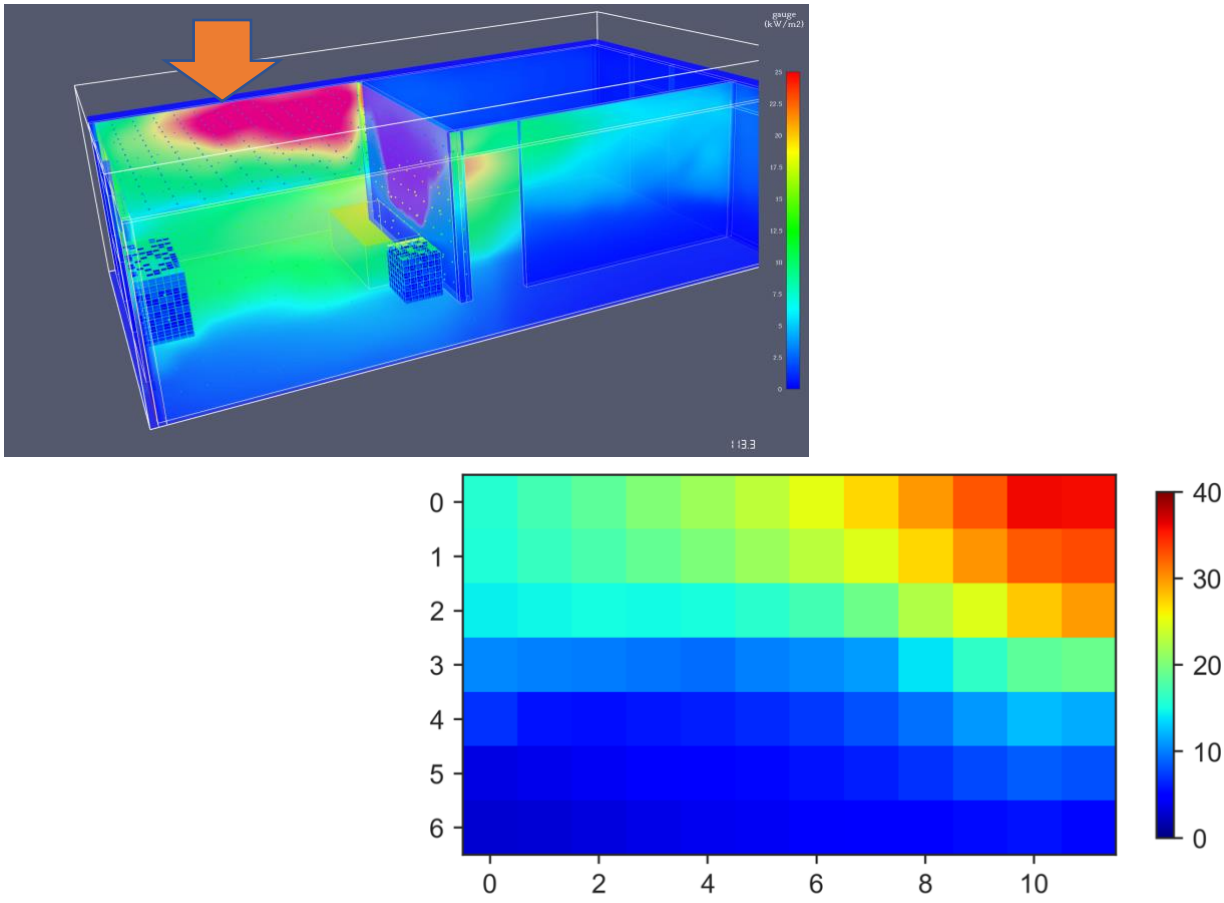

Figure 61: Visualization of heat flux to the compartment used (top) with an orange arrow pointing to the selected wall. Visualization of the heat flux to the selected wall obtained from FDS (bottom). The heat flux is in kW/m^2.

The measured depth of calcination from the full-scale experiments, predicted depth of calcination from the experimental correlation, and predicted depth of calcination from the numerical correlation are compared in Figure 62. The deviations between the predictions and measurements are within 2 mm for most of the wall. These differences could be due to the experimental uncertainties, assumptions used in the numerical model, and limitations of the FDS.

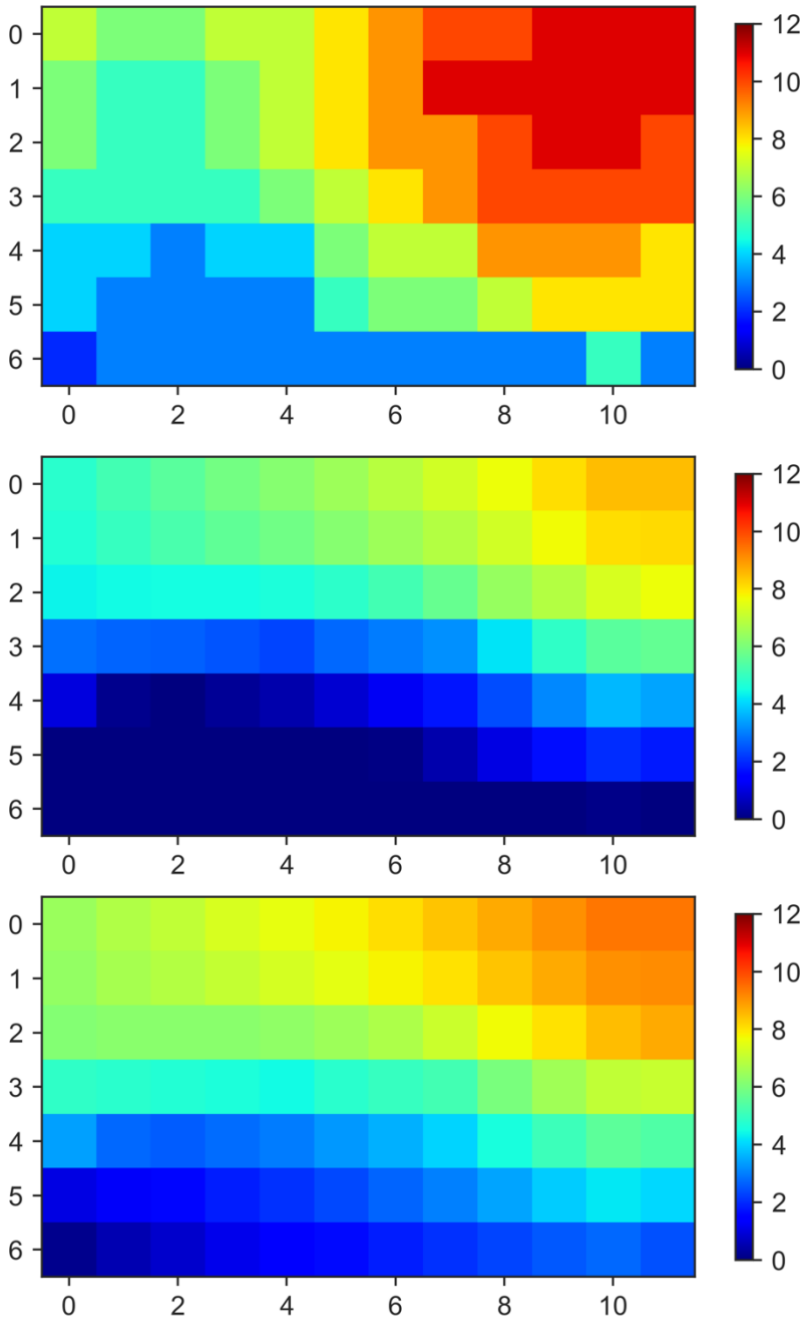

Figure 62: The measured depth of calcination from the full-scale experiments (top), predicted depth of calcination from the experimental correlation (center), and predicted depth of calcination from the numerical correlation (bottom). The depth of calcination is in mm.

3.3: Limitations

The major limitations of the present study are,

1. Due to the local irregularities in the gypsum board, the experimental uncertainties are significant.
2. Experimental studies are limited to regular drywalls. CertainTeed regular drywall panel (model #640365) with a thickness of 0.5 inch (12.7 mm) was used for the study. The results might not be reliable for other kinds of gypsum boards like moisture-resistant gypsum board, mold, and mildew-resistant gypsum board, fire-resistant gypsum board, and sound-absorbing gypsum board.
3. The numerical model considers the gypsum board as a homogeneous porous material. However, local irregularities are present in the commercial gypsum boards. This could affect the predictions.
4. The numerical model neglects the thin paper layers used in commercial gypsum boards
5. The numerical model neglects other materials like fiberglass added to commercial gypsum boards.
6. All the material and thermo-physical properties used in the model are only suitable for the regular gypsum boards. Also, properties of the gypsum boards from different manufacturers may vary.
7. Numerical predictions may not be accurate if the actual fire scenario is significantly different from the initial and boundary conditions used in the model.
8. The correlations developed are only approximate. The correlations may not be reliable for older gypsum boards, painted gypsum boards, and special types of gypsum boards.

4. ARTIFACTS

4.1: List of products

4.1.1: List of publications from the study

1. Rylan Paye, Reese P. Hancock, Shehzad Khan, Shijin P. Kozhumal, Hayri Sezer, “Local and Global Sensitivity Analysis of Gypsum Board Calcination”. 13th US National Combustion Meeting, College Station, TX, USA, March-2023.
2. Muhammad Hasnain, Rylan Paye, Jairo Casa, Trevor Borth, Gregory E. Gorbett, Shijin P. Kozhumal, Hayri Sezer, “3D Mathematical Model for Heat and Mass Transfer Mechanisms in Gypsum Board Exposed to Fire”, 13th US National Combustion Meeting, College Station, TX, USA, March-2023.
3. Shijin P. Kozhumal, Hayri Sezer, “Development of Gypsum Thermo-Chemistry Model with Variable Heating Rate”, Spring Technical Meeting, Eastern States Section of the Combustion Institute, Orlando, Florida, USA, March-2022.
4. Hayri Sezer, Rylan Paye, Carter Geist, Hunter Fries, Trevor Borth, Gregory E. Gorbett, Shijin P. Kozhumal, “TGA, DSC, and FTIR Analysis of Gypsum Plasterboards under Varying Heating Rates”, Spring Technical Meeting, Eastern States Section of the Combustion Institute, Orlando, Florida, USA, March-2022.
5. Shijin P. Kozhumal, Gregory E. Gorbett, Hayri Sezer, “Experimental and Numerical Investigations for the Prediction of Depth of Calcination of Gypsum Plasterboards Under Fire Exposure”, 2022 NIJ Forensic Science Research and Development (R&D) Symposium (Virtual), March-2022.

6. Ethan A. Fowlie, Trevor Borth, Gregory E. Gorbett, Hayri Sezer, Shijin P. Kozhumal, "Experimental and Numerical Investigation of Gypsum Calcination under Fire Exposure", 12th US National combustion meeting, College Station, Texas (Virtual), May-2021.

Published articles have been uploaded to JustGrants webpage.

4.1.2: Articles under review from the study

1. Gregory E. Gorbett, Ethan A. Fowlie, Trevor Borth, Hayri Sezer, Shijin P. Kozhumal, "Experimental Investigation of Gypsum Board Calcination under Radiant Heat Exposure and Depth of Calcination for Forensic Fire Investigation", under review, Fire Technology, 2023.

4.1.3: Technology

4.1.3.1: Depth of calcination predictor

A stand-alone executable to predict depth of calcination based on the exposed heat flux and duration of exposure is developed and shared to public through a GitHub repository available for public access. Users will only need to download, unzip, and double click the executable to open the Depth of Calcination Predictor. Users can enter the values of Heat flux (in kW/m^2) and duration of exposure (in seconds) on the Graphical User Interface. Hence, no programming background is needed to use the tool. Link to the repository is given below.

https://github.com/ShijinKozhumal/NIJ_Project_EKU

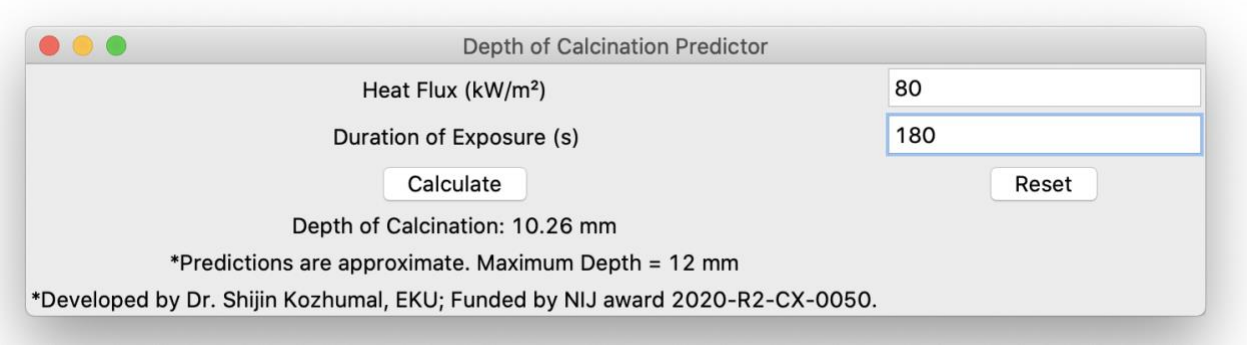

Figure 63: A screenshot of the stand-alone executable developed to predict depth of calcination based on the exposed heat flux and duration of exposure.

4.1.3.2: Comprehensive gypsum thermo-chemistry solver

A more comprehensive executable capable of plotting the transients in temperature and water vapor density at certain locations inside the gypsum board is developed and shared to public through a GitHub repository available for public access. Users will only need to download, unzip, and double click the executable to open the comprehensive gypsum thermo-chemistry solver. Users will need to enter a set input parameter input file provided. Even though the application is more computationally demanding, no programming background is needed to use the tool. Link to the repository is given below. A set of instructions is also included.

https://github.com/ShijinKozhumal/NIJ_Project_EKU

4.2: Data sets generated

4.2.1: Experimental data sets

1. Internal temperature and heat flux data from the radiant burner experiments
2. Internal temperature and heat flux data premixed burner experiments
3. Internal temperature and heat flux data diffusion burner experiments
4. Data sets of mass loss and mass loss rate from TGA

4.2.2: Numerical data sets

1. Internal temperature, vapor pressure, vapor density, air density, and degree of dehydration from numerical simulations with heat flux from 10 to 100 kW/m^2

2. Gypsum thermo chemistry reaction rates for different heating rates and temperature ranges.

Outcomes from the study including datasets, codes, articles are shared to public through the GitHub repository available for public access. Link to the repository is given below.

https://github.com/ShijinKozhumal/NIJ_Project_EKU

4.3: Dissemination activities

4.3.1: Conference presentations

1. 13th US National Combustion Meeting, College Station, TX, USA, March-2023.

   Two oral presentations based on the results from the project.

2. Spring Technical Meeting, Eastern States Section of the Combustion Institute, Orlando, Florida, USA, March-2022.

   Two oral presentations based on the results from the project.

3. NIJ Forensic Science Research and Development (R&D) Symposium (Virtual), March-2022.

   One poster presentation based on the results from the project.

4.3.2: Webinars

On Thursday June 3, 2021, an online webinar was held via zoom. This webinar engaged fire investigators and researchers in a conversation regarding depth of calcination and the use of this technique in fire investigations. Webinar participants were invited via email and social media. The webinar participants were provided with a 2-page handout describing the research project and a

short YouTube video describing the intent of the webinar and the research (https://www.youtube.com/watch?v=_t7U_mwrX3Q)

The webinar started with a brief introduction of the research methods and general objectives of the proposed research. The remaining 45 minutes of the webinar consisted of an open feedback session where the PI and Co-PI fielded questions and suggestions from the participants. Approximately 60 participants attended the webinar synchronously, while approximately 5 watched the recorded session later.

Recorded link of webinar:

https://www.dropbox.com/sh/9se9tuvmmuncsbs/AAAmby7qcASSWt1J-JMJruOwa?dl=0

Or

https://youtu.be/IMUXqKzwYQI

On Saturday April 29, 2023, a second webinar was held via a prerecorded YouTube presentation. The presentation summarized the research methods and results of the completed work and lasted approximately 20 minutes. To reach a broad audience an email was sent out to the previous webinar attendees and those that had shown an interest in the work (~300 email addresses). Also, a LinkedIn post with the link was also sent out to reach the wider fire investigation profession audience. At the time of writing this report, the post had already generated over 1400 impressions, over 32 reactions, and 2 reposts.

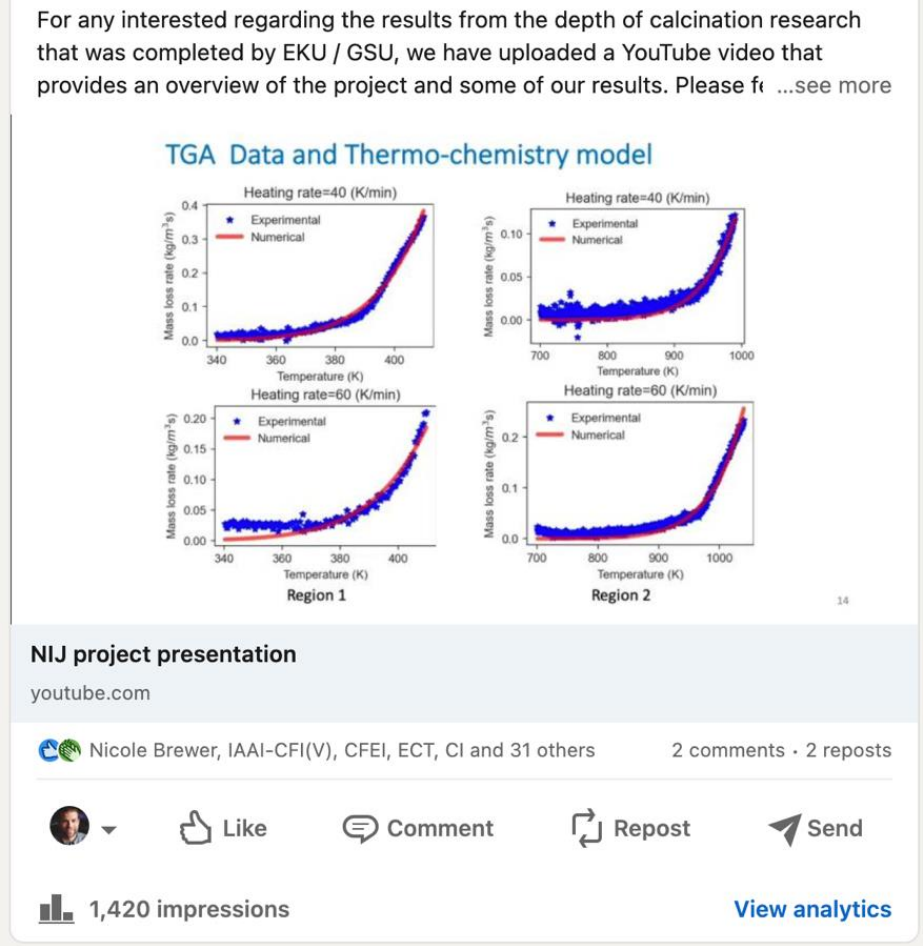

Figure 64: A screenshot of the LinkedIn post discussing the outcomes from the project.

Link to the recording: https://youtu.be/XqGLXazs0MI

5. REFERENCES

Abatzogloua, J. T., & Williams, A. P. (2016). Impact of anthropogenic climate change on wildfire across western US forests. *Proceedings of the National Academy of Sciences, 113*(42), 11770–11775.

Ahmed, N., & Hurst, J. (1997). Coupled heat and mass transport phenomena in siliceous aggregate concrete slabs subjected to fire. *Fire and Materials, 21*, 161-168.

Andesson, L., & Jansson, B. (1987). *Analytical Fire Design with Gypsum – A Theoretical and Experimental Study, Report FSD87-MG001.* Malmo, Sweden: Fire Safety Design.

Ang, C., & Wang, Y. (2004). The Effect of Water Movement on Specific Heat of Gypsum Plasterboard in Heat Transfer Analysis under Natural Fire Exposure. *Construction and Building Materials, 18*(7), 505–515.

Axenenko, O., & Thorpe, G. (1996). The Modelling of Dehydration and Stress Analysis of Gypsum Plasterboards Exposed to Fire. *Computational Materials Science, 6*(3), 281–294.

Bear, J. (1972). *Dynamics of Fluids in Porous Media.* Dover Publications.

Blondeau, P., Tiffonnet, A., Damian, A., Amiri, O., & Molina, J. (2003). Assessment of contaminant diffusivities in building materials from porosimetry tests. *Indoor air, 13,* 302-310.

Carman, S. (2008). Burn Pattern Development in Post-Flashover Fires. *International Symposium on Fire Investigations* (pp. 50-62). Sarasota: Investigations Institute.

Cox, A. (2013, July). Origin Matrix Analysis: A Systematic Methodology for the Assessment and Interpretation of Compartment Fire Damage. *Fire and Arson Investigator-Journal of the International Association of Arson Investigators, 64*(1), 37-47.

Craft, S., Isgor, B., Hadjisophocleous, G., & Mehaffey, J. (2008). Predicting the thermal response of gypsum board subjected to a constant heat flux. *Fire and Materials, 32,* 333-355.

Doerr, S. H., & Santín, C. (2016). Global trends in wildfire and its impacts: perceptions versus realities in a changing world. *Philos Trans R Soc Lond B Biol Sci., 371(1696)*.

Finney, M., Cohen, J., McAllister, S., & Jolly, W. (2013). On the need for a theory of wildland fire spread. *Int. J. Wildland Fire, 22*(1), 25–36.

Fowlie, E. A., Borth, T., Gorbett, G. E., Sezer, H., & Kozhumal, S. P. (2021). Experimental and Numerical Investigation of Gypsum Calcination under Fire Exposure. *12th US National combustion meeting* (pp. 1-10). College Station, Texas: Combustion Institute.

Fowlie, E. A., Sezer, H., Gorbett, G. E., & Kozhumal, S. P. (2020). Numerical Investigation of Heat Transfer and Gypsum Calcination under Fire Exposure. *Spring Technical Meeting, Eastern States Section of the Combustion Institute*, (pp. 1-6). Columbia, SC.

Ghazi Wakili, K., Hugi, E., Wullschleger, L. and Frank, T.H. (2007). Gypsum board in fire—modeling and experimental validation. *Journal of fire Sciences*, *25*(3), 267-282.

Hicks, W., Gorbett, G. E., Hopkins, M. C., Kennedy, P., Kennedy, J., Hopkins, R. L., & Thurman, J. T. (2008). Full-Scale Single Fuel Package Fire Pattern Study. *International Symposium on Fire Investigation Science and Technology.* Ohio: ISFI.

Jeong, S.G., Chang, S.J., Wi, S., Lee, J. and Kim, S. (2017). Energy performance evaluation of heat-storage gypsum board with hybrid SSPCM composite. *Journal of Industrial and Engineering Chemistry*, *51*, 237-243.

King, G., Beretka, J., & Ridge, M. (1971). Chemical Changes in Slabs of Cast Gypsum during Standard Tests of Resistance to Fire. *Journal of Applied Chemistry and Biotechnology, 21*(6), 159–162.

Kontogeorgos, D. and Founti, M. (2010). Numerical investigation of simultaneous heat and mass transfer mechanisms occurring in a gypsum board exposed to fire conditions. *Applied Thermal Engineering*, *30*(11-12), 1461-1469.

Kontogeorgos, D., & Founti, M. (2010). Numerical investigation of simultaneous heat and mass transfer mechanisms occurring in a gypsum board exposed to fire conditions. *Applied Thermal Engineering, 30*, 1461-1469.

Kontogeorgos, D.A. and Founti, M.A. (2012). Gypsum board reaction kinetics at elevated temperatures. *Thermochimica Acta, 529,* 6-13.

Kozhumal, S. P., Hicks, W. D., & Sezer, H. (2019). Numerical Investigation of Gypsum Thermo-Chemistry under Fire Exposure. *11th U. S. National Combustion Meeting* (pp. 1-10). Pasadena, CA: Combustion Institute.

Madrzykowski, D. M., & Fleischmann, C. (2012). Fire Pattern Repeatability: A Study in Uncertainty. *Journal of Testing and Evaluation, 40*(1), 1-11.

Magnussen, B., & Hjertage, B. (1976). On mathematical modeling of turbulent combustion with special emphasis on soot formation and combustion. *Proc. Combust. Inst., 16,* 719–729.

Mann, & Putaansuu. (2009). Studies of the Dehydration/Calcination of Gypsum Wall Board. *International Association of Arson Investigators* (pp. 38-44). Crofton, MD: IAAI.

McGarry, A., & Milke, J. (1997). *Full-Scale Room Fire Experiments Conducted at the University of Maryland.* University of Maryland. Gaithersburg: National Institute of Standards and Technology.

McGrattanan, K., McDermott, R., Floyd, J., Hostikka, S., Forney, G., & Baum, H. (2012). Computational fluid dynamics modelling of fire. *International Journal of Computational Fluid Dynamics, 26*(6-8), 349–361.

Mealy, C., Wolfe, A., & Gottuk, D. (2013). *Forensic Analysis of Ignitable Liquid Fuel Fires in Buildings, Grant No. 2009-DN-BX-K232.* USA: Department of Justice.

Mehaffey, J., Cuerrier, P., & Carisse, G. (1994). A Model for Predicting Heat Transfer through Gypsum-Board/Wood-Stud Walls Exposed to Fire. *Fire and Materials, 18*(5), 297-305.

National Academy of Science. (2009). *Strengthening Forensic Science in the United States: A Path Forward.* Washington D.C.: National Institute of Justice.

NFPA. (2017). *Guide for Fire and Explosion Investigations.* Quincy, MA: National Fire Protection Association.

NFPA. (2021). *Guide for Fire and Explosion Investigations.* Quincy, MA: National Fire Protection Association.

NFPA 400. (2019). *Hazardous Materials Code.* Quincy, MA (USA): National Fire Protection Association.

Paye, R., Hancock, R. P., Khan, S., Kozhumal, S. P., & Sezer, H. (2023). Local and Global Sensitivity Analysis of Gypsum Board Calcination. *13th US National Combustion Meeting.* College Station, TX.

Posey, E., & Posey, J. (1983). Using Calcination of Gypsum Wallboard to Reveal Burn Patterns. *Fire and Arson Investigator Journal of the International Association of Arson Investigators, 3*(83).

Radeloff, V. C., Hammer, R. B., Stewart, S. I., Fried, J. S., Holcomb, S. S., & Mckeefry, J. F. (2005). The wildland–urban interface in the united states. *Ecological Applications, 15*(3), 799–805.

Rethoret, H. (1945). *Fire Investigations* . Toronto, Canada: Recording and Statistical Corp, Ltd.

Riahi, S. (2012). *Development of Tools for Smoke Residue and Deposition Analysis. NIJ Grant No. 2007-DN-BX-K236.* Department of Justice (USA) .

Riahi, S., & Beyler, C. (2011). Measurement and Prediction of Smoke Deposition from a Fire Against a Wall. *Fire Safety Science, 10*, 641-654.

Riahi, S., Beyler, C., & Hartman, J. (2013). Wall Smoke Deposition from a Hot Smoke Layer. *Fire Technology, 49*, 395-409.

Ryan, J. (1962). Study of Gypsum Plasters Exposed to Fire. *Journal of Research of the National Bureau of Standards – C. Engineering and Instrumentation, 66C*(4), 373–387.

Sanders, J., & Gallagher, P. (2002). Kinetic analyses using simultaneous TG/DSC measurements: Part I: decomposition of calcium carbonate in argon. *Thermochimica Acta, 388*(1–2), 115–128.

Schroeder, R. (1999). *Post-Fire Analysis of Construction Materials, Dissertation.* . Berkeley: University of California.

Schwertz, F., & Brow, J. E. (1951). Diffusivity of water vapor in some common gases. *The Journal of Chemical Physics, 19*(5), 640-646.

Shanley, J., Kennedy, P., & Ward, J. (1997). *USFA Fire Burn Pattern Test* (Vols. FA-178). Emmitsburg, MD: United States Fire Administration.

Sobol, I. M. (1993). Sensitivity Estimates for Nonlinear Mathematical Models. *Mathematical Modeling & Computational Experiment (English Translation)*, 407-414.

Sobol, I. M. (2001). Global Sensitivity Indices for Nonlinear Mathematical Models and Their Monte Carol estimates. *Mathematics and Computers in Simulation, 55*(1-3), 271-280.

Sultan, M. (1996). A Model for Predicting Heat Transfer Through Noninsulated Unloaded Steel-Stud Gypsum Board Wall Assemblies Exposed to Fire. *Fire Technology, 32*(3), 239–259.

The Engineering Toolbox. (n.d.). Retrieved from https://www.engineeringtoolbox.com/

Wakili, K. G., Hugi, E., Wullschleger, L., & Frank, T. (2007). Gypsum board in fire - modeling and experimental validation. *Journal of Fire Sciences, 25*, 267-282.

www.globalgypsum.com. (2013). *Gypsum wallboard in the USA.* Retrieved from http://www.globalgypsum.com: http://www.globalgypsum.com/magazine/articles/679-gypsum-wallboard-in-the-usa

Zehfuß, J. and Sander, L. (2021). Gypsum plasterboards under natural fire—Experimental investigations of thermal properties. *Civil Engineering Design, 3*(3), 62-72.